RI 9273

REPORT OF INVESTIGATIONS/1989

Physical and Computer Modeling of Roof Bolt Systems

By S. M. Dar, T. W. Smelser, and H. C. Pettibone

BUREAU OF MINES

UNITED STATES DEPARTMENT OF THE INTERIOR

Mission: As the Nation's principal conservation agency, the Department of the Interior has responsibility for most of our nationally-owned public lands and natural and cultural resources. This includes fostering wise use of our land and water resources, protecting our fish and wildlife, preserving the environmental and cultural values of our national parks and historical places, and providing for the enjoyment of life through outdoor recreation. The Department assesses our energy and mineral resources and works to assure that their development is in the best interests of all our people. The Department also promotes the goals of the Take Pride in America campaign by encouraging stewardship and citizen responsibility for the public lands and promoting citizen participation in their care. The Department also has a major responsibility for American Indian reservation communities and for people who live in Island Territories under U.S. Administration.

Report of Investigations 9273

Physical and Computer Modeling of Roof Bolt Systems

By S. M. Dar, T. W. Smelser, and H. C. Pettibone

UNITED STATES DEPARTMENT OF THE INTERIOR
Manuel Lujan, Jr., Secretary

BUREAU OF MINES
T S Ary, Director

Library of Congress Cataloging in Publication Data:

Dar, S. M.
Physical and computer modeling of roof bolt systems / by S. M. Dar, T. W. Smelser, and H. C. Pettibone.

(Report of investigations / Bureau of Mines, United States Department of the Interior; 9273)

Includes bibliographical references.

1. Mine roof bolting. 2. Mine roof control–Computer simulation. 3. Engineering models. I. Smelser, T. W. II. Pettibone, Howard C. III. Title. IV. Series: Report of investigations (United States. Bureau of Mines); 9273.

TN23.U43 [TN289.3] 622 s–dc20 [622'.28] 89-600062
CIP

CONTENTS

ILLUSTRATIONS

ILLUSTRATIONS—Continued

ILLUSTRATIONS–Continued

TABLES

UNIT OF MEASURE ABBREVIATIONS USED IN THIS REPORT

deg	degree	in/in	inch per inch
ft	foot	lb	pound
ft/lb	foot per pound	lb/ft^3	pound per cubic foot
ft · lbf	foot pound (force)	mm	millimeter
gal/min	gallon per minute	pct	percent
h	hour	psi	pound per square inch
in	inch	V	volt
in^2	square inch	yd^3	cubic yard

PHYSICAL AND COMPUTER MODELING OF ROOF BOLT SYSTEMS

By S. M. Dar,[1] T. W. Smelser,[2] and H. C. Pettibone[3]

ABSTRACT

The U.S. Bureau of Mines constructed a full-scale model of a 15-ft-wide coal mine entry to use in combination with finite-element analyses to investigate roof support systems and various types of roof bolts. The objective was to enhance understanding of the fundamental mechanics of the interaction between rock and supports and the relative integrity of bolted mine roof as a function of roof bolt type, length, spacing, and tension, and the basic characteristics of the roof strata. The laboratory test results, when correlated with computer simulations using finite-element analysis and underground verification tests, should provide a basis for designing safer, more cost-effective roof control systems and help to establish guidelines for employing fully grouted resin and mechanically anchored bolting systems. The background for this research, the research approach, the methods and equipment employed, and the results are described in this report.

[1]Mechanical engineer.
[2]Supervisory mechanical engineer.
[3]Research civil engineer (retired).
Spokane Research Center, U.S. Bureau of Mines, Spokane, WA.

INTRODUCTION

During the last 30 years, the use of roof bolts for the support and stabilization of U.S. coal mine excavations has increased, until today roof bolting is the primary support system. The result has been a significant reduction in the number of fatal and nonfatal roof fall accidents in underground coal mines, although roof fall accidents still occur where bolts have been installed. In practice, most roof bolting plans are based almost entirely on trial and error and inevitably lead to underdesign or overdesign with regard to bolt length, spacing, tension, and type. Underdesign causes safety problems, and overdesign is a financial burden to the coal mine operator. A set of comprehensive guidelines for the industry is needed to encourage the selection and design of roof bolting plans that will maximize safety and minimize cost. Such guidelines must be adaptable to the site-specific geology of a given coal mine as well as provide specific design criteria.

Although a number of theories have been proposed and a great amount of research has been carried out regarding the mechanics of rock reinforcement and mine roof behavior, there is still no consensus on criteria for the design and installation of roof bolt systems. In particular, there is an incomplete understanding of how much tension should be applied to mechanically anchored roof bolts when they are installed in order to achieve a stable mine roof under specific geologic and mining conditions.

As part of its mission to improve mine safety, the U.S. Bureau of Mines is performing basic research on roof bolt performance under a variety of geologic conditions. A physical model, computer simulations using finite-element analysis, and field verification were chosen for this research because they were technically and economically feasible. Underground testing alone has proven too complex, costly, and time consuming and has yielded limited results. On the other hand, a physical model allows precise measurement of the performance of different bolt types under controlled test conditions using a wide range of roof bolting parameters. Although the model constructed was idealized and limited in size, it served as a reliable basis for validating the use of bolts for rock reinforcement and for verifying the accuracy of computer modeling. Computer modeling using the finite-element approach enables evaluation of the extremely variable and complex site-specific problems encountered in an underground mine environment in a rapid and cost-effective manner. Small-scale underground tests to verify the finite-element predictions serve to increase confidence that this multifaceted approach can establish practical guidelines for roof bolting under various mining conditions. However, this report reviews physical and computer modeling studies only, because sufficient field data were not available for comparison at the time of reporting.

PHYSICAL MODEL

The model is a full-sized reproduction of a coal mine entry housed at the Bureau's Spokane Research Center (SRC) (fig. 1). This model consists of two supporting concrete pillars, 3 ft wide, 6 ft high, and 15 ft long, separated by a clear span of 15 ft. The pillars are capped by six roof slabs, one on top of another, each 1 ft thick by 15 ft wide by 21 ft long. The model entry was constructed of 90 yd^3 of fine-grained concrete having a design strength of 5,000 psi, which simulates a competent shale. Surrounding the concrete entry, and tied into a structural testing floor, is a 150-ton structural steel reaction frame supporting a servocontrolled hydraulic loading system. Loads from the hydraulic cylinders are distributed over the model surface through rubber-faced steel pads approximately 30 in square. This system is capable of applying about 3 million lb vertically and 1.8 million lb horizontally and has vertical and horizontal shear capabilities of 0.5 and 0.9 million lb, respectively. A system of hydraulic supports in the model mine entry is capable of providing simulated premining and postmining support.

The roof slabs, with roof bolts installed, are extensively instrumented with gauges that monitor strain in the bolts, total load on certain types of bolts, slab deflection, strain within slabs and pillars, interlaminar slip between slabs, temperatures within and around the model, movement of the pillars, and entry closure. A minicomputer and data acquisition system control the testing operation on a real-time basis. Real-time data, displayed on a cathode-ray tube, keep the model operators constantly informed of critical strains within the model and the bolting systems.

Roof bolt holes were drilled into the roof slabs in a 4- by 4-ft pattern, and parallel tests were performed to compare conventional mechanically anchored steel bolts with resin-grouted steel bolts.

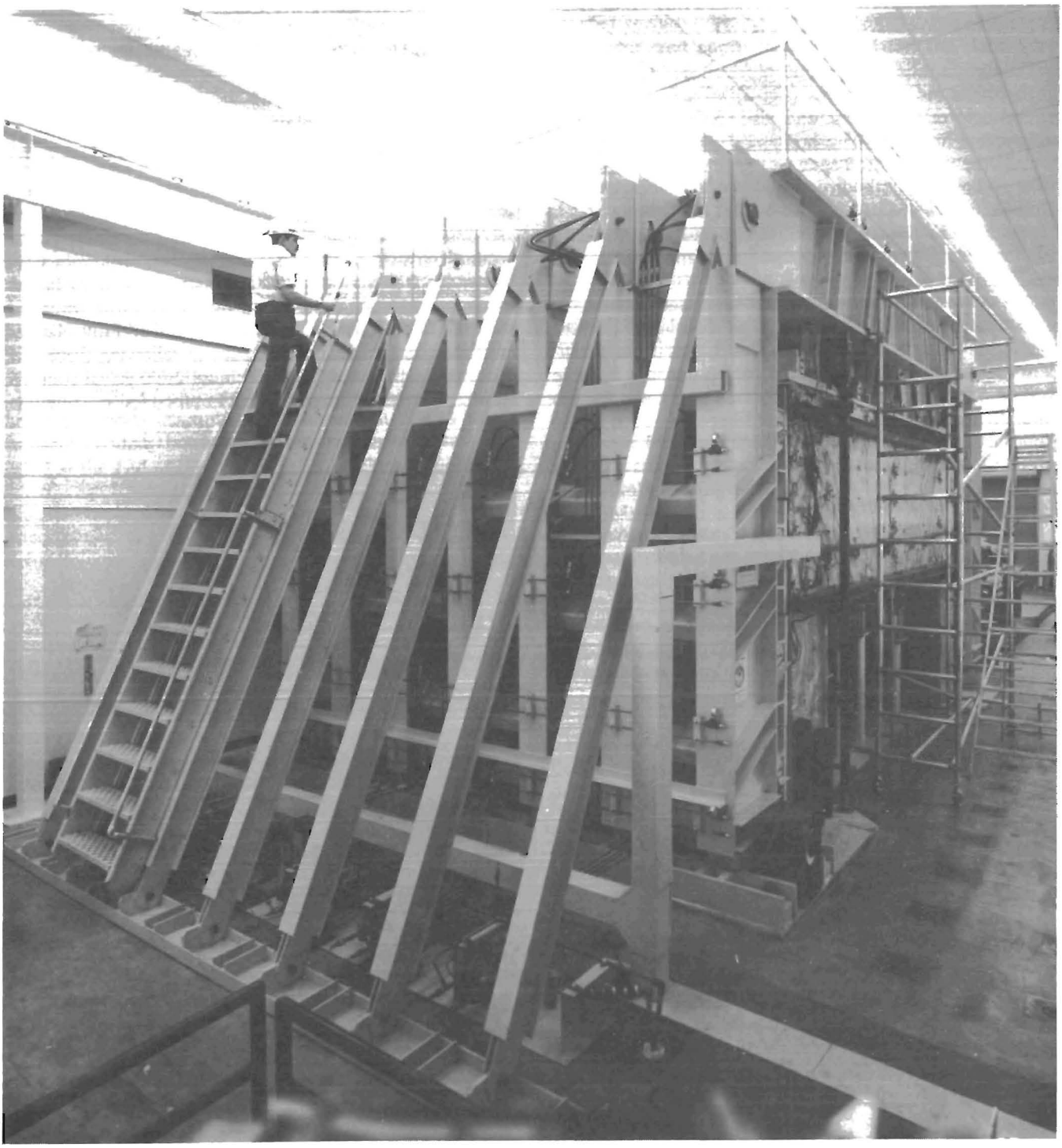

Figure 1.–Full-scale model of mine entry.

CONSTRUCTION OF MODEL COAL MINE ENTRY

The dimensions of the model were chosen to maintain the approximate dimensions (fig. 2) of a typical underground coal mine opening and also to fit within the existing space at SRC. The horizontal and lateral dimensions of the unsupported span were selected to allow four rows of bolts in both directions at 4-ft spacings. The immediate roof was assumed to consist of six layers, each 1 ft thick. The immediate roof thus could accommodate bolt lengths of 4 to 6 ft and could also approximate the bedding of an actual mine roof.

The roof slabs and pillars are separated from each other by a layer of 6-mil polyethylene sheeting to prevent bonding of the concrete and to produce a uniform coefficient of friction in the laminated roof (appendix B, table B-3). A 5,000-psi, sand-portland cement grout was used to simulate a competent shale. Steel fiber was added to the grout mix to help eliminate shrinkage and cracking and to extend the useful life of the slabs. Eighty pounds of 50- by 0.5-mm steel fiber was used per cubic yard of grout in the slabs.

The simulated mine entry was cast in place on the structural test floor at SRC. The 3- by 6- by 15-ft pillars and the 15- by 21- by 1-ft slabs were emplaced at 1-week intervals using plywood forms fabricated on-site. The slabs were supported by temporary shoring designed to allow a maximum vertical deflection of the slabs, under full dead load, of 0.005 in. Seven-inch-square cutouts were provided in the bottom form so that 20 mechanical jacks could be placed under the concrete slabs to support them fully before the temporary shoring was removed. This ensured that the concrete slabs would be fully supported at all times and so prevented unwanted creep strains from developing in the slabs.

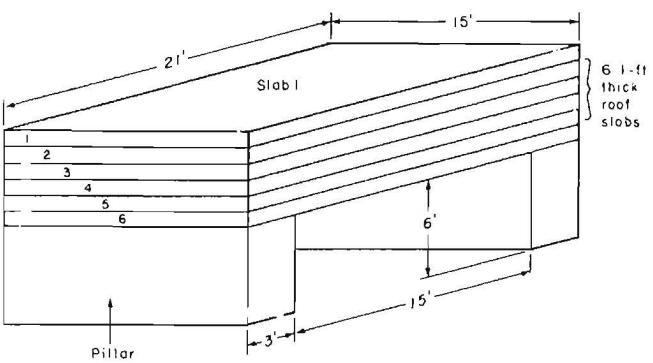

Figure 2.–Dimensions of model mine entry.

Concrete Placement

The concrete was delivered in ready-mix trucks; the steel fibers were added and mixed; and the mixture was transferred from the truck to the forms using a 1/2-yd^3 bucket on an overhead crane in the structures bay at SRC.

The concrete in the 6-ft-high pillars was placed in 1-ft lifts. Each lift was thoroughly vibrated with an immersion-type vibrator. The slabs were placed in two 6-in lifts, and again the concrete was thoroughly vibrated with an immersion-type vibrator. Concrete was carefully placed around the instruments by hand (fig. 3). Markers were suspended from strings over each instrument so the instruments would not be disturbed by the vibrator while the second lift of concrete consolidated. Carefully planned emplacement procedures and care in following these procedures resulted in the emplacement of 90 yd^3 of concrete without damage to any of the 121 embedded instruments.

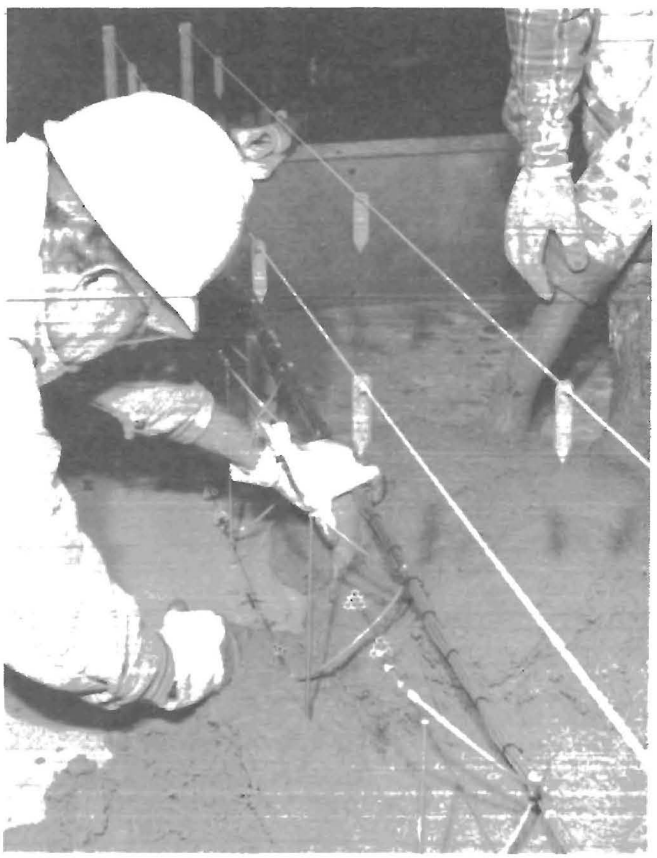

Figure 3.–Placing concrete around embedment strain gauges.

Quality Control

Tests to evaluate the material properties of the concrete were conducted following the procedures outlined by the American Society for Testing and Materials (ASTM).[4] The concrete in each truck was agitated at a fast rate and then tested to make sure the load met slump, temperature, and air specifications. The samples consisted of twenty-four 6- by 12-in cylinders, four flexure beams, and four shear samples. Twelve cylinders, two flexure beams, and two shear samples were cast from half of the first lift. After half of the second lift had been emplaced, the second set of samples was taken from the concrete remaining in the truck.

Eight cylinders were tested at 7, 14, and 28 days to determine their compliance with the strength specifications. The remaining 16 cylinders were separated into 2 groups of 8 and evaluated at the beginning and end of the test period. Samples from structural beams were similarly divided; however, the shear samples were all tested at the end of the test period. The large number of concrete specimens provided reliable, statistically significant figures for the desired concrete properties of the model coal mine entry. The results showed acceptable uniformity in strength and moduli, and the values obtained were used as input for computer modeling of the physical model.

Curing Procedures

Steps were taken to control the hydration rate of the concrete and to ensure dimensional stability. Each pillar had the forms stripped away 1 day after concrete placement. The pillars were then cured for 28 days with wet burlap. A resin-based curing compound was applied at four times the normal amount, and the pillars were completely wrapped in 6-mil polyethylene. The curing compound and plastic cover served as moisture seals to reduce moisture loss.

Experience obtained during a Bureau contract at the U.S. Army Corps of Engineers, Construction Engineering Research Laboratory, Champaign, IL, showed that differential drying or differential temperatures in the concrete can cause curling of large, unreinforced slabs. Because of the potential for such problems, the following curing and insulation procedures were used.

Two sets of slab forms were built, and they remained in place for at least 7 days after concrete placement. Immediately after the forms were stripped, any projections were ground off and an epoxy curing compound was applied along the sides and ends of the slabs at four times the normal amount. As soon as the compound cured, 6-mil polyethylene was taped temporarily in place over the exposed surface. The top face of each slab was sprayed with water, and approximately 4 h later, the slabs were covered with a 6-mil layer of polyethylene and a 2-in concrete curing (insulation) blanket. The polyethylene sheet on the top of slabs 1 through 5 were left in place permanently to prevent concrete bonding between layers and to ensure a more uniform and predictable coefficient of friction. Three and one-half inches of fiberglass were also placed under the bottom form of slab 6 (fig. 2) to minimize temperature differentials in the slabs during the initial curing period. Temperature readings taken from the sensors buried in the slabs showed that this method was successful. The top of slab 1 was sealed with an epoxy curing compound, which successfully retarded curling. The top was also coated with an antiskid vapor barrier.

LABORATORY TEST SYSTEM

Reaction Frame

The entire reaction frame and how it interacted with the structural testing floor is depicted in figure 4. The 15-ft-long spreader beams under the structural test floor were necessary because the load being transferred through the intermediate bolts securing the base plate to the floor was 90 kips, which was 50 pct higher than the allowable 60 kips per tiedown hole. The unusually high loads being placed on the floor caused concern, and during initial testing, the floor was very carefully monitored, as described later.

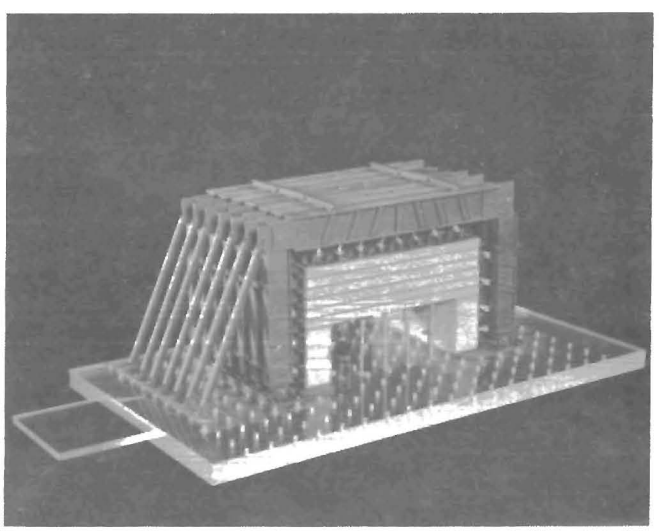

Figure 4.–Scale model of model mine entry.

[4]American Society for Testing and Materials (Philadelphia, PA). C 39, C 78, C 143, C 172, C 192, C 684, C 873 in 1979 Annual Book of ASTM Standards: Part 14, Concrete and Mineral Aggregates.

The reaction frame is a pinned structure; hence, the diagonal brace on the left side is necessary to ensure stability of the frame. To facilitate disassembly of the frame in preparation for placing a new concrete entry, the frame was designed in modules, as shown in figure 4. Connections between the modules are bolted, while all other connections are welded, and the hydraulic lines are supplied with quick disconnects.

The load plates that apply the load to the outer surface of the concrete entry were designed for minimal deflection to ensure uniform distribution of the load over the concrete surface. Ribbed rubber padding was glued to the load face of each plate to take up minor irregularities in the concrete surface and further ensure uniform distribution of the load.

The 25 hydraulic cylinders were installed in the mine entry to simulate premining and postmining conditions. These hydraulic jacks are shown in figure 5, which also shows the 20 mechanical supports that continuously support the roof slabs while the model is not being used. The complete test system, including all instruments and several safety features, is shown in figure 1.

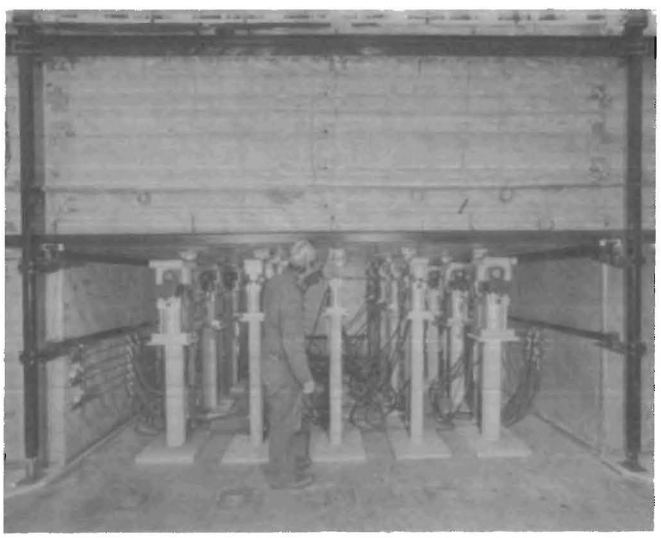

Figure 5.–Hydraulic supports being placed in model mine entry.

Hydraulic Loading System

The main hydraulic power unit used to load the model was a 9.3-gal/min variable displacement pump. The 121 hydraulic cylinders, which applied load to the model as shown in figure 6, are 3,000-psi cylinders and range in diameter from 3-1/4 to 8 in. The loading configuration was determined from a global analysis of stress distributions around a typical mine opening (see the section on "Loading Analysis" and appendix A). The closed-loop, servocontrolled, electrohydraulic system is divided into 11 zones.

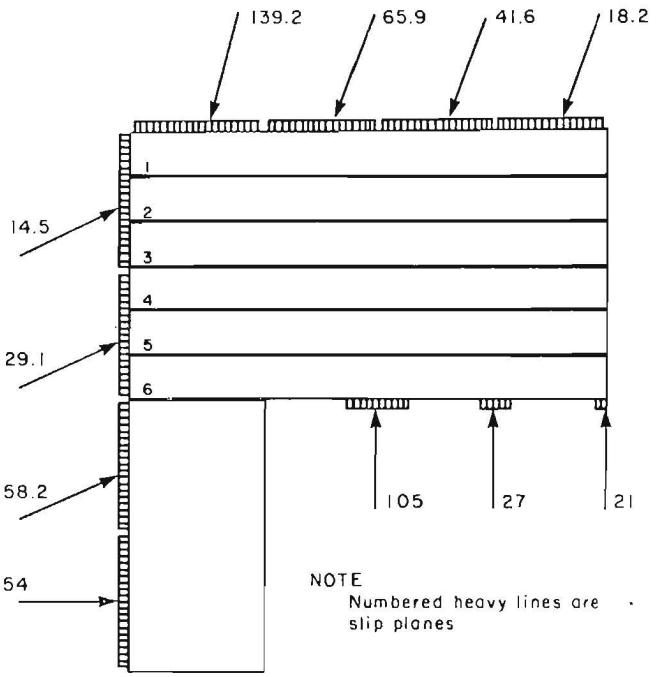

Figure 6.–Direction and amount of applied loads. Loads are total per cylinder, kips, including 25-pct overload.

Instrumentation

The simulated concrete coal mine entry contains 106 embedded concrete strain meters. Sixty-five of the gauges are 4-in-long single gauges mounted with their long axes parallel to the 21-ft length of the roof slabs. The gauges are arranged in two lines, each situated 18 in. in from the east and west faces of the model (fig. 7). Thirteen three-gauge rosettes composed of 2-in-long embedded concrete strain gauges were placed in the slabs in both horizontal and vertical directions. A pair of vertical rosettes and three temperature sensors are illustrated in figure 8. Seventeen platinum probe temperature sensors measure the temperature at two points in the air around the model, six points in the pillars, and nine different locations in the roof slabs.

Loads on the heads of the 16 mechanically anchored bolts and on the 16 resin-grouted steel bolts are monitored with rock bolt load cells such as the one shown in figure 9. These load cells have been used successfully in past research at SRC and were available from existing inventory. All load cells were recalibrated before being used.

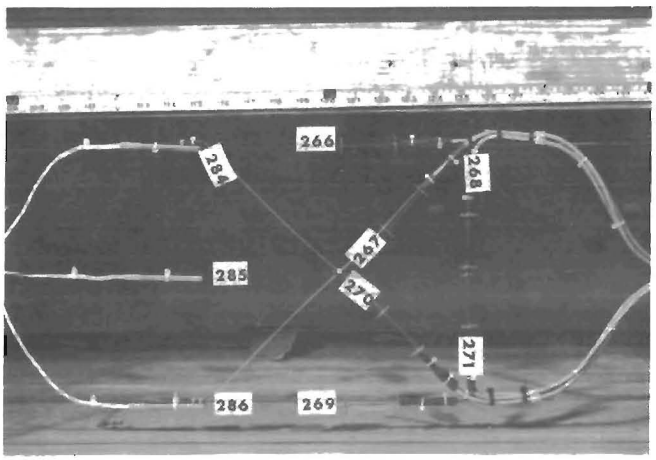

Figure 8.–Vertical strain-gauge rosettes (266-271) and temperature sensors (284-286).

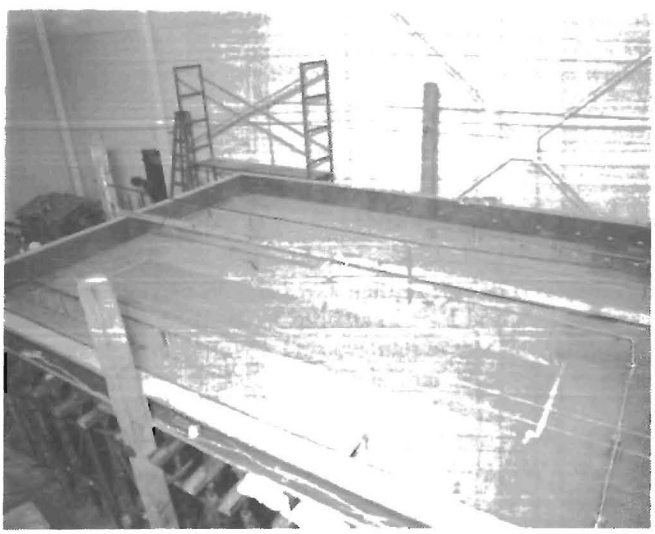

Figure 7.–Embedded instrumentation in slab 6.

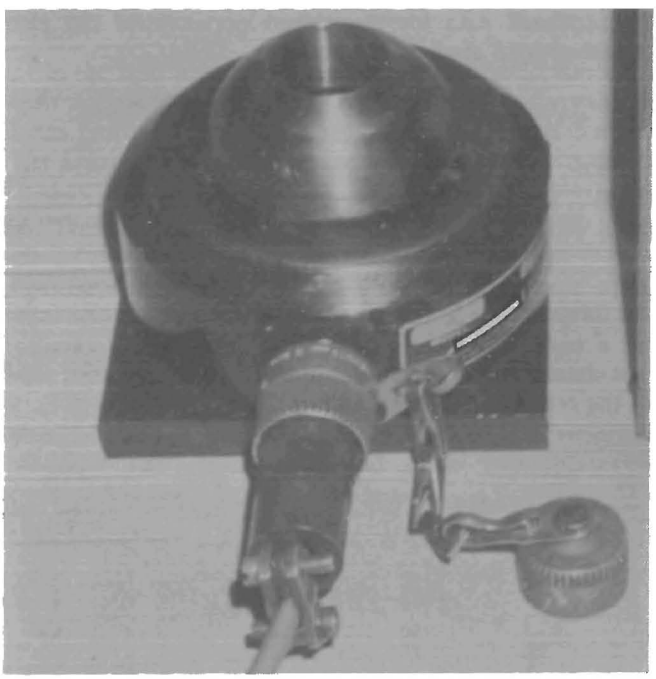

Figure 9.–Roof bolt load cell.

Thirty-four direct current differential transformers (DCDT's) measure the interlaminar slip at each of the six slip joints. Another 29 DCDT's measure vertical deflection of the bottom and top slabs. Five of the seven DCDT's on the east face of the bottom slab are shown in figure 5. The black structural framework supports the deflection DCDT's, but the interlaminar slip DCDT's are mounted directly on the concrete structure.

Hydraulic cylinder efficiency tests were necessary to determine friction losses in the cylinder. These tests indicated that efficiency could drop to 85 pct at low pressures, but could go as high as 98.5 pct at high pressures. To determine the exact efficiency of the 11 different hydraulic systems, 13 custom-designed, strain-gauged clevis pins were used. These special load cells measure load produced by any selected hydraulic cylinder. A statistical sampling of the 125 hydraulic cylinders was analyzed to produce calibration curves for each system.

Oil pressure supplied to each of the 11 banks of hydraulic cylinders was measured with strain-gauge-type pressure transducers. The transducers not only supplied the feedback data for the closed-loop control but also furnished load application data.

Computer and Data Acquisition System

The minicomputer operates with ASSEMBLER, BASIC, and FORTRAN languages and controls the model on a real-time basis. The central processing unit has 48,000 words of mapped memory, 315,000 words of diskette storage, and 10 megabytes of hard disk storage. Approximately 650 full scans may be stored on one magnetic tape. The data acquisition system can monitor 300 channels of instruments. Figure 10 is a general view of the computer control panel.

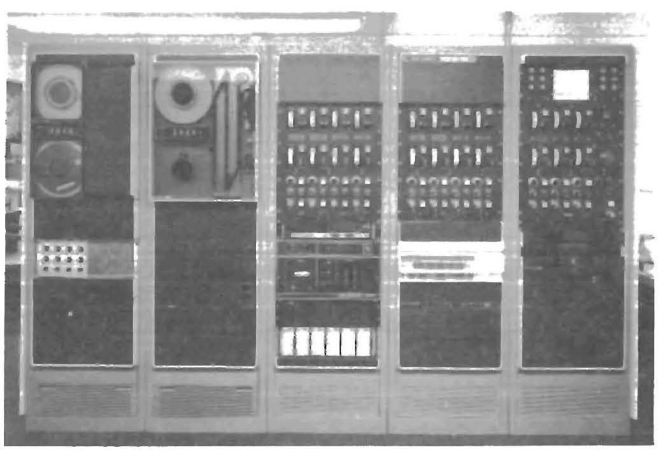

Figure 10.–Computer control panel.

PHYSICAL MODEL TEST PROGRAM

The purpose of the model test program was to acquire data (strain, slab deflection, interlaminar slip, and bolt load) for the mine entry system in both the unbolted and the bolted states using mechanically anchored bolts and resin-grouted bolts. The data can serve to verify the computer code used to model the structure and to increase fundamental knowledge about roof bolting systems.

The two types of roof bolts tested are shown in figure 11. The mechanically anchored bolt is tensioned to put a compressive load on the strata. In coal mining, a resin-grouted bolt is generally an untensioned, fully grouted, steel dowel. Both bolt types use identical bearing plates under the bolt head.

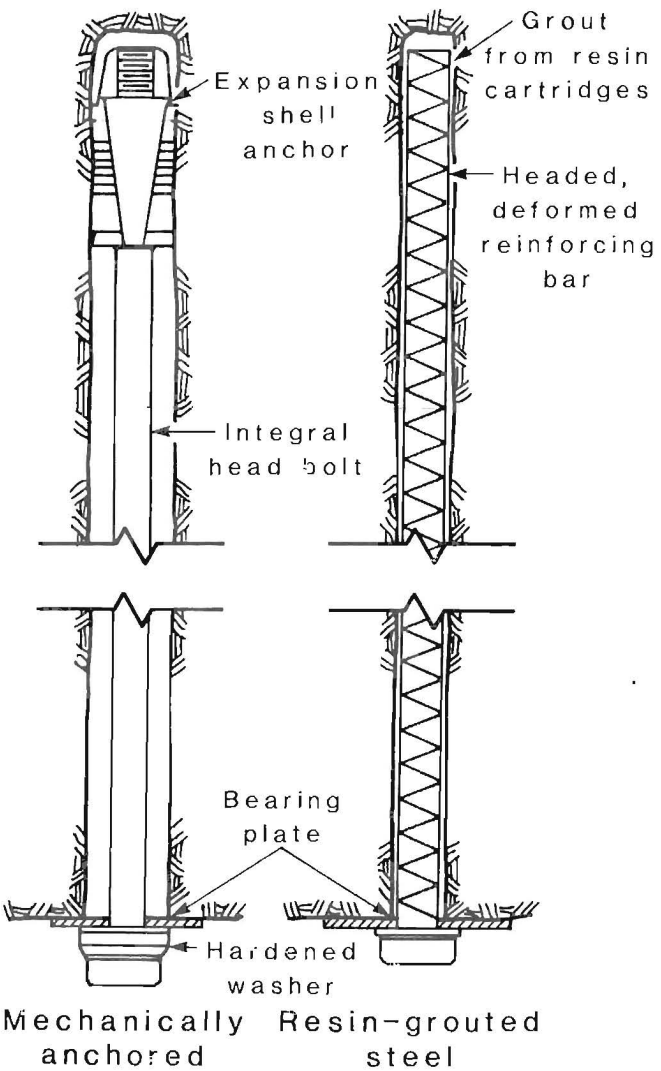

Figure 11.–Two types of roof bolts.

The initial testing on the model determined dead-load stresses by first fully supporting the dead weight of the slabs with the 25 premining and postmining hydraulic jacks in the entry. The mechanical jacks were released, and then the hydraulic load was decreased in 10-pct increments until the roof slabs were supporting themselves fully.

A grid pattern of sixteen 1-in-diameter holes, spaced 4 ft on center, was wet-drilled into the roof slabs. The bolt pattern is shown in figure 12. No. 6, grade 60 resin-grouted steel bolts were installed in each of the holes. A typical live-load test was performed by first retracting all load pads on the outside of the model and applying dead load to the model, as previously described. Next, the load pads were moved into contact with the model, and loads were applied in 5-pct increments of maximum load. Loading was stopped at either a midspan deflection on the bottom slab of 0.04 in or an internal longitudinal tensile strain in the concrete slab of 50×10^{-6} in/in. This limited the responses to 50 pct of maximum breaking capacity of the model. Slab deflection was the controlling factor in all tests.

After live-load testing with all bolts installed, the bolts were removed in three stages and the tests were repeated. First, the four bolts in the geometric center of the pattern were removed. Then the four remaining bolts near the midspan on the east and west sides of the model roof were taken out. Finally, the four remaining bolts adjacent to each rib of the entry were removed. The bolts were removed by overcoring with a custom-designed, thin-walled diamond bit and then reaming the hole to a 1-3/8-in diameter.

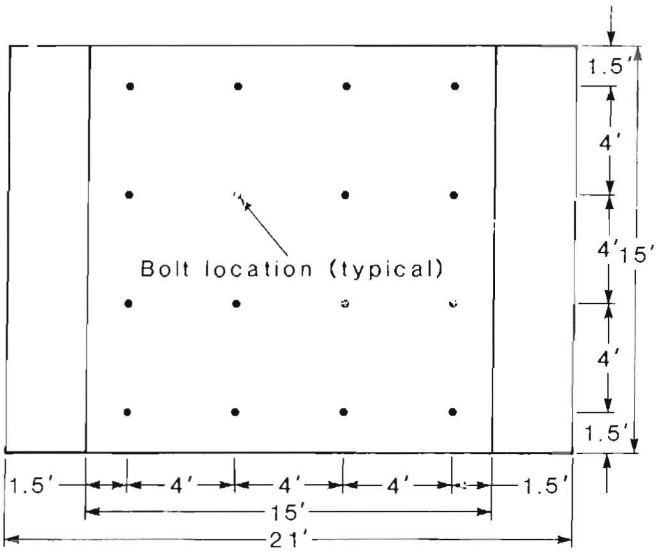

Figure 12.–Bolt pattern.

In the next phase, 3/4-in-diameter, grade 55, mechanically anchored steel bolts were inserted into the reamed holes and tensioned to 13 kips using an impact wrench. The tension was measured by rock bolt load cells rather than with a torque wrench. Live-load testing then continued at 9, 6, and 3 kips with all bolts installed. The three-stage sequence of bolt removal was repeated as described above for the resin-grouted bolts.

COMPUTER MODELING OF PHYSICAL MODEL

One objective of this investigation was to establish the validity of finite-element models of roof bolt support systems in mine openings. This evaluation was accomplished by constructing analytical models that approximated the geometry and loading characteristics of the physical model opening and comparing the results of the analyses with results of full-scale laboratory model testing. Although, in most cases, geometry of mine openings can be assumed to be constant, in the real world, loading intensities vary from mine to mine, even at the same depths, because mine geometry, physical properties of overburden, and geologic characteristics of the surrounding media all influence load intensities. For a given situation, however, information gained from an analytical model can be used to predict the performance of different roof bolting systems in a full-scale physical model.

Laboratory test models are, however, subject to certain constraints with respect to geometry and load intensities. Given the capacity of the existing full-scale model test facility at SRC, constraints arose partly because of the size of the real mine opening actually chosen and partly because of heavy load intensities in the neighborhood of the mine roof. Therefore, certain simplifying assumptions consistent with the geometry and load intensities of the physical model were incorporated into the analytical model. The rationale behind these assumptions is discussed below.

LOADING ANALYSIS

In 1971, a numerical analysis was made at SRC to determine the loading configuration for a physical model that would simulate the stress distribution about a mine opening in an infinite stress field. Though coal mines exist at considerably greater depths, a depth of approximately 100 ft was assumed. Loading on the roof of a mine opening is generally caused by the weight of the overburden. Assuming a weight density of rock in the range of 140 to 150 lb/ft^3, a load factor of about 1 psi results for every foot of depth. However, because of the "inclusion effect" of the mine opening, this load is not uniformly distributed over the width of the roof. To arrive at more accurate load intensities around the mine opening, reference was made to a finite-element analysis of a rectangular opening subjected to an assumed uniform vertical pressure of 1,360 psi on the horizontal boundary at a distance of approximately 500 in above the horizontal centerline of the opening. This analysis was based on a linear elastic

approach using the ASOLID computer program. The horizontal and vertical dimensions of the surrounding mass and the opening, including various material properties used in the analytical model, are shown in figure 13.

With these large dimensions, the inclusion effect of the opening and the Poisson's effect were negligible in the vicinity of the outside boundaries. All boundaries other than the top surface were considered roller supported to approximate the freedom of movement in a mining situation. The top boundary was far enough from the opening for a valid assumption of uniform pressure. For these reasons, the loading shown in figure 13 and the corresponding responses shown in figure 14 (and subsequently in figures 15 and 16) are referred to as "global loading" and "global analyses," respectively. The stress distribution in the neighborhood of the mine opening is shown in figure 14, where the first, second, and third rows are the resulting vertical normal, shear, and horizontal normal stresses, respectively.

To check the statics of the stress distribution, the reader should refer to figure A-1 in appendix A, where a portion of the mine entry shown in figure 14 has been isolated. To maintain equilibrium, shear stresses must occur in the directions indicated on figure A-1.

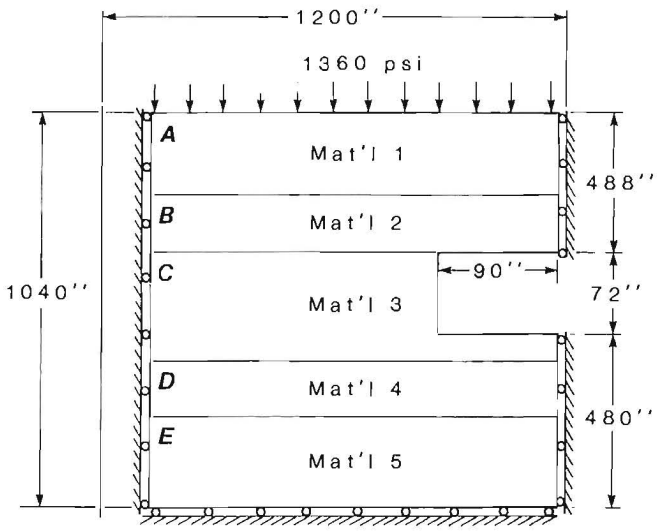

A $E = 1.85 \times 10^6$ psi
$\nu = 0.2$
$G = 0.77 \times 10^6$ psi

B $E = 1.30 \times 10^6$ psi
$\nu = 0.2$
$G = 0.54 \times 10^6$ psi

C $E = 0.55 \times 10^6$ psi
$\nu = 0.3$
$G = 0.21 \times 10^6$ psi

D $E = 1.4 \times 10^6$ psi
$\nu = 0.3$
$G = 0.54 \times 10^6$ psi

E $E = 4.5 \times 10^6$ psi
$\nu = 0.2$
$G = 1.87 \times 10^6$ psi

Figure 13.–Global model loading and geometry.

SELECTION OF COMPUTER CODES

The immediate roof of a coal mine opening usually consists of distinct beds. Because of the geologic discontinuities inherent in actual mining situations, the load-carrying capacity of the immediate roof is reduced significantly compared with the capacity of a continuous slab of the same thickness and similar material properties. One basic aim of this project was to establish technical criteria for support of the immediate roof, using roof bolts to make the roof layers act as a reinforced rock unit. Therefore, it was necessary to employ a numerical analysis method that could incorporate features such as joints, bedding planes, and roof bolts. Joints and bedding planes are defined differently: Bedding planes constitute depositional horizons, whereas joints are fractures in the rock that occur primarily as a result of external stresses. Both ANSYS and BMINES computer codes were employed to corroborate the analytical results. These codes were first used to model continuous media without slab interfaces (unlayered solids), using the material properties and load distributions of the global analysis (fig. 13) for comparison with the ASOLID results (fig. 14). The resulting quantities from the analysis using BMINES are shown in figure 15, where the first, second, and third rows are vertical normal stress, shear stress, and horizontal normal stress, respectively. As can be seen, figures 14 and 15 compare very favorably with each other, validating the use of BMINES.

After the validity of the BMINES code when applied to solid continuous media was verified, stress distribution around the mine-opening was determined for a depth of 100 ft by multiplying the quantities in figure 15 by a factor of 100/1360 = 0.0735 (fig. 16), which is the ratio of the loading under consideration to the global loading shown in figure 13. Figure 17 shows stress intensities taken from figure 16 at sections A-A and B-B, which formed the boundaries of the physical model after these loads were corrected for the dead-load contributions of the model; that is, the applied stresses on the boundary were equal to total live load minus dead load of the physical model. These loads were applied on the boundary of the physical model by means of steel pads (fig. 17). The practical aspects of the application of these load intensities and the geometrical constraints of the laboratory model are discussed below.

GEOMETRICAL BOUNDARY CONDITIONS AND LOADING ANALYSIS

For the analytical model to represent the physical model in all respects, it was necessary to impose some restrictions on the loading intensities and on the boundary conditions of the analytical model. These constraints may contradict some of the information provided by the global analyses shown in figures 14 through 16, but they will not cause significant changes in the critical regions. For example, it would be impossible to construct a full-scale physical model and maintain the displacements at the

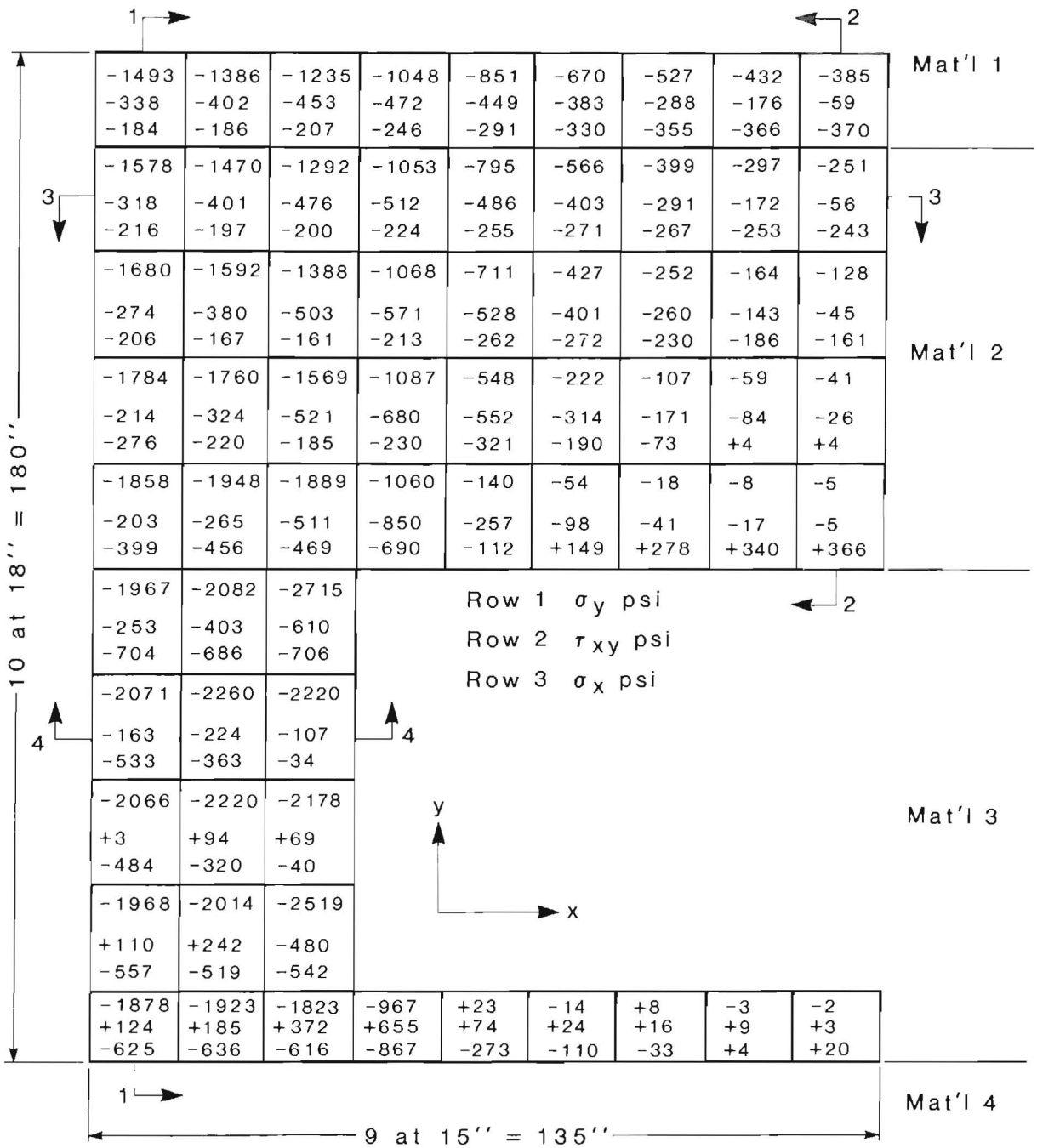

Figure 14.–Analytical stress distributions around mine opening caused by global loading, using ASOLID code. Source, figure 13.

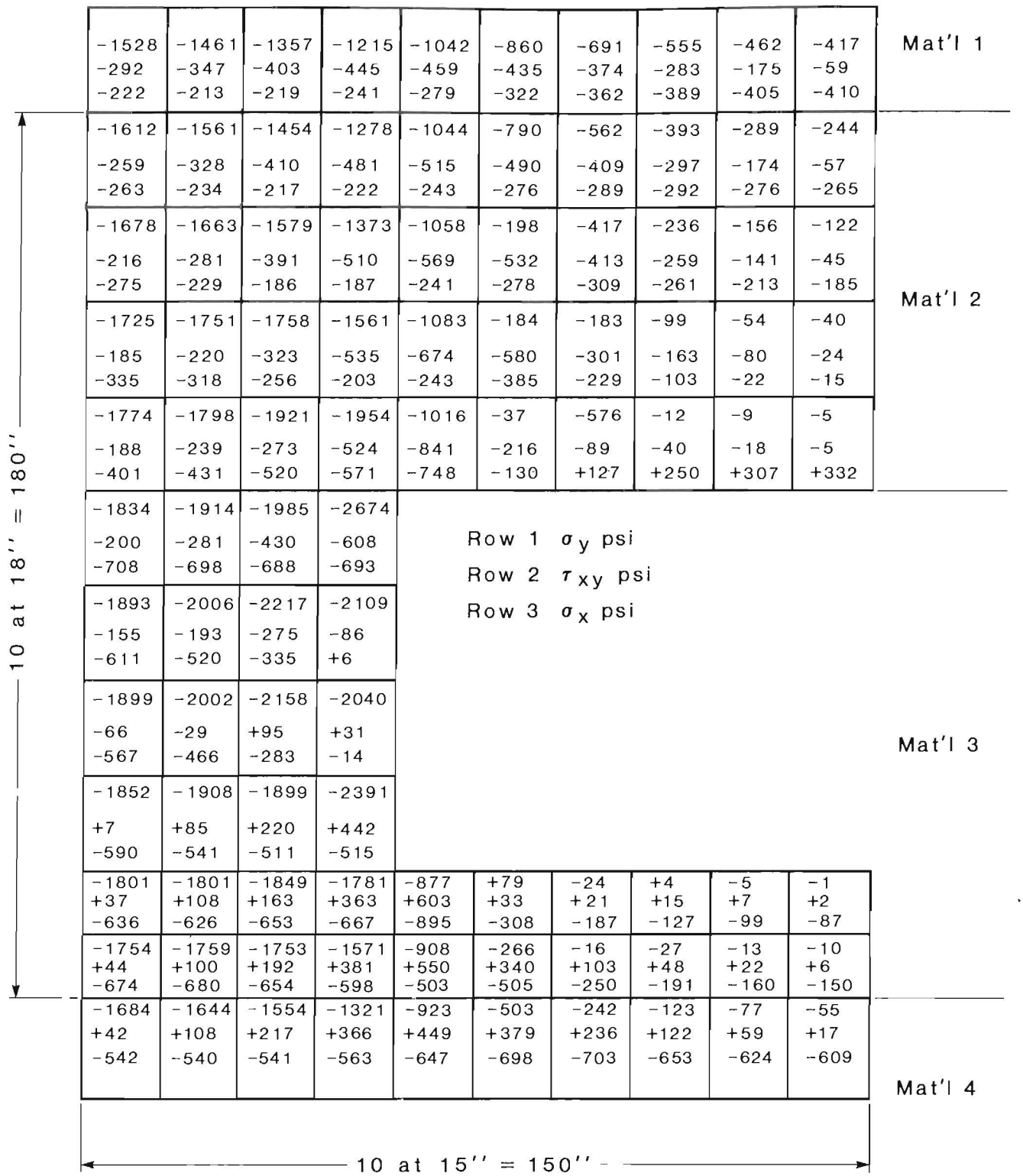

-1528 -292 -222	-1461 -347 -213	-1357 -403 -219	-1215 -445 -241	-1042 -459 -279	-860 -435 -322	-691 -374 -362	-555 -283 -389	-462 -175 -405	-417 -59 -410
-1612 -259 -263	-1561 -328 -234	-1454 -410 -217	-1278 -481 -222	-1044 -515 -243	-790 -490 -276	-562 -409 -289	-393 -297 -292	-289 -174 -276	-244 -57 -265
-1678 -216 -275	-1663 -281 -229	-1579 -391 -186	-1373 -510 -187	-1058 -569 -241	-198 -532 -278	-417 -413 -309	-236 -259 -261	-156 -141 -213	-122 -45 -185
-1725 -185 -335	-1751 -220 -318	-1758 -323 -256	-1561 -535 -203	-1083 -674 -243	-184 -580 -385	-183 -301 -229	-99 -163 -103	-54 -80 -22	-40 -24 -15
-1774 -188 -401	-1798 -239 -431	-1921 -273 -520	-1954 -524 -571	-1016 -841 -748	-37 -216 -130	-576 -89 +127	-12 -40 +250	-9 -18 +307	-5 -5 +332
-1834 -200 -708	-1914 -281 -698	-1985 -430 -688	-2674 -608 -693						
-1893 -155 -611	-2006 -193 -520	-2217 -275 -335	-2109 -86 +6						
-1899 -66 -567	-2002 -29 -466	-2158 +95 -283	-2040 +31 -14						
-1852 +7 -590	-1908 +85 -541	-1899 +220 -511	-2391 +442 -515						
-1801 +37 -636	-1801 +108 -626	-1849 +163 -653	-1781 +363 -667	-877 +603 -895	+79 +33 -308	-24 +21 -187	+4 +15 -127	-5 +7 -99	-1 +2 -87
-1754 +44 -674	-1759 +100 -680	-1753 +192 -654	-1571 +381 -598	-908 +550 -503	-266 +340 -505	-16 +103 -250	-27 +48 -191	-13 +22 -160	-10 +6 -150
-1684 +42 -542	-1644 +108 -540	-1554 +217 -541	-1321 +366 -563	-923 +449 -647	-503 +379 -698	-242 +236 -703	-123 +122 -653	-77 +59 -624	-55 +17 -609

Figure 15.–Analytical stress distributions around mine opening caused by global loading, using BMINES code. Source, figure 13.

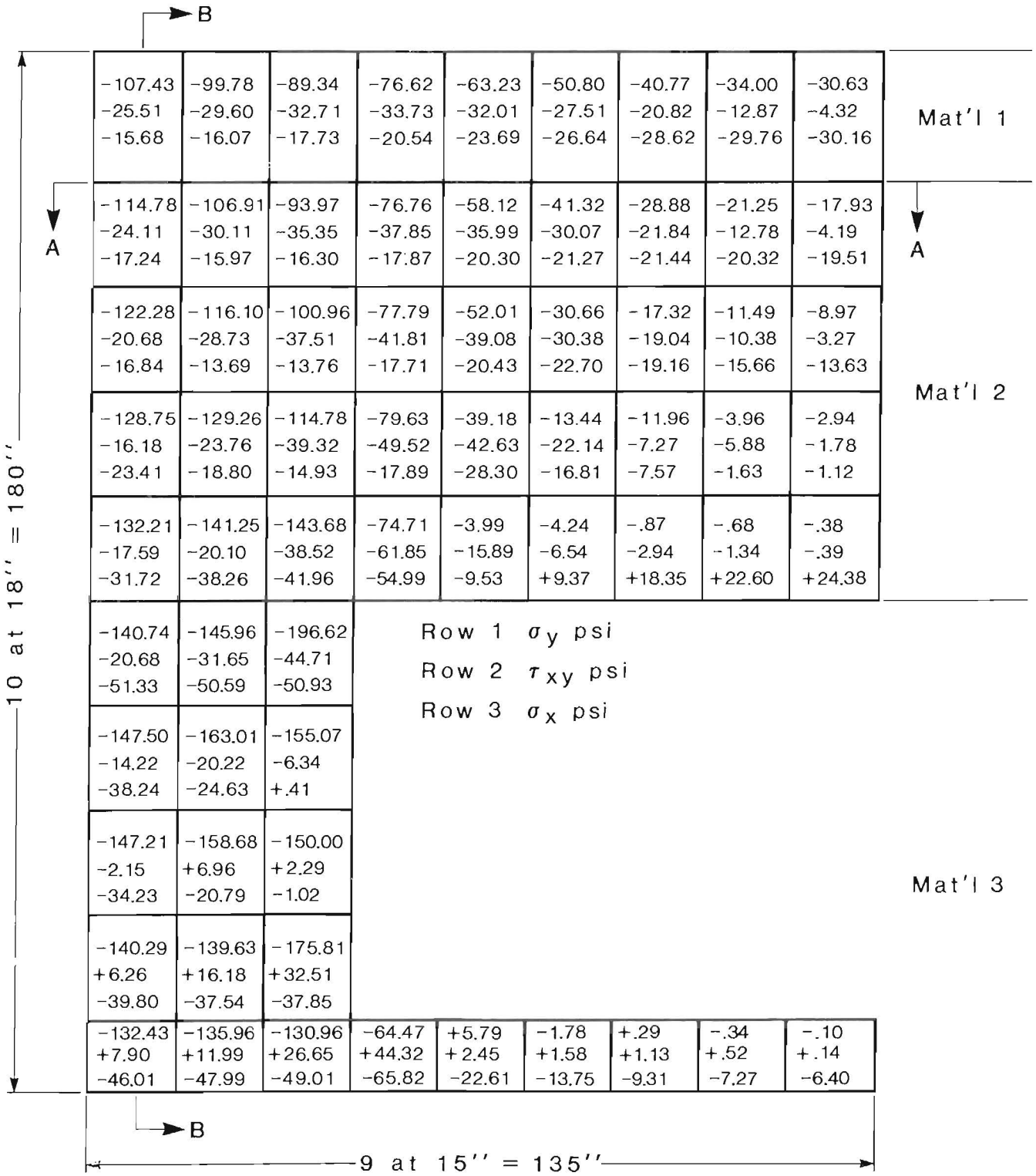

Figure 16.–Analytical stress distributions around mine opening caused by global loading, corrected for 100-ft depth.

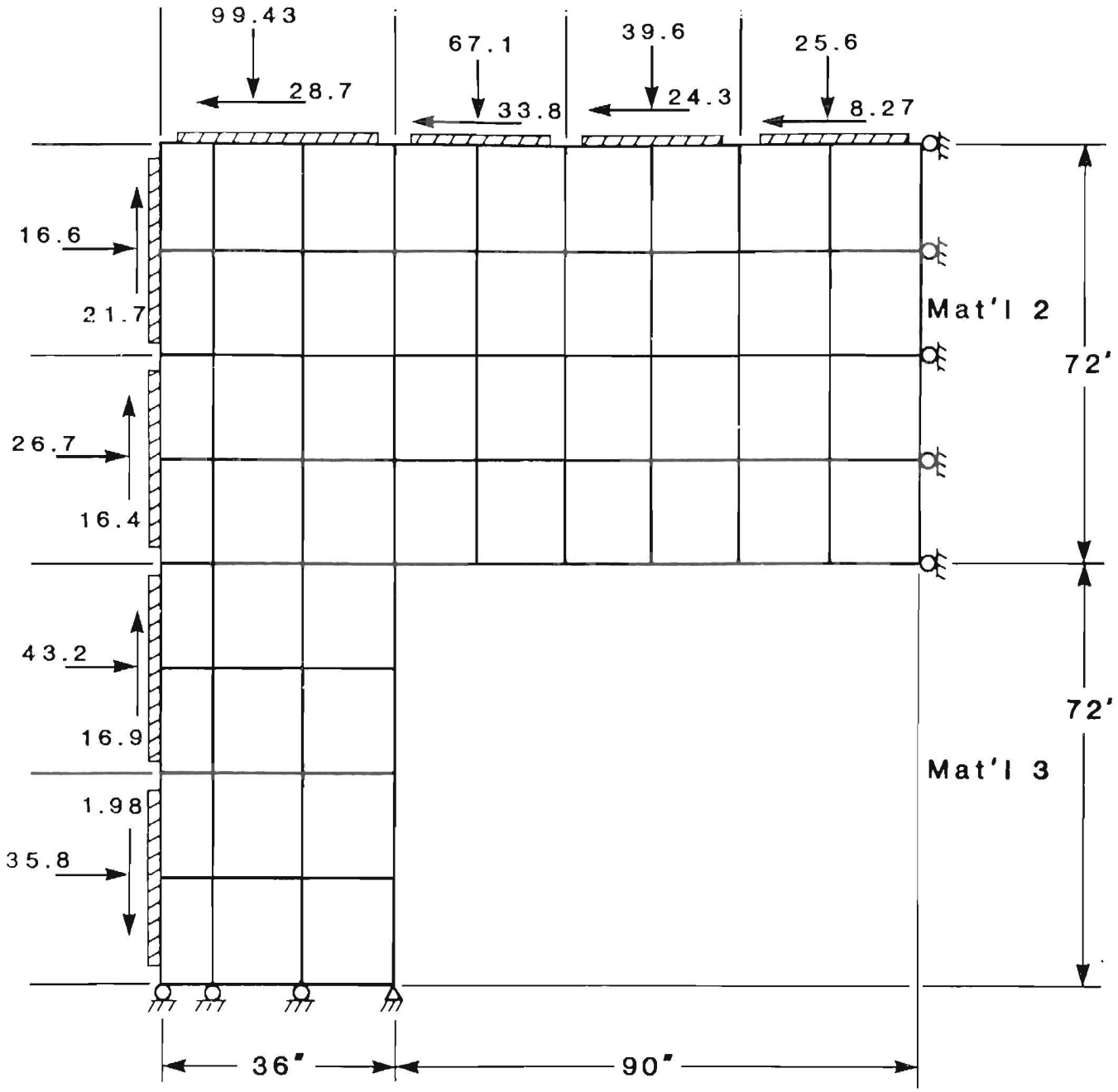

Figure 17.–Load intensities on boundary of physical model. All values in pounds per square inch.

bottom of the pillars or at the center of the span, as is done in the global analysis. However, if roof displacements relative to pillar displacements are examined, the analytical and physical models should give comparable results, provided the boundaries of the analytical model are loaded with the stress distributions given in figure 16. This result is verified in figure 18, where stresses applied on the boundary of the physical model after correction for dead load were subtracted from figure 16 and applied to the analytical model as nodal point loads. The resulting stresses, along with the boundary constraints, which represent the behavior of the physical model, are also shown in figure 18. Despite the fact that all boundary requirements of an actual mine cannot be satisfied in the laboratory (for example, it was assumed that $\delta y = 0$ along the pillar base and $\delta x = 0$ at the innermost point of the pillar, assumptions that violate field or stress conditions in the real world), the results in figure 18 compare favorably with those shown in figure 16, which were derived from a global analysis. In the global analysis, no boundary constraints were imposed around the immediate boundary. However, the physical model boundary constraints around the mine opening shown in figures 17 through 19 did not significantly affect the stress distributions in the regions of interest, for example, bottom midspan and span-pillar interaction regions. This justifies calculations of the boundary restraints of the model.

The boundary loads shown in figure 18 consist of normal and shear loads. An examination of the ratios of shear forces to normal forces at the boundaries shows that they ranged from 0.4 to 1.4 on the load pads. This means that a coefficient of friction as high as 1.4 would be needed to prevent the pad(s) from slipping because of high shear forces. Achieving such a frictional resistance is impractical. A literature survey revealed that the coefficient of friction of steel on concrete ranges from 0.2 to 0.4, and it was decided to limit the coefficient of friction to 0.4. This changed the applied state of stress on the boundaries of the structure, causing a different stress distribution in the model. To avoid any significant changes in the critical regions, namely in the interaction between the pillars and the span under shear stresses and in the center of the span under bending stresses, many trial loads were evaluated using a computer. The best choice of load application is illustrated in figure 19, which shows that the bending tensile stresses in the bottom region of the span and the shear stresses around the region of the pillar-span interface compare satisfactorily with the corresponding data in figure 18.

MODEL MATERIALS

The material properties used in the analytical model were those of the global analysis (figs. 13-14). The physical model was intended to incorporate the properties of coal shales. Extensive testing of samples from various regions of the country has shown that the approximate compressive strength of coal shale is 5,000 psi. However, the compressive strength of the concrete used in the physical model measured between 5,500 and 6,500 psi. Therefore, for analytical equations requiring data on material properties, a compressive strength of 6,250 psi was assumed for the concrete in the physical model. Using code 8.3.1 of the American Concrete Institute, the modulus of elasticity of concrete is

$$E_c = 57{,}000 \sqrt{f_c'}, \qquad (1)$$

where f_c' = compressive strength of the concrete, psi.[5]

Therefore,

$$E_c = 57{,}000 \sqrt{6{,}250} = 4.5 \times 10^6 \text{ psi}, \qquad (2)$$

where $\upsilon = 0.15$.[6]

Using this value for E_c and the loads on the boundaries shown in figure 19, the stress distribution around the model mine opening was calculated and is depicted in a finer mesh pattern in figure 20.

SLIP ELEMENT MODELS

The analytical modeling discussed so far represents the geometry and loading of a mine opening constructed in a continuous, unbedded medium. However, the mine model tested in the laboratory is not in a monolithic and continuous medium. To simulate the bedded structure found in coal mines, the model mine roof was constructed of six concrete layers separated with polyethylene sheeting and resting on two concrete pillars. Slab interfaces present difficulties in finite-element analysis both in a model and around coal mine openings. However, these interfaces can be modeled with joint elements. This requires that interface material models be formulated as part of the computer modeling analysis. The interface material models in codes such as BMINES and ANSYS accommodate options for two- and/or three-dimensional joint elements. These elements are intended to represent various types of interfaces, including joints, faults, bedding planes, and in general, any planes or axisymmetric surfaces that may maintain or break physical contact and that may slide relative to one another.

BMINES CODE

The joint element described by Goodman and Dubois[7] is nonlinear and requires an iterative solution with the stiffness matrix formulated after each iteration. For the purpose of mathematical modeling, the joint material is

[5]Wang, C. K. and C. G. Salmon. Reinforced Concrete Design. Harper and Row, 4th ed., 1985, 15 pp.

[6]These values for E_c and υ were also verified by laboratory triaxial tests.

[7]Goodman, R. E., and J. Dubois. Duplication of Dilatancy in Analysis of Jointed Rocks. J. Soil Mech. and Found. Div., ASCE, v. 98, No. SM4, Apr. 1972, pp. 399-422.

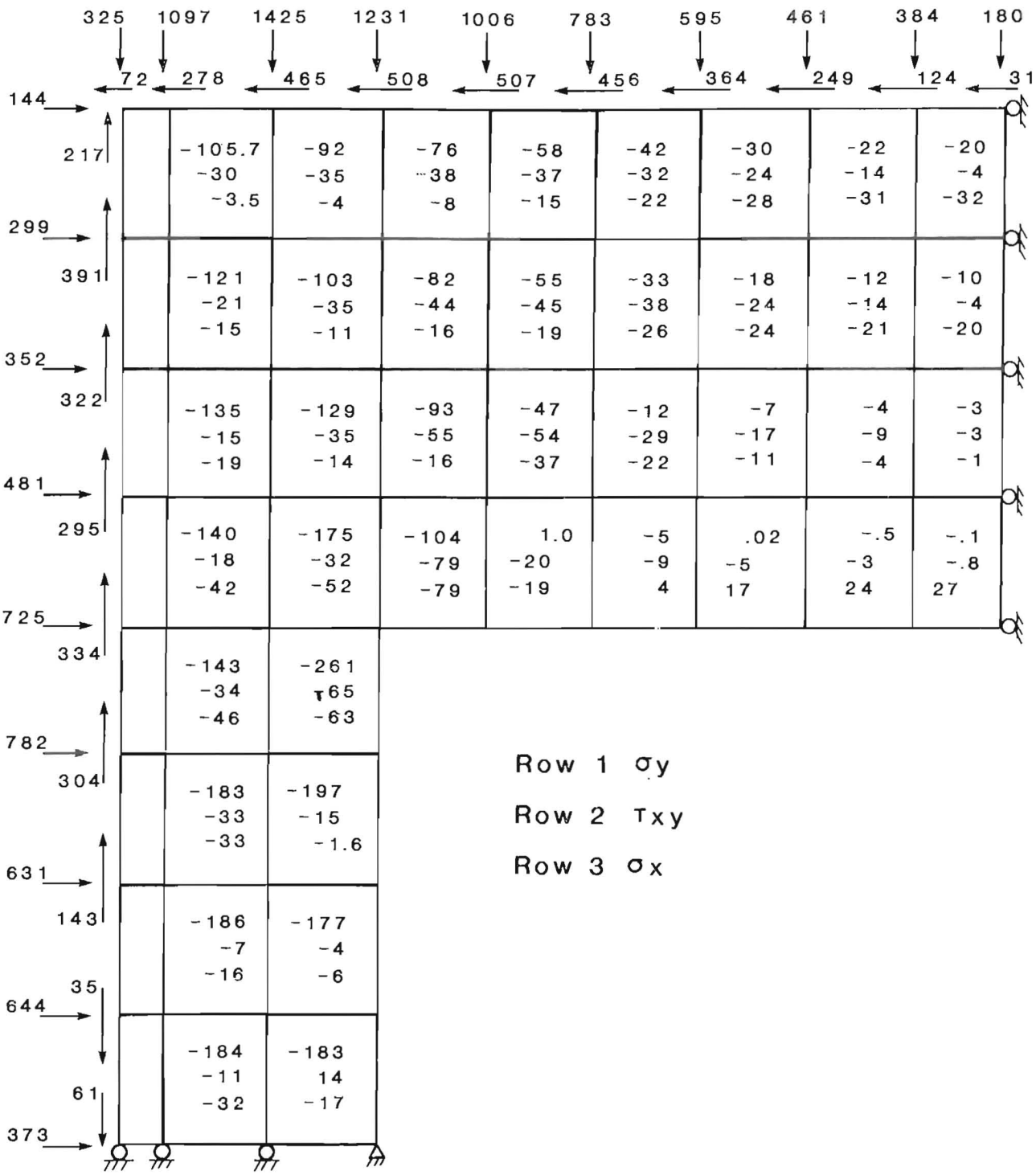

Figure 18.–Nodal load intensities and resulting normal stress distributions in physical model. All values in pounds per square inch. Source, figure 17.

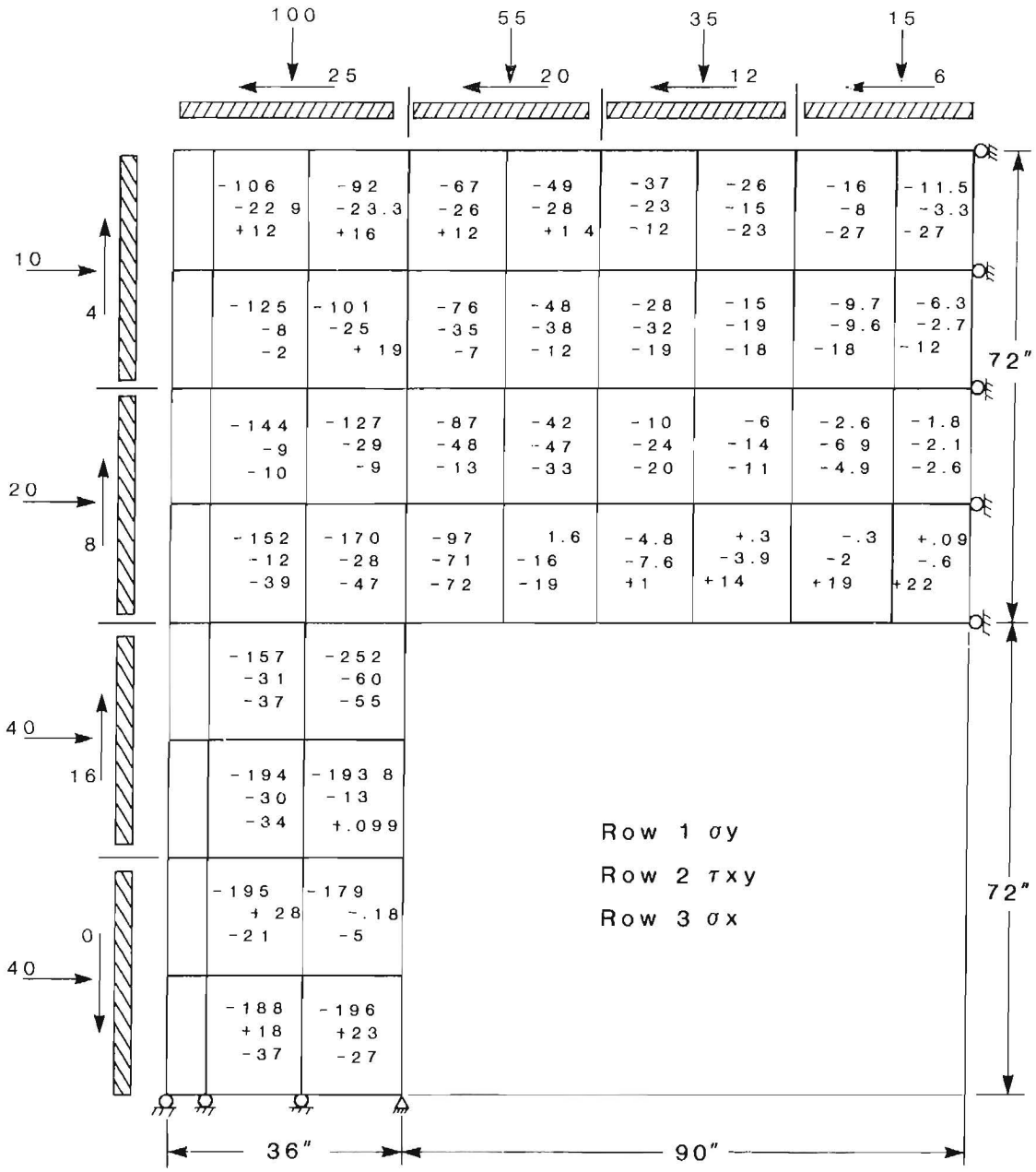

Figure 19.–Modified pad-load intensities applied on boundary of physical model and resulting stress distributions. All values in pounds per square inch.

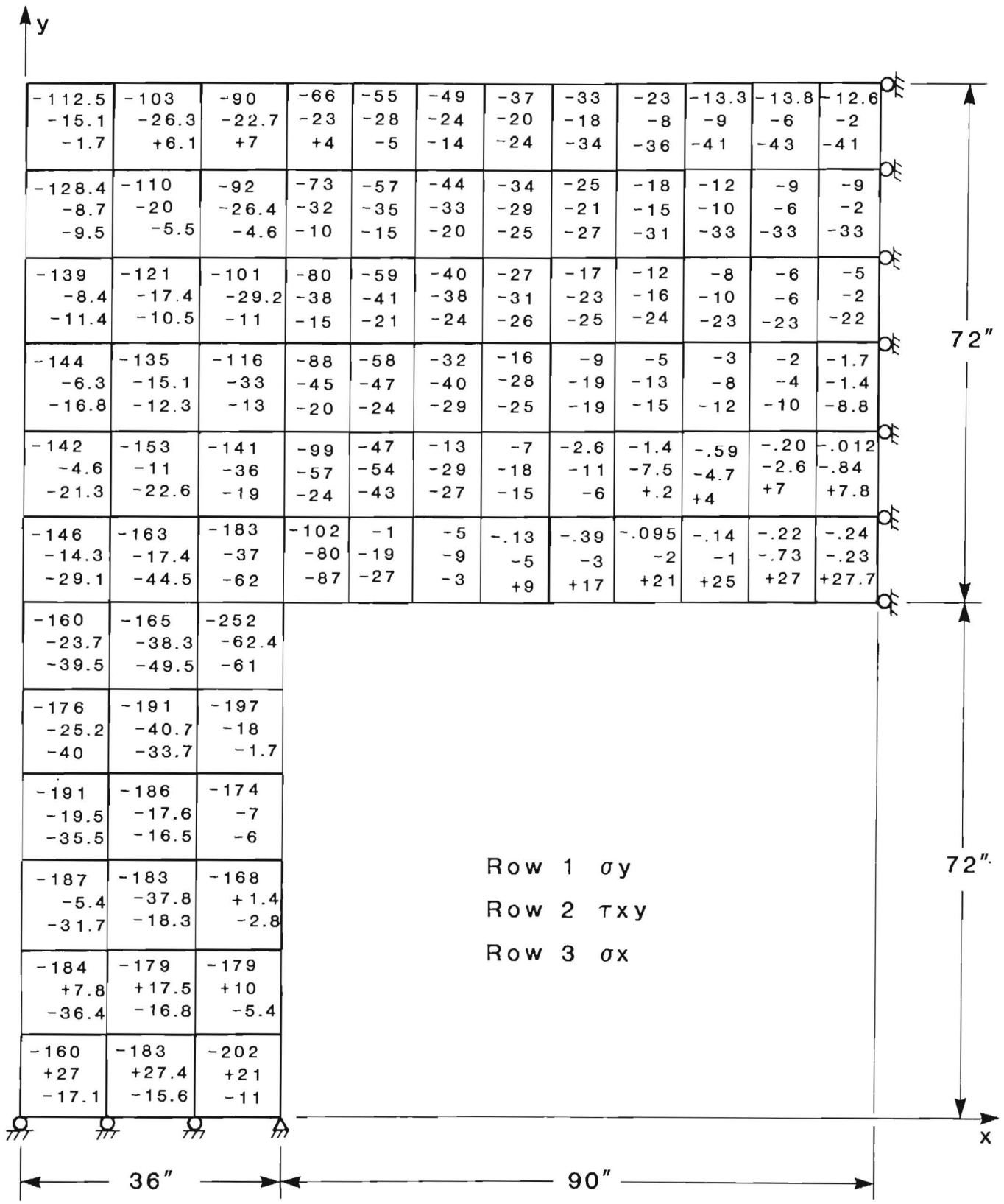

Figure 20.–Stress distribution in physical model using actual material properties and applied loads shown in figure 19. All values in pounds per square inch.

assumed to have a finite thickness and a finite volume, although both may be quite small compared with adjacent material elements. Using this thickness along with the dimensions of the joint, it is possible to define the element. The deformation across the interface distorts the region, making it possible to define joint element strains in a manner completely analogous to that of computing strains in a continuum element.

The mechanical response of a joint element, as in the case of a continuum element, consists of elastic and plastic components. Plastic strains in the directions normal to, and along, the plane of the joint are referred to as "dilatation" and "slip," respectively. The element is capable of supporting only compression in the direction transverse (normal) to the surfaces and only shear along (tangential to) the surfaces. Consequently, normal and shear stiffnesses (K_n and K_s) of the joint must be known. These stiffness values, in general, vary from situation to situation and are often controversial. The values used in this analysis were based on laboratory tests performed on concrete blocks at SRC in the manner outlined by Goodman and Dubois.[8] These results are discussed briefly in the following section.

Shear Stiffness Coefficient

The shear strength parameters required by the BMINES code are peak shear strength, τ_p, and residual shear strength, τ_r. These quantities are functions of normal stress and are qualitatively sketched in figure 21*A*. Two slab blocks or disks separated by a joint are subjected to a constant normal stress while a gradually increasing unidirectional shear stress is applied. The displacement results in the corresponding shear strain, which determines $G(K_s)$, the elastic shear modulus of the joint. During this loading, all the shear elastic strain is recoverable and no slip occurs until the peak shear strength, τ_p, is reached. At this point, finite slip begins, causing some damage to the asperities and reducing the shear strength until it levels off at the residual shear strength, τ_r. The transition from τ_p to τ_r takes place linearly with increasing plastic slip strain. The data accumulated from stiffness tests and the method of testing are discussed in appendix B. Average values for shear coefficients required by BMINES are presented in table B-4.

Normal Stiffness Coefficients

For the determination of normal stiffness, K_n, two blocks separated by a joint are subjected to constant, unidirectional shear stress while normal stress is gradually increased. This loading results in a bilinear curve of the type shown qualitatively in figure 21*B*. Here, E_1 represents the modulus for fully bonded behavior while E_2 applies to the debonding transition zone marked at the normal stress level, σ_1. A tensile strength up to σ_c can be held by the joint if the joint is still intact. If either debonding or prior slip have occurred, the tensile strength of the joint, σ_c, is considered zero (fig. 21*C*). The stress-strain behavior of the polyethylene-separated joint, given by various tests, is also presented in appendix B. Based on these tests, average values for E_1, E_2, σ_1, and σ_c (table B-4) are 413,000, 33,000, 57.8, and 0 psi, respectively. A qualitative plot of this phenomenon is shown in figure 21*C*.

[8]Work cited in footnote 7.

ANSYS Code

The interface slip element provided in ANSYS is simple compared with that in BMINES and requires very few parameters. The sliding of the two surfaces is based on Coulomb friction. The element may be initially preloaded in the normal direction or it may be given a gap specification, δ (fig. 22*A*). Angle Θ in figure 22*A* defines the interface plane, which, for the horizontal slab, is zero. A specified stiffness acts in the normal and tangential directions when the gap is closed and not sliding. The value of normal stiffness, K_n (fig. 22*B*), is to be entered as the stiffness of the surface materials of the contact. The only other material property required is the interface coefficient of friction, μ, for the polyethylene sheet. In a normal direction, when the normal force, F_n, is negative, the interface remains in contact and responds as a linear spring. A positive normal force indicates debonding. In the tangential direction, for normal force $F_n < 0$ and tangential force $F_s > \mu |F_n|$, the interface does not slide and responds as a linear spring in the tangential direction. When $F_n < 0$ and $F_s > \mu |F_n|$, sliding occurs, and shear stiffness, K_s, degenerates to virtually a zero slope (indicated by the dashed line in figure 22*C*). For a detailed description of the interface, the reader is referred to the ANSYS manual.[9]

FINITE-ELEMENT MODEL MESH

In order to form a more accurate picture of the variation of stresses and displacements in the physical model (fig. 2), a more refined mesh was used (fig. 23). The element sizes over the span length and in the neighborhood of the span-pillar region were made small enough (6 by 3 in) to interpolate the stresses and/or displacements without significant errors. Toward the base of the pillars, the size of the elements was 6 by 6 in. The selection of proper element sizes, not only over span length but also through the thickness of each slab, is the key to obtaining the true stress distribution over each slab. If recording instruments are installed in the desired locations, comparisons can be made between observed quantities.

[9]Swanson Analysis Systems, Inc. (Houston, PA). ANSYS–Engineering Analysis System, Volumes I and II. Feb. 1982, 500 pp.

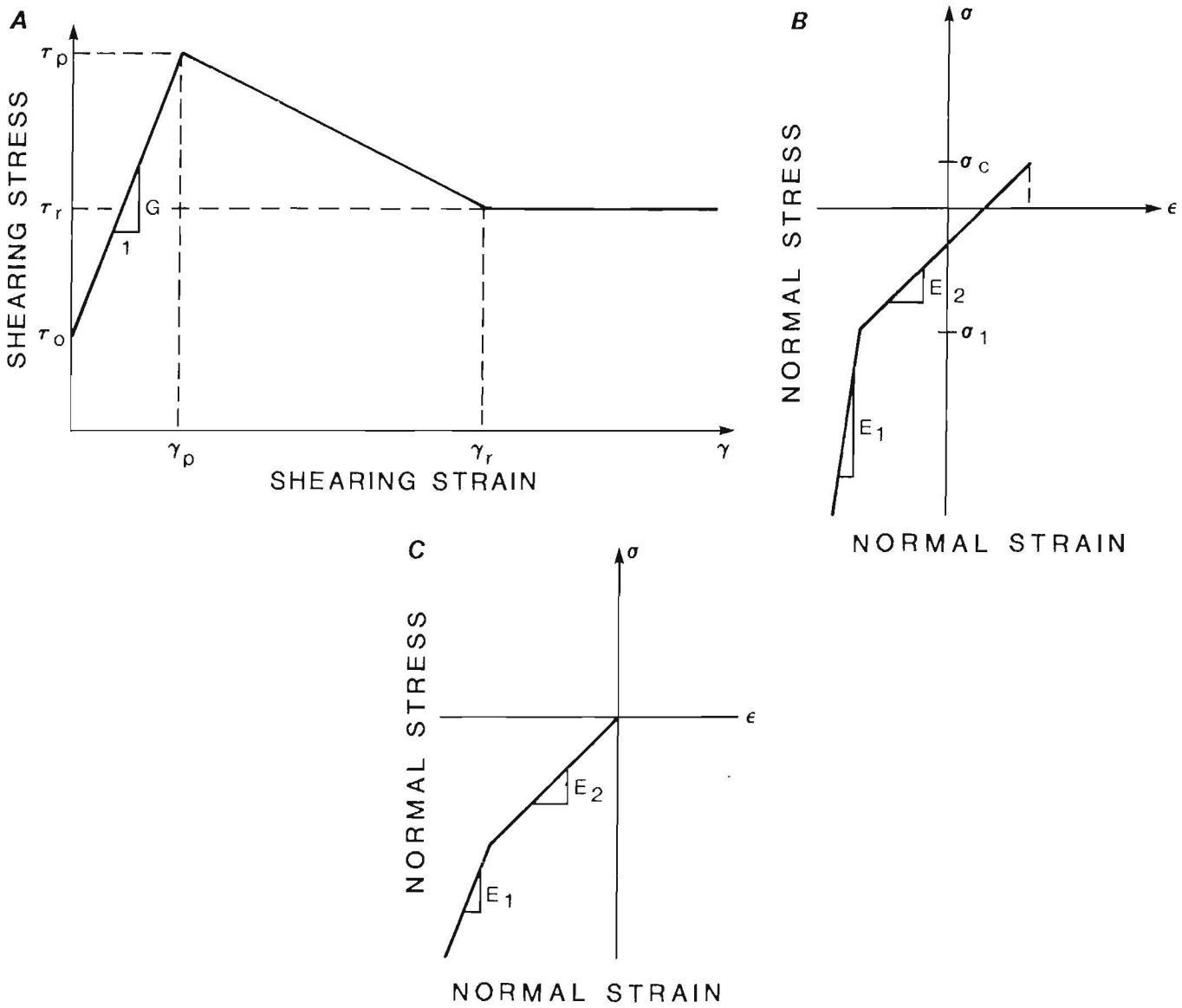

Figure 21.–Qualitative load deformation behavior of joint used in BMINES. *A*, Shear stiffness coefficients; *B*, normal stiffness coefficients for intact media; *C*, normal stiffness coefficients with zero tensile strengths.

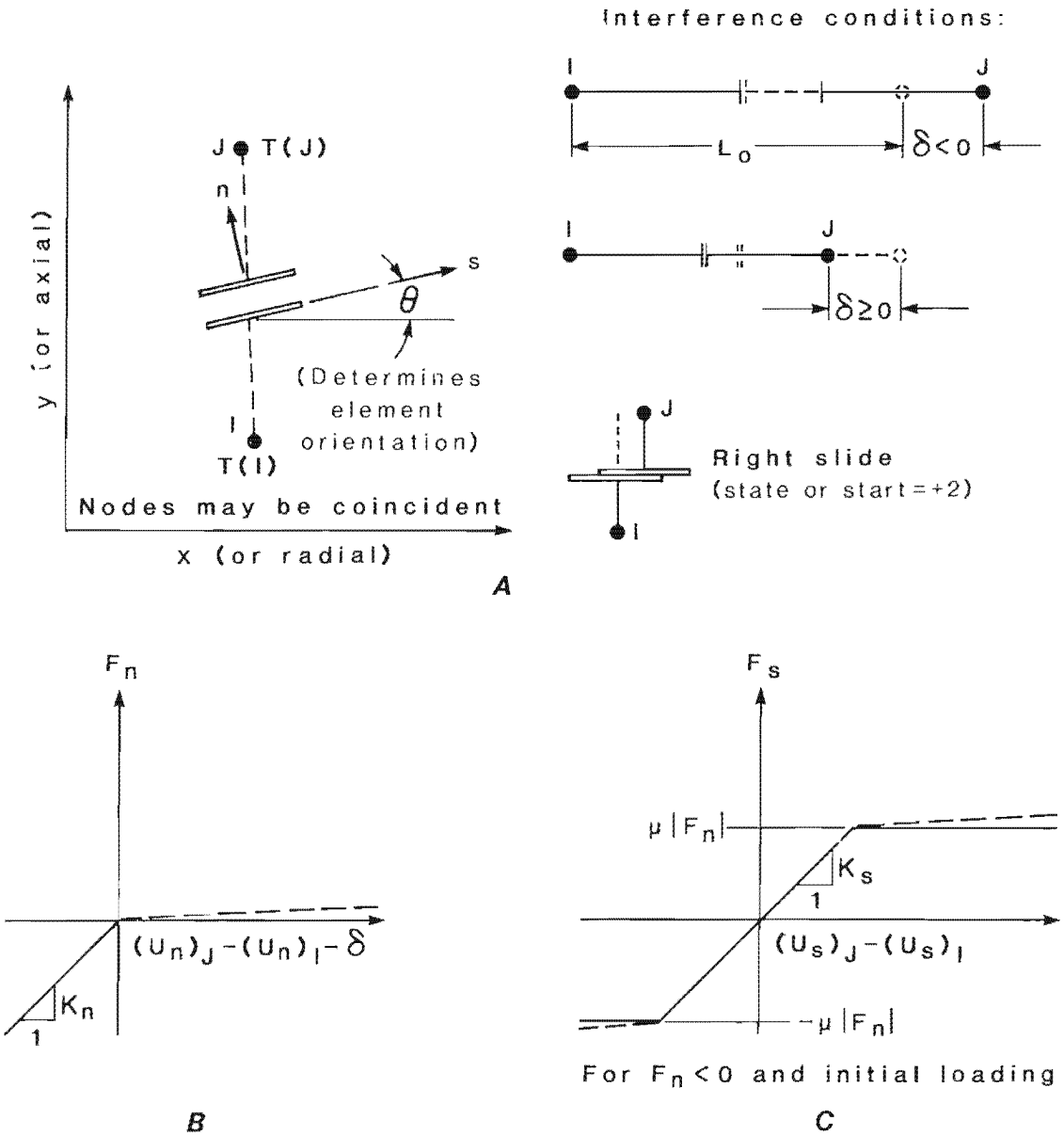

Figure 22.–Qualitative load deformation behavior of joint used in ANSYS. *A*, Gap element with parameters; *B*, normal stiffness coefficient; *C*, shear stiffness coefficient.

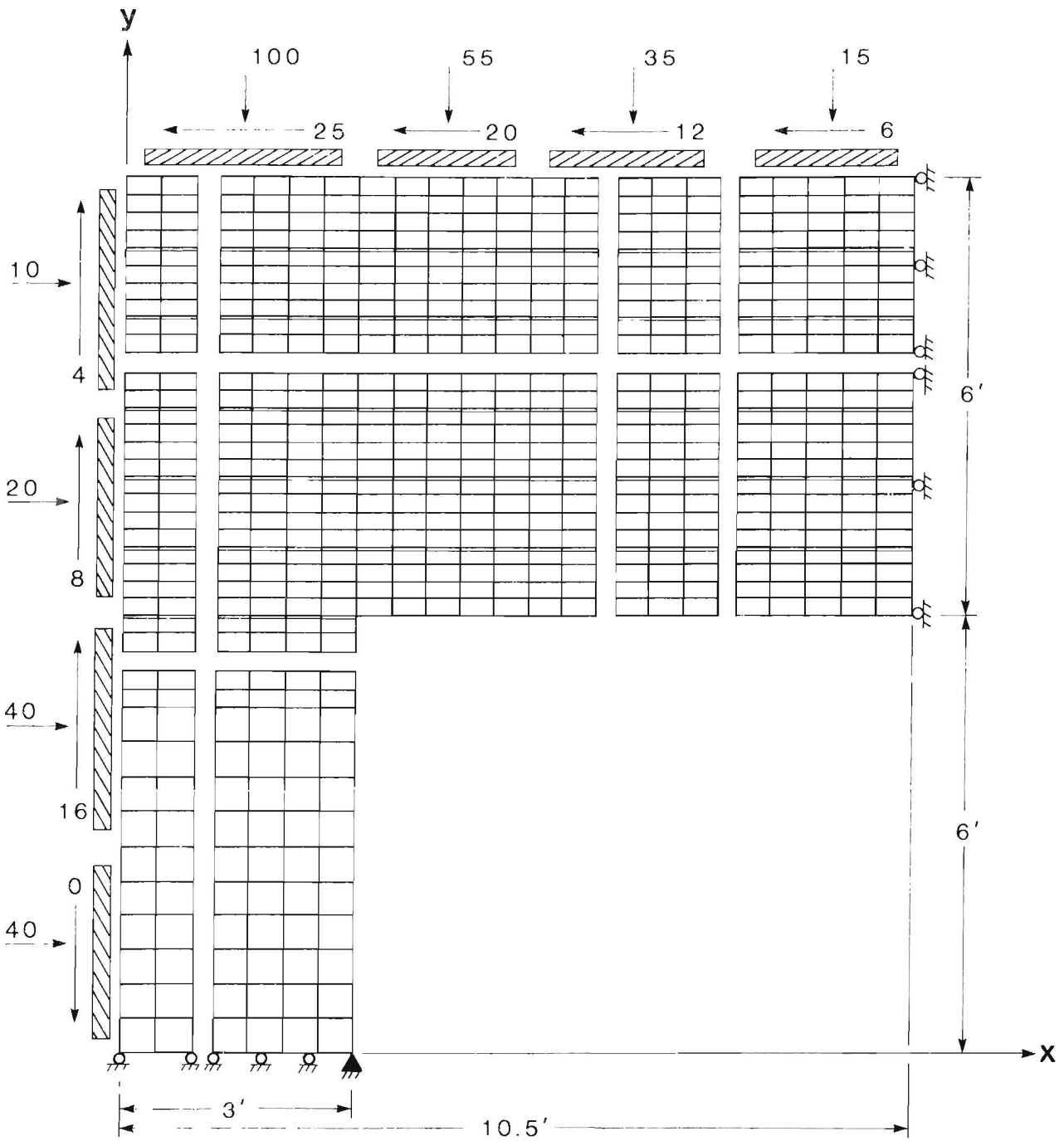

Figure 23.–Physical model with refined mesh size and slip planes. All values in pounds per square inch.

PHYSICAL AND COMPUTER MODEL RESULTS

UNBOLTED, DEAD-LOAD RESULTS

A comparison of predicted and observed values for dead-load conditions establishes the validity of the analytical model with greater confidence than would using any other loading condition. This is because the dead-load condition is less susceptible to experimental errors that may be inherent in externally induced loads (live loads). The results of static analyses on the layered model for dead-load and dead- and live-load conditions are presented in appendix C.

Because of the nonlinear nature of the interfaces between slabs, the experimental and analytical models must be loaded or unloaded in small increments. Accordingly, the support system of the open span in the physical model was released gradually in 10 load increments until full dead-load conditions were reached. A theoretical analysis of dead-load conditions using an equal number of increments was also performed. The dead-load experiment was repeated three times. The average values of observed deflections of some of the points along the lower edge of the span, together with those predicted for the unlayered solid and layered computer models, are shown in table 1.

Although deflection in the midsection of a layered structure is many times greater than that for an unlayered solid structure, this situation should not be considered unusual. Even with the same geometry and under identical loading conditions, the relative stiffness values, the number of bedding planes, and the pillar widths will all influence the results. Results show that the data from the layered analytical models, except for those points at the outer rib edge, compare favorably with the data from the physical model. Complete profiles of the deflection curves of slab 1 (top slab) and slab 6 (bottom slab) are given in figure 24. The two experimental curves are plotted in figure 24 and pertain to the opposite edges of the physical model. Despite some slight deviation between the two experimental curves, there is very good agreement on deflections across the roof span between the analytical and the experimental results.

It should be noted that both the BMINES and ANSYS codes give essentially identical responses despite different interpretations and definitions of joint material models in each code. The small discrepancies between the predicted and the measured values at the outer edges of the model can be attributed partly to the insensitivity of the deformation gauges at very low values and partly to the curling effect of the slabs at the corners. As expected, this deviation at the corners appears to be less pronounced in the lower slabs than in the top slab.

The experimental longitudinal strains caused by dead loads in slabs 2, 5, and 6 are plotted in figure 25 along with the corresponding predicted values. As in the case of the deflections, BMINES and ANSYS codes give nearly identical predictions for the longitudinal strains. Comparison of the predicted strains with observed values shows that, for a major portion of the model, the agreement is very good. The close agreement between the two codes could be attributed to small deflections in situations where nonlinear joints under BMINES behave similarly to linear joints under ANSYS.

Some of the observed strain values that seem to deviate significantly from the predicted quantities are thought to be of questionable accuracy. For example, in figure 25*B*, the observed strains measured at the top and bottom of slab 5 near its midsection are -12.7×10^{-6} in/in and $+7.5 \times 10^{-6}$ in/in, respectively. The value of $+7.5 \times 10^{-6}$ in/in is incorrect because (1) the strain value at the identical location on slab 2 (fig. 25*A*) reads $+9.3 \times 10^{-6}$ in/in; however, the strain value in slab 5 (fig. 25*B*), because of its position relative to slab 2, must necessarily be greater than that registered on slab 2 at a corresponding location, and (2) geometrical and load symmetries require that the midsection of the structure be experiencing pure bending, and this is confirmed by the predicted values. If the strain reading of the bottom gauge in slab 5 at midsection is assumed to be approximately 12.7×10^{-6} in/in rather than 7.5×10^{-6} in/in, the comparison between the predicted and the observed values is excellent. The sensitivity of the gauges at low readings must be carefully determined before their accuracy is accepted.

Table 1.–Comparison of vertical deflections at various points along bottom of slab 6 (y = 72 in) for unbolted, dead-load conditions, inches

(Plus sign refers to tensile and minus sign to compressive stresses)

Position[1]	x, in	Analytical			Experimental
		Layered		Unlayered solid[2]	
		BMINES	ANSYS		
Outer rib edge	0	+0.00266	+0.00290	-0.00310	-0.0002
Inner rib edge	36	-.00138	-.00143	-.00054	-.0020
Midspan	126	-.01210	-.01230	-.00144	-.0125

[1]See figure 20 for x and y coordinates.
[2]BMINES.

In slab 6 (fig. 25*C*), readings of top gauges (compressive strains) at and near the midsection of the structure appear to be inaccurate. The top gauge reading is -10×10^{-6} in/in at the midsection of the model and the corresponding bottom gauge reading (tensile strain) is $+15 \times 10^{-6}$ in/in. If these magnitudes are compared with the corresponding top gauge readings in slab 5 (-12.7×10^{-6} in/in) (fig. 25*B*), one must conclude that compressive strain in slab 6 should be greater than -12.7×10^{-6} in/in. Also, recognizing that pure bending will dominate in the neighborhood of the midsection, more valid midsection gauge readings would be around -15×10^{-6} in/in rather than -10×10^{-6} in/in. These comments are equally applicable to observed readings on either side of the midsection. If observed values are compared with predicted values, it can be seen that the responses almost overlap each other and an excellent correlation can be established.

Each of the top five slabs, which are supported elastically by the neighboring slab, should bend about its own neutral axis. The shear forces (although small) along the top and bottom longitudinal surfaces of each of these slabs are approximately the same magnitude but act in opposing directions; thus, they induce negligible axial stress but nevertheless influence the pure bending stresses. Slab 6, however, is supported by the two pillars. The shear force developed along the interacting surface between slab 6 and the pillars does not entirely neutralize the shear force along the top surface of slab 6. This induces axial stresses in addition to bending stresses. Compared with the bending stresses in the middle of the span, these coupled stresses over the pillars reach significant levels. An examination of the strains in slabs 2 through 6 reveals a significant buildup of stresses in the portion of the slabs over the pillars. These stresses are at least of the same magnitude as the stresses in the midsection of the structure. At the midsection, stresses are predominantly of a bending nature; near the edges, they are coupled with axial stresses as well. As the distance from the pillar

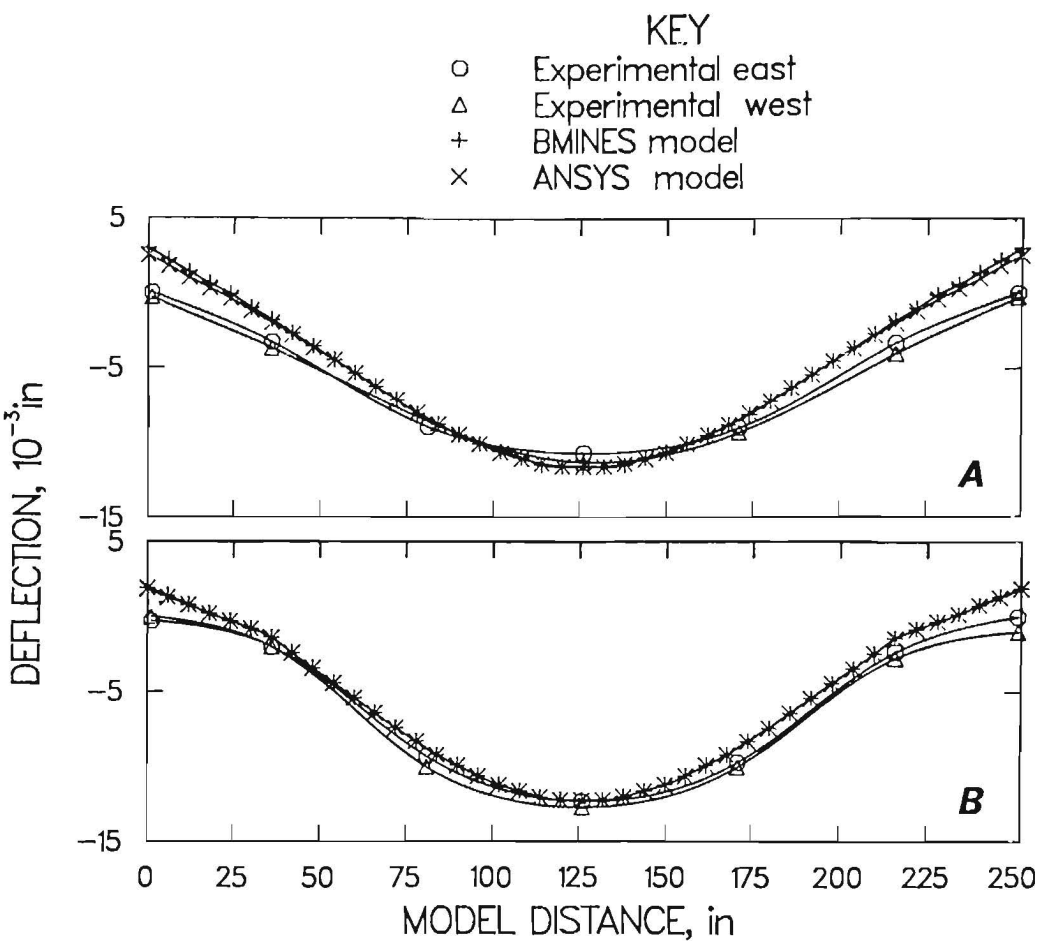

Figure 24.–Predicted and observed vertical deflection profiles under dead load without bolts. *A*, **Lower edge of slab 1;** *B*, **lower edge of slab 6.**

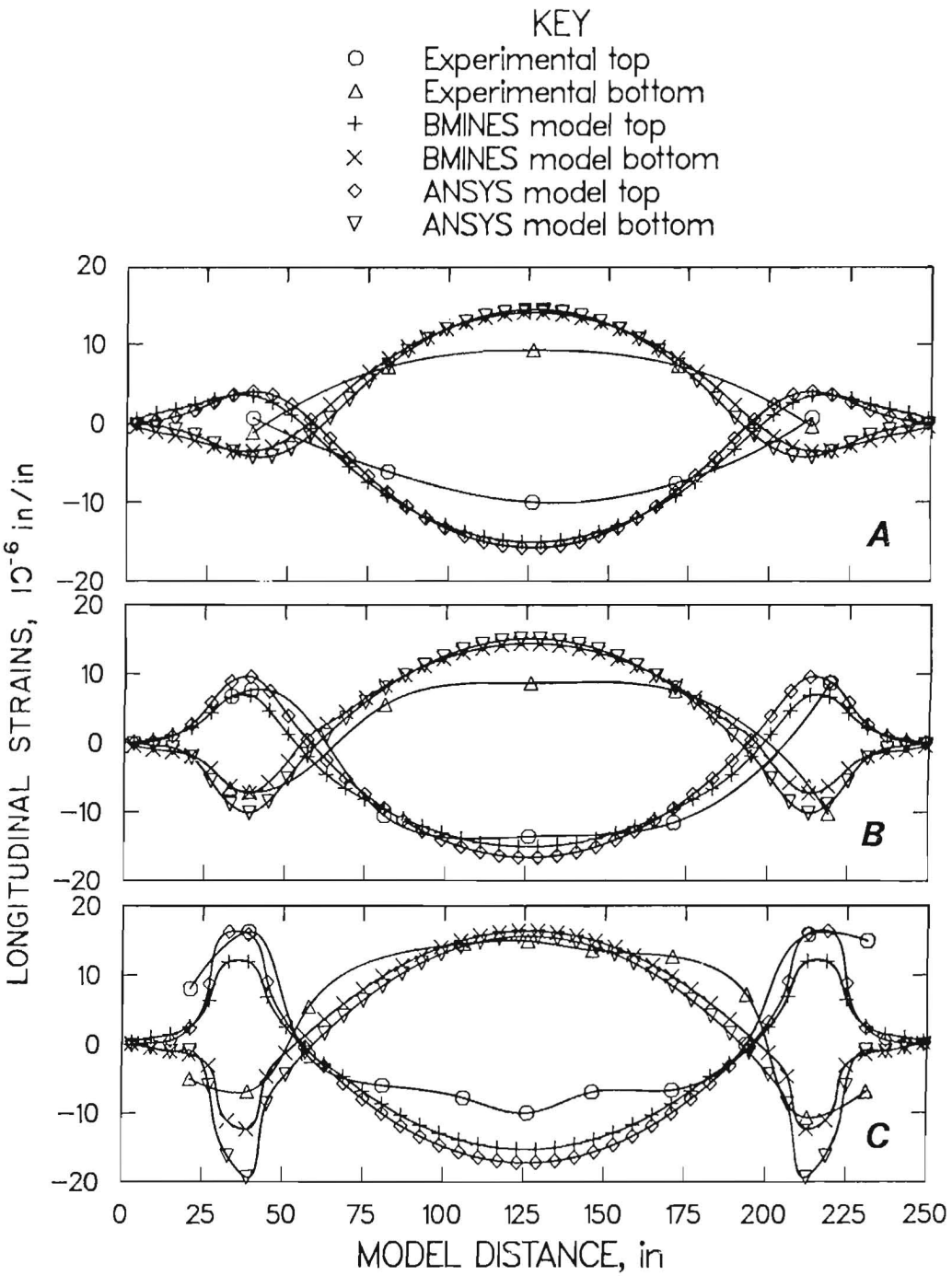

Figure 25.–Predicted and observed profiles of longitudinal strains under dead load without bolts. Measurements were taken 1-1/2 in from top and bottom edges of slabs as indicated in key. *A*, slab 2; *B*, slab 5; *C*, slab 6.

toward the midsection increases, the effect of axial stress decreases, and pure bending becomes predominant.

In deflection as well as strain analyses, the responses showed reasonably good agreement between the observed and the predicted quantities. The predictions of the BMINES and ANSYS codes were almost identical. All these comparisons were sufficiently favorable to confirm the validity of the analytical models for unbolted, dead-load cases.

UNBOLTED, LIVE-LOAD RESULTS

To avoid premature structural failure, it was prudent not to load the physical model to failure. The conditions for maximum live loading were (1) limit strains at critical sections (that is, midspan) to 50×10^{-6} in/in (in tension) and (2) limit maximum vertical deflection to 40×10^{-3} in. To be conservative, the live load was limited to 40 pct for the unbolted case and 40 to 70 pct for the bolted case, depending upon the type of bolt (fig. 19).

Live load was applied in small increments. Data were recorded for 20, 40, and 60 pct of the full live load as shown in figure 19. Deflection profiles of the lower edges of slabs 1 and 6 are plotted in figure 26, together with a number of observed values. The theoretical values given by BMINES and ANSYS appear identical to each other, but both tend to deviate from the experimental values, particularly in the pillar-span regions. In addition, the observed behavior is asymmetrical. This may suggest uneven deformation of the floor, to which deformation gauges are attached by a framework. Another possible cause of deviation at certain locations may have been inconsistency in the amount of actual pressure applied on the pads by the hydraulic system. Dead-load cases lack these sources of possible errors (fig. 24), and the experimental and the theoretical comparisons were excellent for dead-load conditions, thus validating the analytical model. Despite discrepancies, overall comparisons of deflection, strain, and stress appear to be satisfactory.

Figure 27 illustrates plots of strain variations across the model for slabs 2, 5, and 6 and shows that the theoretical values from BMINES and ANSYS compare very well with each other. The observed values, despite the lack of sufficient data (because of the failure of many of the embedded strain gauges), generally follow the predicted pattern. Any deviations from predicted values can be explained by the manner in which dead-load strain comparisons were analyzed. From these observations and analyses, it is reasonable to conclude that the stress distribution in a mine opening with horizontal beds can be predicted analytically with good results.

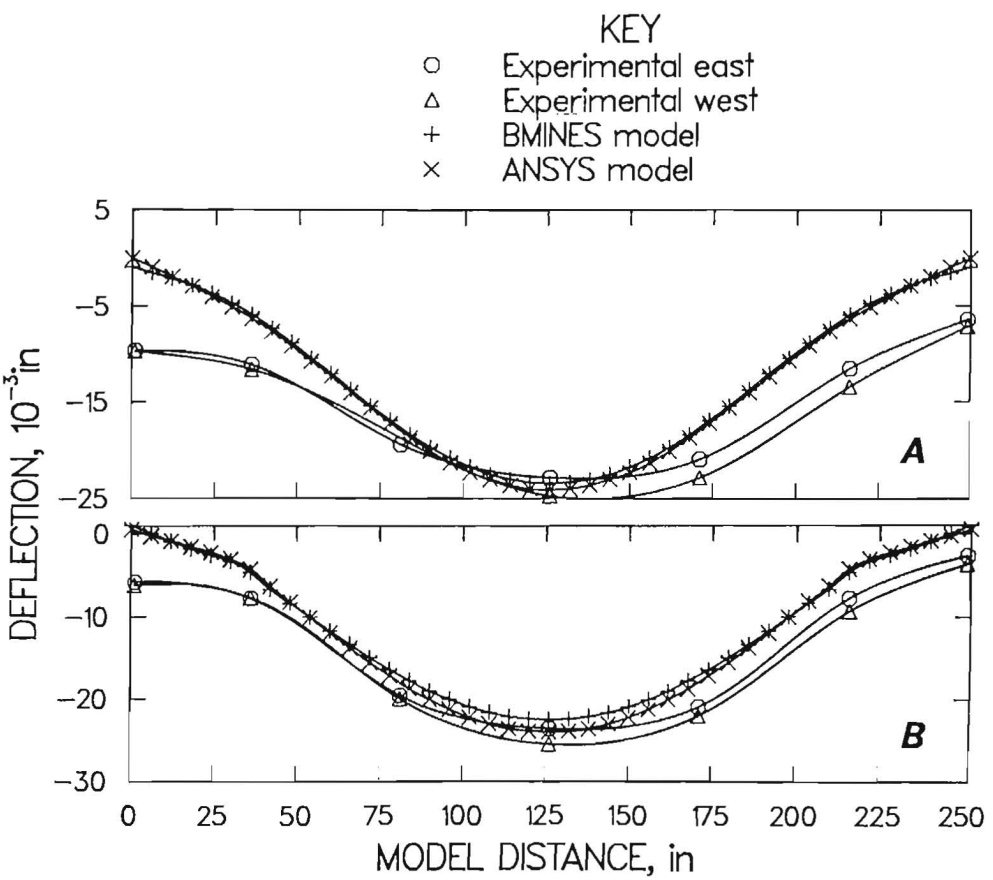

Figure 26.–Predicted and observed vertical deflection profiles under dead and 40-pct live loads without bolts. *A*, Lower edge of slab 1; *B*, lower edge of slab 6.

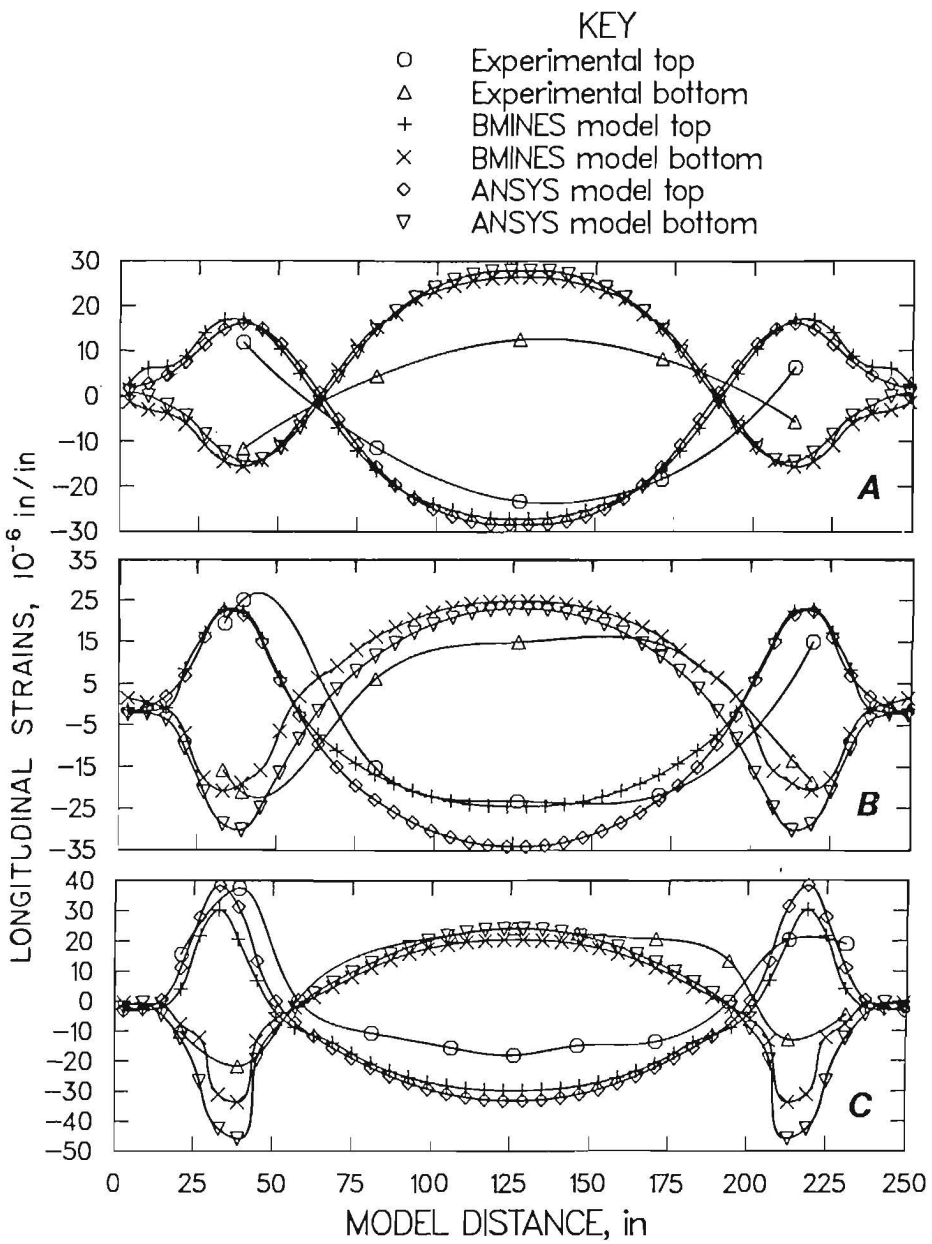

Figure 27.–Predicted and observed profiles of longitudinal strains under dead and 40-pct live loads without bolts. Measurements were taken 1-1/2 in from top and bottom edges as indicated in key. *A*, Slab 2; *B*, slab 5; *C*, slab 6.

ANALYSIS OF BOLTED ROOF

A second goal of this investigation was to analyze the performances of different types of roof bolt systems used to reinforce layered mine roofs. The degree of roof stability gained by the use of any roof bolt system will depend upon bolt type, as well as such factors as bolt spacing, bolt length, height of the immediate roof, and amount of pretensioning. Theoretically, roof bolts increase the strength of the surrounding medium either by compressing the bedded strata, by causing significant shear resistance between layers, or by introducing resistance to shearing along the length of a bolt. These phenomena result in redistribution of stresses, and the behavior of the immediate roof begins to resemble that of a single unit rather than that of a loosely jointed rock mass. Analytical modeling of roof bolts and comparisons of their performance with experimental data are discussed in the following sections. Both mechanically anchored and resin-grouted roof bolts with constant lengths and spacings are discussed.

MECHANICALLY ANCHORED BOLT SYSTEM

Mechanically anchored bolts are typically constructed of 3/4-in-diameter steel and equipped with expansion anchors. A bolt is inserted into a 1-3/4-in-diameter drill hole and, with a bearing plate against the collar of the hole, is torqued to activate the anchor until the desired tension is reached (fig. 11). In the physical model, bolts 5 ft long were anchored in slab 2 with the load-bearing plates placed along the lower edge of slab 6. A series of dead-load tests were conducted, after which 20-, 40-, and 60-pct live-load tests under various bolt tensions, ranging from 0 to 15 kips, were performed. A 4-ft rectangular bolt pattern was used for all test configurations (fig. 12). A mechanically anchored bolt, attached to the rock at two ends and free along its length, does not resist any shear along its length. It does narrow joint gaps by compressing the strata through tension applied to the bolt to create shear resistance between those portions of the strata separated by the joint. Results of tests where bolt spacing, bolt length, and bolt tension were varied will be discussed later.

The BMINES three-dimensional truss element was used to model the bolt. This is an elastoplastic isoparametric element capable of transmitting only one component of stress, either axial tension or compression. Its classification as a three-dimensional element stems from its mechanical behavior, which is formulated in terms of three translational degrees of freedom at each end.

The mechanically anchored bolt was also modeled using ANSYS and the three-dimensional cable or compression-only spar element. This element has a unique feature, that is, a bilinear stiffness matrix where stiffness is removed if the element goes into compression. The element operates either as a cable (taking tension only) or as a compression-only spar. It is nonlinear and requires an iterative solution with the stiffness matrix reformulated for each iteration.

Deflections

Figure 28 shows theoretical deflection profiles of the lower edge of slab 6 for bolt tensions of 3, 6, 9, 13, and 15 kips under dead load. The 5-ft-long bolts were installed on 4-ft spacings. Both observed and predicted values for the deflections are included in these plots, except that the experimental bolts were not subjected to 15 kips of tension (fig. 28*E*). The agreement between observed and predicted values was fairly good. Although curling on the edges of the slab still persisted for bolts under low tension, it decreased as the tension in the bolt was increased. Comparisons of the vertical deflection for the 40-pct live-load conditions were very satisfactory, differing by 2×10^{-3} in, which was within instrument precision. The data for the vertical deflections under 40-pct live load and variable bolt tensions are plotted in figure 29. The effect of installed tension is shown in figure 30, where midspan deflections of the bottom edge of slab 6 are plotted as functions of installed bolt tensions for dead- and live-load combinations. Under dead-load conditions, a reduction in midspan deflection of 60 pct was observed when the bolt tension was increased from 3 to 13 kips (table 2).

Table 2.–Comparison of vertical deflection components at midspan under low and high overburden loads, with and without tensioned bolts

(Tension in bolts equal to 13 kips)

	Deflection, in		Difference, pct
	Unbolted	Bolted	
BMINES:			
Dead load . . .	0.0121	0.0085	26
Dead plus 100-pct live load	.0396	.0358	3
ANSYS:			
Dead load . . .	.0134	.0072	46
Dead plus 100-pct live load	.0395	.0347	12

Longitudinal Strains

For simplicity, only longitudinal strain distributions near the top and bottom surfaces of slab 6 are discussed. The strain variations in slab 6, under dead-load conditions for installed tensions of 3, 6, 9, and 13 kips, are plotted in figure 31; both theoretical and experimental results are included in these plots. The strains in the bolted cases were generally lower than those in the unbolted cases, depending upon the amount of installed bolt tension. Comparison of the strain in the unbolted condition (fig. 25*C*) with the corresponding strain under a bolt tension of 13 kips (fig. 31*D*) shows an overall compressive strain decrease of 50 pct.

The variation of strains across the span of slab 6, under dead load and 40-pct live load, is shown in figure 32 for installed bolt tensions of 3, 6, 9, and 13 kips. As the tension was increased in the bolt, the reduction of all longitudinal normal strains in the slabs became very significant. This is especially evident with regard to compressive strains. The two theoretical curves predicted by ANSYS and BMINES are almost identical. The strain variation patterns in the experiment are similar to the theoretical variations. Any deviations in magnitudes were probably due to errors in live-load applications on the physical model and to faulty readings of the strain gauges at specific locations.

The effects of bolting are evident from these diagrams (fig. 31), which show decreases in compressive strains on either side of the bolts. These decreases appear as dents in the strain diagram and become more and more conspicuous with increases in bolt tension.

Table 3 gives quantitative information on longitudinal strains at distances of 3 in on either side of the bolt (at x = 54 in and 102 in) across the interface (average y = 84 in) of slabs 5 and 6.

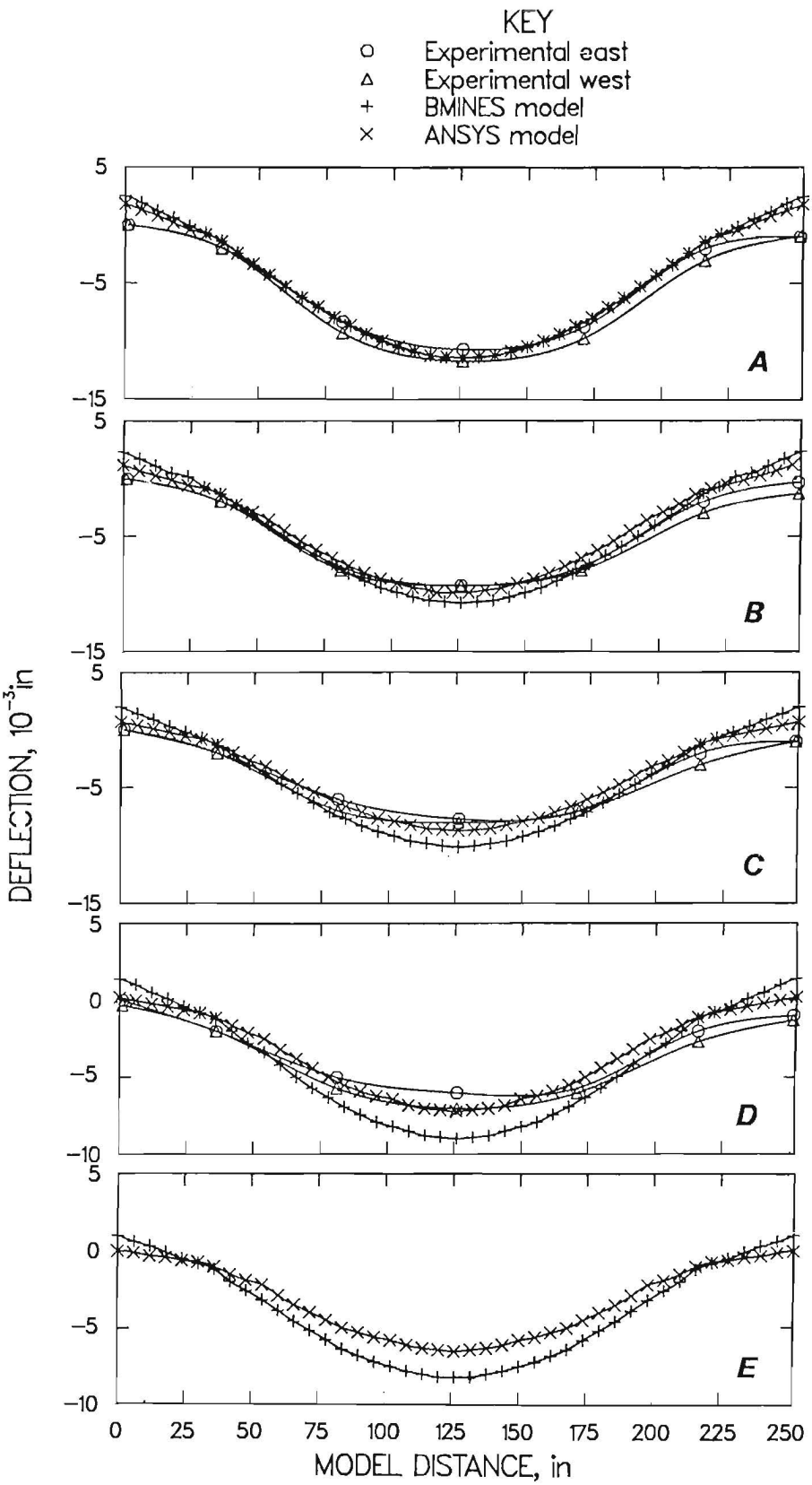

Figure 28.–Predicted and observed vertical deflection profiles of lower edge of slab 6 under dead load using 5-ft-long mechanically anchored bolts spaced 4 ft apart. Tension was applied to (*A*) 3 kips, (*B*) 6 kips, (*C*) 9 kips, (*D*) 13 kips, (*E*) 15 kips (no observed values available).

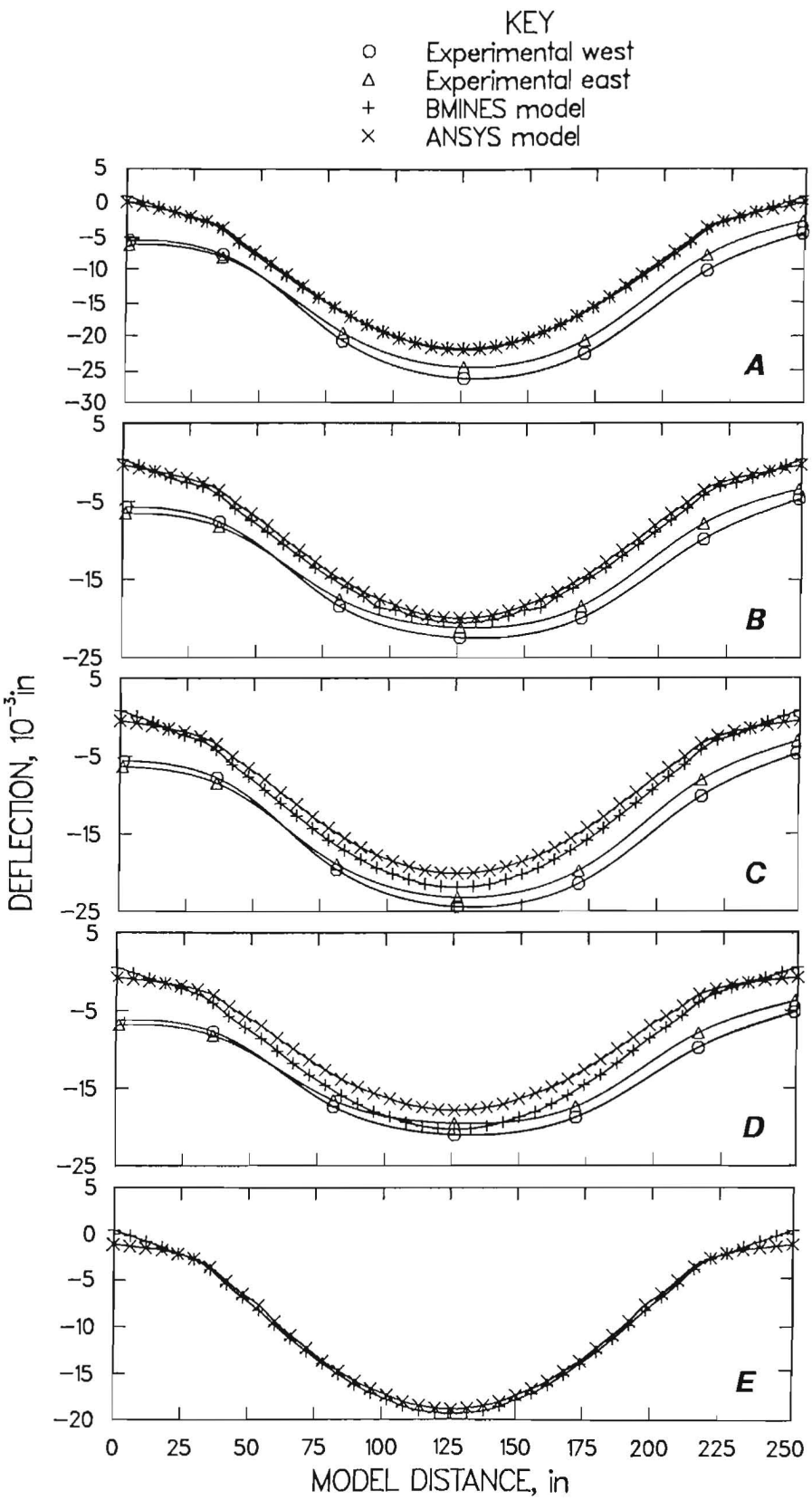

Figure 29.–Predicted and observed vertical deflection profiles of lower edge of slab 6 under dead and 40-pct live loads using 5-ft-long mechanically anchored bolts spaced 4 ft apart. Tension was applied to (*A*) 3 kips, (*B*) 6 kips, (*C*) 9 kips, (*D*) 13 kips, (*E*) 15 kips (no observed values available).

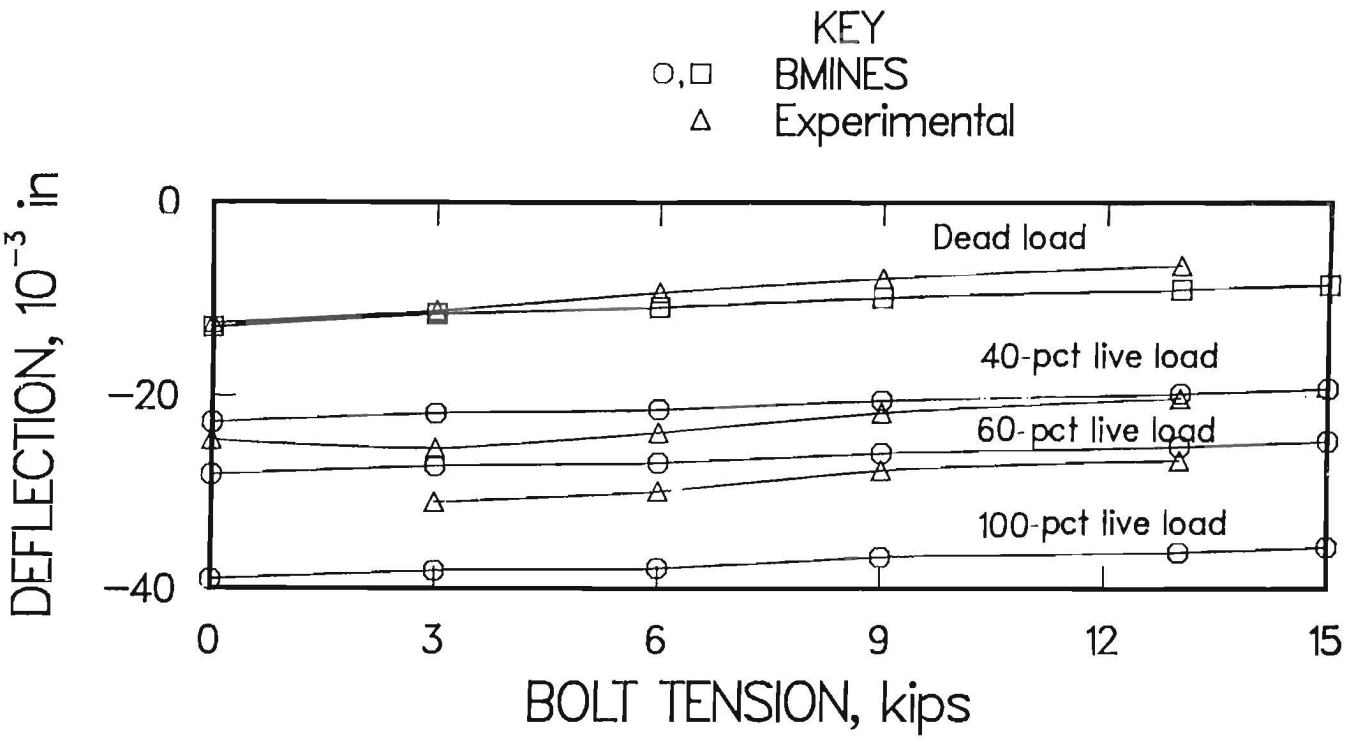

Figure 30.–Predicted and observed vertical deflection profiles of bottom point at centerline of slab 6 as a function of bolt tension under various loads.

It is apparent that mathematical modeling of mechanically anchored bolts can be done with reasonable accuracy by BMINES and ANSYS. Each code has advantages and limitations. ANSYS is simpler and much easier to use and requires very few parameters as input. For consideration of small deflections, ANSYS is recommended, although cost effectiveness should also be evaluated.

BMINES, on the other hand, has a very versatile joint element and requires a large number of input parameters compared with ANSYS. The accuracy of such parameters is sometimes questionable, and thus any accuracy gained in theoretical development is often outweighed by the approximate character of the input. For large deflections, BMINES will yield more accurate results than ANSYS. Because the BMINES code was already available at SRC, and therefore its use was more cost effective, the analyses were based primarily on BMINES.

Stresses

In slab 6, maximum tensile stresses occurred along the bottom edge, at midsection, and along the top edge near the roof pillar corner. In an unbolted state and under dead-load conditions, each slab appeared to bend about its own neutral axis in an almost pure manner. As the slabs were compressed by bolting under tension, redistribution of stresses caused neutral axes to shift toward the upper half of the layers as shear stresses developed along joint surfaces between slabs. The bending stresses in this state decreased significantly, depending on the bolt tension. For a bolt tension of 13 kips, the bending stresses at midsection in the bottom slab decreased by 20 pct compared with those in an unbolted slab. Addition of normal stresses through axial loading of bolts did not change the tensile stress in the midspan of the bottom layer, but instead reduced the compressive stress in the midspan of the top layer of slab 6 by 30 pct.

In contrast to the bottom of slab 6, upper slabs continued to undergo the nearly pure bending observed in the unbolted condition. Shear was developed along both the upper and lower surfaces of these layers, negating effects caused by axial stresses, although to a lesser degree than that observed in slab 6. However, horizontal bending stresses in these slabs showed decreases similar to those in slab 6 (table 4).

Slabs under live-load conditions experienced responses similar to those of slabs under dead-load conditions. When a heavier load was placed on the structure, the joints between slabs tended to debond, and reinforcement caused by bolt action decreased. When bolt tension was increased from 0 to 13 kips, the reduction in bending stress under live-load conditions at the corresponding location was approximately 10 pct.

Table 3.–Theoretical longitudinal strains at lower edge of slab 5 (y = 85.5) and top edge of slab 6 (y = 82.5), 10^{-6} in/in

(Tension in bolts equals 13 kips. Plus sign refers to tensile and minus sign to compressive stress. Measurements were taken 3 in on either side of bolt)

Position[1]	Layered				Unlayered solid	
	Unbolted		Bolted			
	Dead load	40 pct of live load	Dead load	40 pct of live load	Dead load	40 pct of live load
	BMINES					
x = 51 in:						
Slab 5	-2.050	-10.83	-2.80	-9.70	+0.2865	-3.136
Slab 6	-.0039	+1.949	+4.22	+4.18	+.2656	-3.507
x = 57 in:						
Slab 5	+1.041	-3.706	-.92	-3.85	+.6544	-2.125
Slab 6	-1.179	-6.444	+2.75	-.48	+.8851	-1.698
x = 99 in:						
Slab 5	+13.59	+21.49	+9.51	+19.41	+2.832	+3.295
Slab 6	-14.26	-27.89	-5.74	-19.72	+3.346	+4.198
x = 105 in:						
Slab 5	+14.49	+22.92	+9.30	+19.88	+2.974	+3.501
Slab 6	-15.20	-29.21	-5.35	-19.95	+3.565	+4.468
	ANSYS					
x = 51 in:						
Slab 5	+4.37	-9.01	-1.76	-13.65		
Slab 6	+3.30	+.06	+8.38	+8.87		
x = 57 in:						
Slab 5	-1.15	-2.14	-4.91	-7.77		
Slab 6	-.33	-7.10	+7.55	+4.23		
x = 99 in:						
Slab 5	+13.10	+20.30	+7.89	+16.02		
Slab 6	-14.61	-29.33	-2.98	-16.91		
x = 105 in:						
Slab 5	+14.12	+21.91	+8.26	+17.01		
Slab 6	-15.63	-30.89	-2.64	-17.15		

[1]See figure 20 for x and y coordinates.

Table 4.–Midspan variation of normal stresses (in pounds per square inch) under dead loads as a function of bolt tension

(Bolts are 5 ft long on 4-ft spacings. Plus sign refers to tensile and minus sign to compressive stresses)

	y, in[1]	Bolt tension, kips					
		0	3	6	9	13	15
Slab 6:							
Bottom	73.5	+73.81	+69.05	+68.39	+66.78	+64.88	+62.65
Top	82.5	-68.55	-63.48	-56.29	-48.97	-39.31	-33.30
Slab 5:							
Bottom	85.5	+64.99	+64.13	+59.46	+53.24	+47.51	+41.91
Top	94.5	-67.56	-66.89	-62.20	-57.92	-50.00	-46.35

[1]See figure 20.

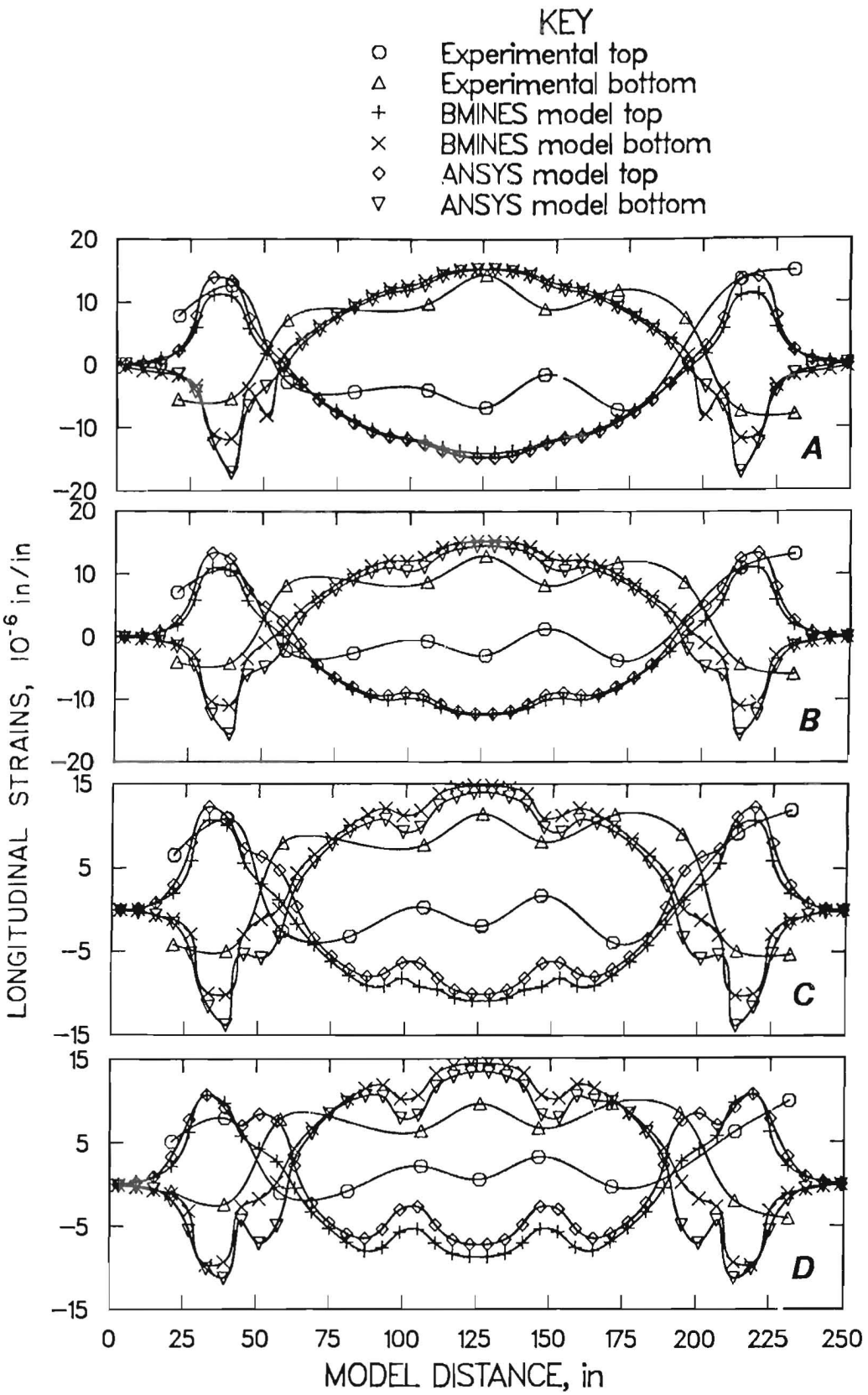

Figure 31.–Predicted and observed profiles of longitudinal strains on slab 6 under dead load using 5-ft-long mechanically anchored bolts spaced 4 ft apart. Measurements were taken 1-1/2 in from the top and bottom edges as indicated in key. Tension was applied to (*A*) 3 kips, (*B*) 6 kips, (*C*) 9 kips, (*D*) 13 kips.

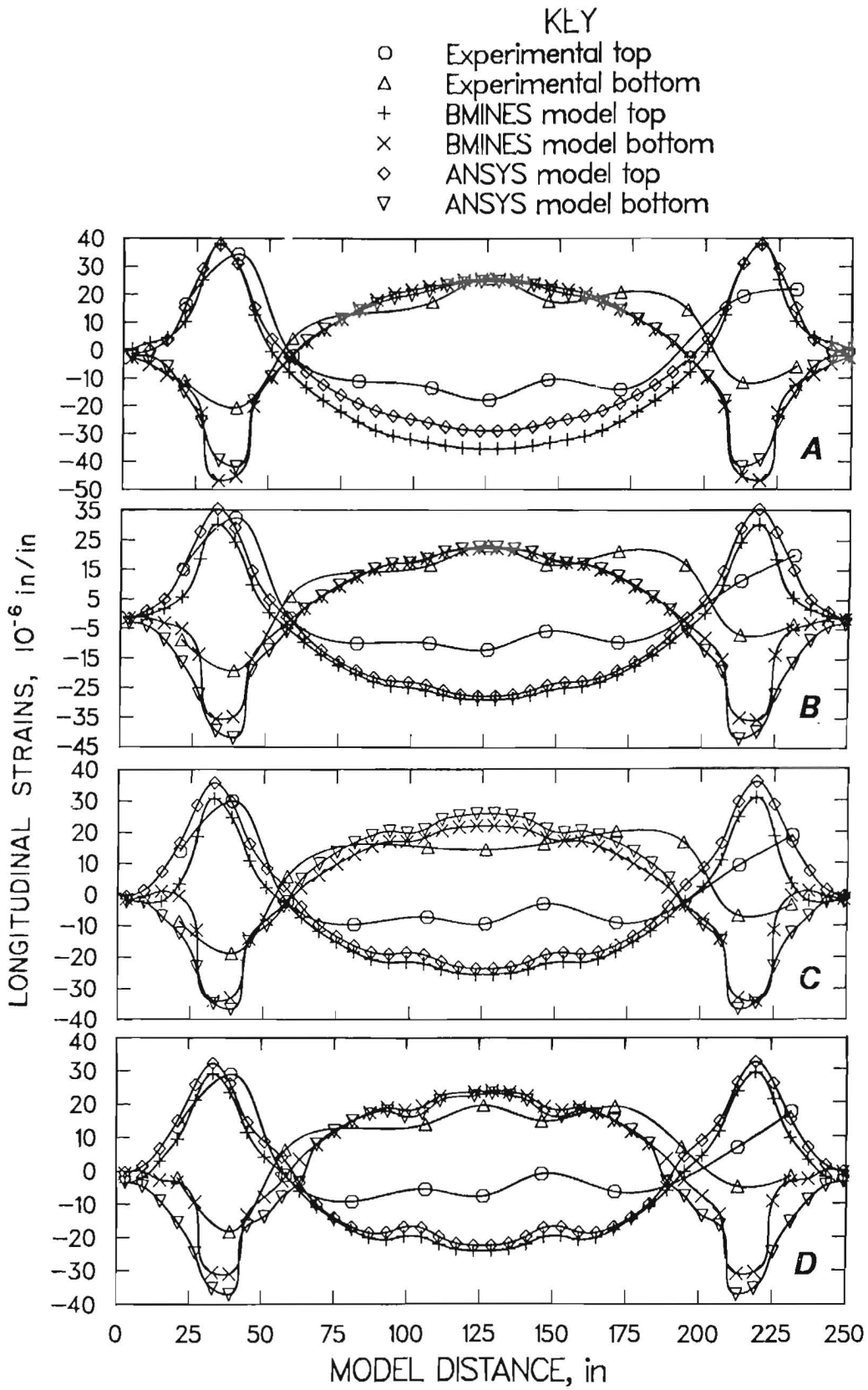

Figure 32.–Predicted and observed profiles of longitudinal strains on slab 6 under dead and 40-pct live loads using 5-ft-long mechanically anchored bolts spaced 4 ft apart. Measurements were taken 1-1/2 in from the top and bottom edges as indicated in key. Tension was applied to (*A*) 3 kips, (*B*) 6 kips, (*C*) 9 kips, (*D*) 13 kips.

RESIN-GROUTED BOLT SYSTEM

Unlike mechanically anchored bolts, resin-grouted bolts establish a bond between the bolt material and the enclosing medium over the entire axial surface of the bolt. As a result, bolts reinforce the bedded medium by creating shear resistance across a joint and through a slab, thus restricting slip between layers (fig. 33). Modeling of such a bolt requires different types of input for the BMINES and ANSYS codes. These models are described below.

Modeling Considerations

The BMINES code, as noted, is usable for planar joints extending from one end of the model to the other with no solids between the layers. The code does not permit joining of nodes on either side of the joint to form solid elements as is usually done for a solid model. The only recourse was to model a resin-grouted bolt with a fictitious slip element where the bolt passed through the slip plane. This element, indicated by nodes 1, 2, 3, and 4 in figure 33*A*, was modified from the regular slip element by assigning it very high shear and normal stiffness properties. To ensure connectivity between the layers at the interface, this slip element was assigned nonzero cohesion. The cohesive strength of the slip was assumed to be the shear strength of the bolt. Other model properties for the

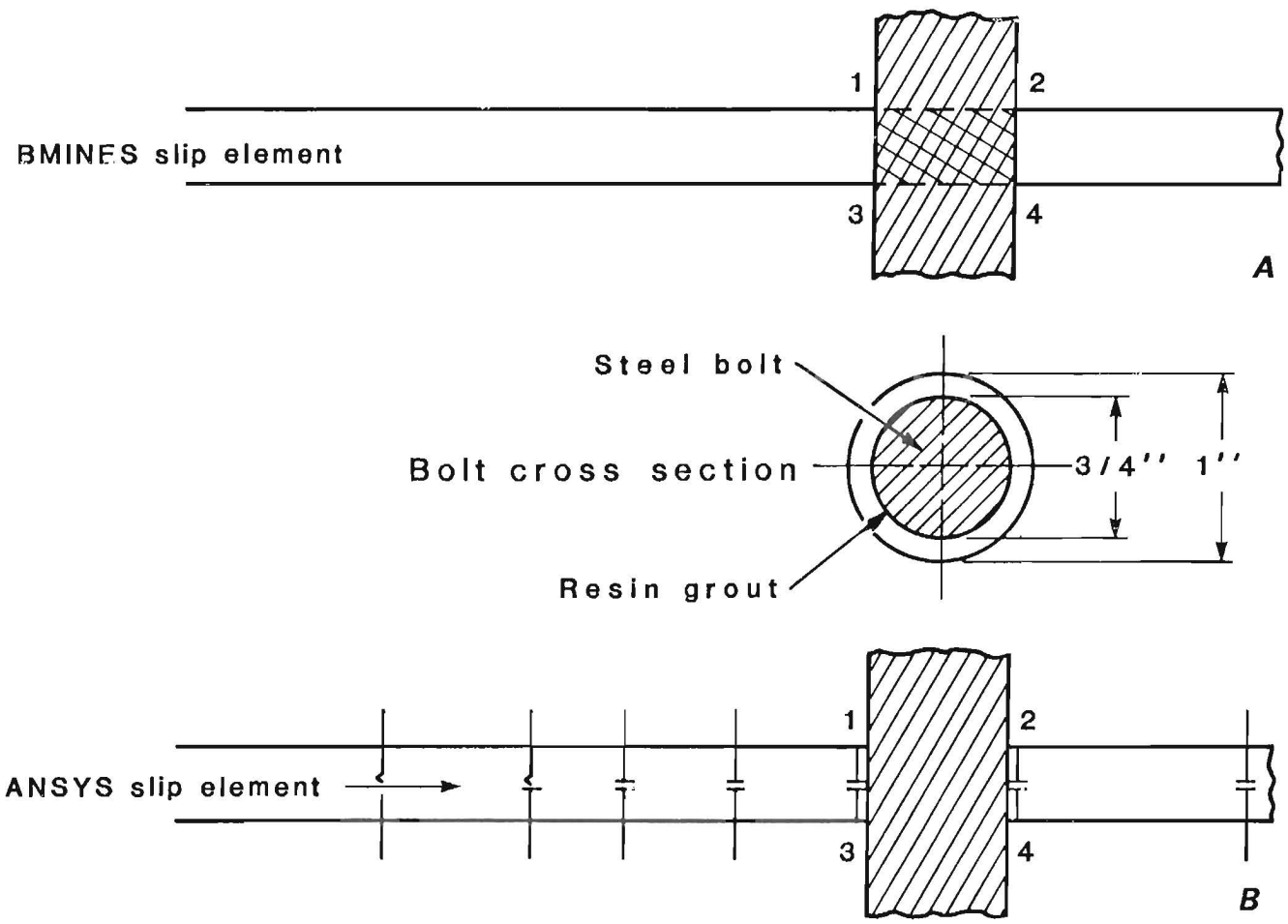

Figure 33.–Slip regions occupied by resin-grouted bolt modeled with (*A*) BMINES and (*B*) ANSYS codes.

resin-grouted bolt and the fictitious slip element were determined in the following manner:

If D_g = diameter of resin-grouted bolt,

D_s = diameter of steel portion of bolt,

A_g = gross area covered by resin-grouted bolt (that is, cross-sectional area of drill hole),

A_s = area of steel portion of bolt,

and A_r = cross-sectional area of resin surrounding bolt,

then $A_g = \frac{\pi}{4}(D_g)^2$

$= \frac{\pi}{4}(1)^2 = 0.7854 \text{ in}^2$,

$A_s = \frac{\pi}{4}(D_s)^2$

$= \frac{\pi}{4}(3/4)^2 = 0.4416 \text{ in}^2$,

and $A_r = A_g - A_s$

$= 0.7854 - 0.4416$

$= 0.3438 \text{ in}^2$.

The force-deformation relation is given by

$$F = \frac{AE}{L}\Delta,$$

where F = force in the member, lb,

A = cross-sectional area of the member, in^2,

E = modulus of elasticity in compression of the material, psi,

L = axial length of the member, in,

and Δ = axial deformation of the member, in.

If F_s, F_r, and F_g are forces resisted by steel area, resin area, and gross area of the bolt, respectively, then

$$F_g = F_s + F_r$$

$$\text{or } \frac{A_g E_g \Delta_g}{L_c} = \frac{(A_s)(E_s)(\Delta_s)}{L_s} + \frac{(A_r)(E_r)(\Delta_r)}{L_r}$$

because $\Delta_g = \Delta_s = \Delta_r$, and $L_g = L_s = L_r$.

From this, the elasticity modulus of the grouted bolt system can be calculated:

$$E_g = \frac{(A_s E_s + A_r E_r)}{Ag}$$

$$= \frac{(0.4416)(30 \times 10^6) + (0.3438)(1 \times 10^6)}{0.7854}$$

$$= 17.3 \times 10^6 \text{ psi.}$$

The resulting shear modulus is

$$G_g = \frac{E_g}{2(1 + \upsilon_c)}$$

$$= \frac{17.3 \times 10^6}{2(1 + 0.25)} = 6.9 \times 10^6 \text{ psi.}$$

The bulk modulus is

$$K_g = \frac{E_g}{3(1\text{-}2\upsilon)} = \frac{17.3 \times 10^6}{3(0.2 \times 0.25)}$$

$$= 11.5 \times 10^6 \text{ psi.}$$

In contrast to BMINES, ANSYS does not restrict the slip element (interface element) to the entire length of the slip plane; the slip element in ANSYS ensures connectivity across the joint in the region of the bolt. This is indicated by the interface nodes 1, 2, 3, and 4 in figure 33*B*. Modeling of this joint was based upon much simpler theoretical considerations, compared with the BMINES slip element theory. ANSYS requires only the shear modulus of the solid medium on either side of the joint (an average value if the medium across the joint possesses different material properties) and the thickness of the joint, thus allowing any chosen material to occupy the joint space. Accordingly, the resin-grouted bolt was modeled using ANSYS in the same manner as any other solid element having pertinent model values as needed in BMINES. Some parameters usually used in the slip element option of BMINES, for example, cohesion, shear strength, etc., are not required in ANSYS because the joint is based on Coulomb friction.

Deflections

The dead-load vertical deflection profiles of the model with resin-grouted bolts spaced 4 ft apart are shown in figure 34 for the lower edges of slabs 1 and 6, respectively. The results from both the BMINES and ANSYS codes closely agree with each other and also compare satisfactorily with observed values. A reduction in the vertical deflection at the lower edge of the midsection of 10 pct compared with the unbolted case is observed for both predicted and observed values.

The indicated deflection profiles for combined dead and 40-pct live loads, shown in figure 35*A* for the lower edge of slab 1 and in 35*B* for the lower edge of slab 6, show deviations similar to those observed under mechanically bolted conditions. Even though the experimental values are not identical to theoretical values on either side of the midsection, a maximum deviation of 5×10^{-3} in does not appear to be sufficient to raise doubts about the comparisons. Some of these results should be examined with regard to the inherent probability of inaccuracies of live-load applications. For a model of this size having live loads of high magnitudes, these deviations may be considered to be within instrument accuracy. Table 5 gives quantitative information on the deflections for unbolted conditions and for resin-grouted bolts under dead and live loads. Some of these data have been used for comparison with the mechanically bolted response and are plotted in figure 36. This comparison reveals that bolt tensions ranging from 6 to 9 kips are required for the mechanically anchored bolts to achieve the same effectiveness in reducing deflection at the midspan as the nontensioned, resin-grouted bolt systems.

Strains

Variations of longitudinal strains under dead loads in the top and bottom layers (1-1/2 in from the top and bottom surfaces) of slabs 2, 5, and 6 are shown in figure 37. The decreases in the magnitudes of the strains are very significant compared with those encountered under unbolted conditions (fig. 25*C*). The abrupt changes of strain in the neighborhood of the bolts are noteworthy compared with the corresponding strains for mechanically anchored bolts (fig. 31). The resin-grouted bolts appear to correlate better with the theoretical values. This might indicate that the magnitudes of the applied prestresses are different from the values assumed in the analytical modeling of mechanical bolts. This is also evident from figure 38, which shows plots of longitudinal strains in slabs 2, 5, and 6 under dead- and live-load combinations. Compared with unbolted conditions, very significant decreases in strain occur. In slab 6, for example, compressive strain readings at the midsection decreased from 30×10^{-6} in/in under unbolted conditions to 24×10^{6} in/in under resin-grouted conditions. The magnitudes of tensile strains did not show such reductions because any reduction in horizontal bending strain was accompanied by axial strain caused by resultant shear forces in slab 6.

Table 5.–Comparison of observed and predicted deflections (in inches) along lower edge of slab 6 (y = 72 in)

(Bolts are resin grouted on 4-ft spacings)

Dead load plus--	x = 0 in	x = 36 in	x = 81 in	x = 126 in
0-pct live load:				
Unbolted:				
Predicted	+0.0027	-0.0014	-0.0087	-0.0121
Observed	-.0003	-.0023	-.0098	-.0125
Bolted:				
Predicted	+.0021	-.0013	-.0079	-.0109
Observed	-.0003	-.0021	-.0086	-.0112
40-pct live load:				
Unbolted:				
Predicted	+.0008	-.0041	-.0163	-.0217
Observed	-.0045	-.0081	-.0206	-.0246
Bolted:				
Predicted	+.0004	-.0042	-.0153	-.0202
Observed	-.0043	-.0080	-.0203	-.0250
60-pct live load:				
Unbolted:				
Predicted	+.0005	-.0051	-.0207	-.0277
Observed	ND	ND	ND	ND
Bolted:				
Predicted	+.0002	-.0052	-.0192	-.0253
Observed	-.0056	-.0103	-.0250	-.0305
100-pct live load:				
Unbolted:				
Predicted	+.0003	-.0073	-.0296	-.0396
Observed	ND	ND	ND	ND
Bolted:				
Predicted	-.0002	-.0072	-.0271	-.0358
Observed	ND	ND	ND	ND

ND No data.

PARAMETRIC ANALYSIS

A basic goal of this investigation has been to verify results from analytical modeling using the physical laboratory model to achieve values for longitudinal strains and vertical deflections. For both unbolted and bolted conditions, the physical model of a mine opening has proven to be very useful for verifying the analytical model. The joint elements in BMINES and ANSYS codes can be used successfully for modeling bedded roof strata.

Mechanically Anchored Bolts

The analytical results indicate that for low bolt tensions of 3 kips, changes in deflection profiles at the bottom edge of slab 6 were inconsequential even when the bolt length and the spacing were varied. This can be seen in figure 39, where midspan deflections of the bottom edge of slab 6 are not significantly different for bolts 3 to 5 ft long spaced from 3 to 12 ft apart. This may be because low bolt tension exerted little squeezing of slab layers, and no significant shear resistance was developed between the layers. For high bolt tensions under unbolted conditions, reductions in midspan deflections appeared to become significant only for 5-ft-long bolts spaced at 4 ft or less (fig. 40). When a condition in which a 5-ft-long bolt under a tension of 15 kips is compared with an unbolted condition, midspan deflection decreases by 9, 11, and 56 pct for bolt spacings of 4, 3, and 0.5 ft, respectively (fig. 41). Figure 40 also shows that very small bolt spacings under high bolt tensions were required to develop adequate shear resistance between layers comparable to that achieved by a solid model. For an intermediate bolt tension of 9 kips and a bolt length of 5 ft, the decrease in midspan deflection from the unbolted state amounted to 7 and 9 pct for bolt spacings of 4 and 3 ft (fig. 42).

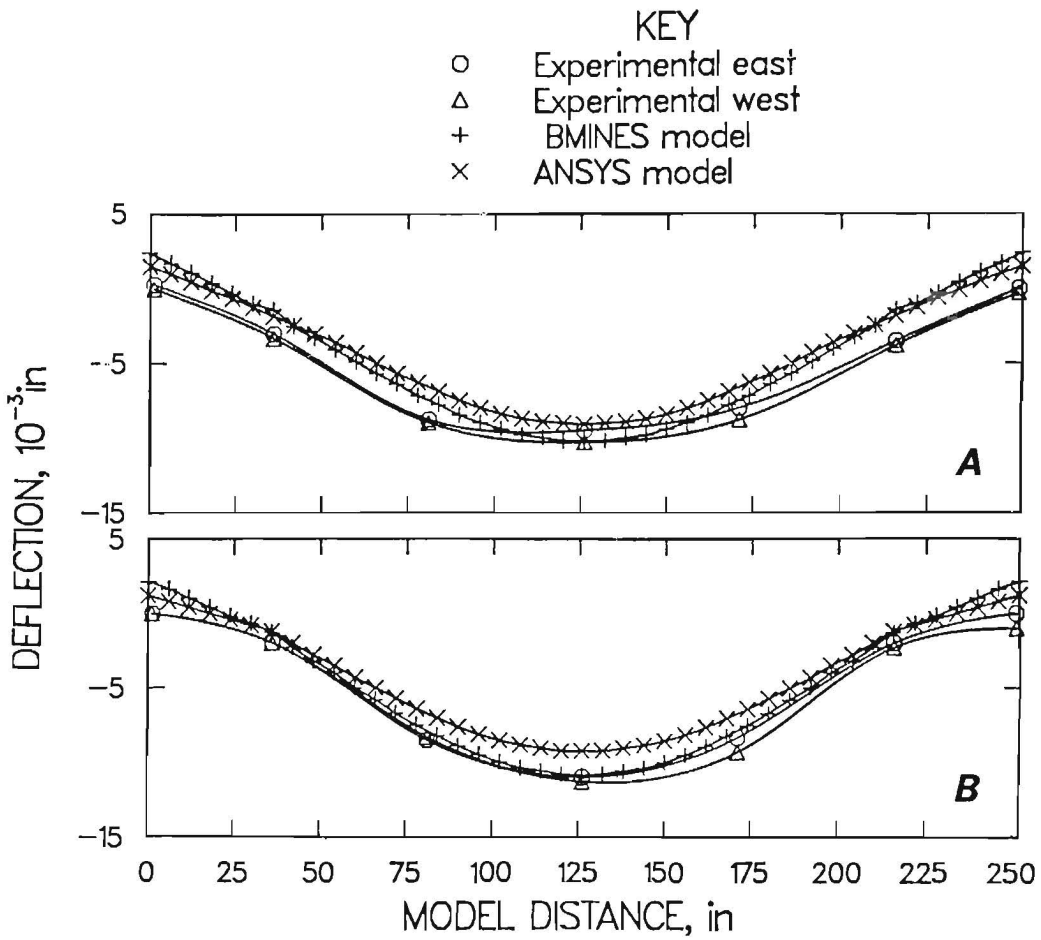

Figure 34.–Predicted and observed vertical deflection profiles under dead load using 5-ft-long resin-grouted bolts spaced 4 ft apart. *A*, Lower edge of slab 1; *B*, lower edge of slab 6.

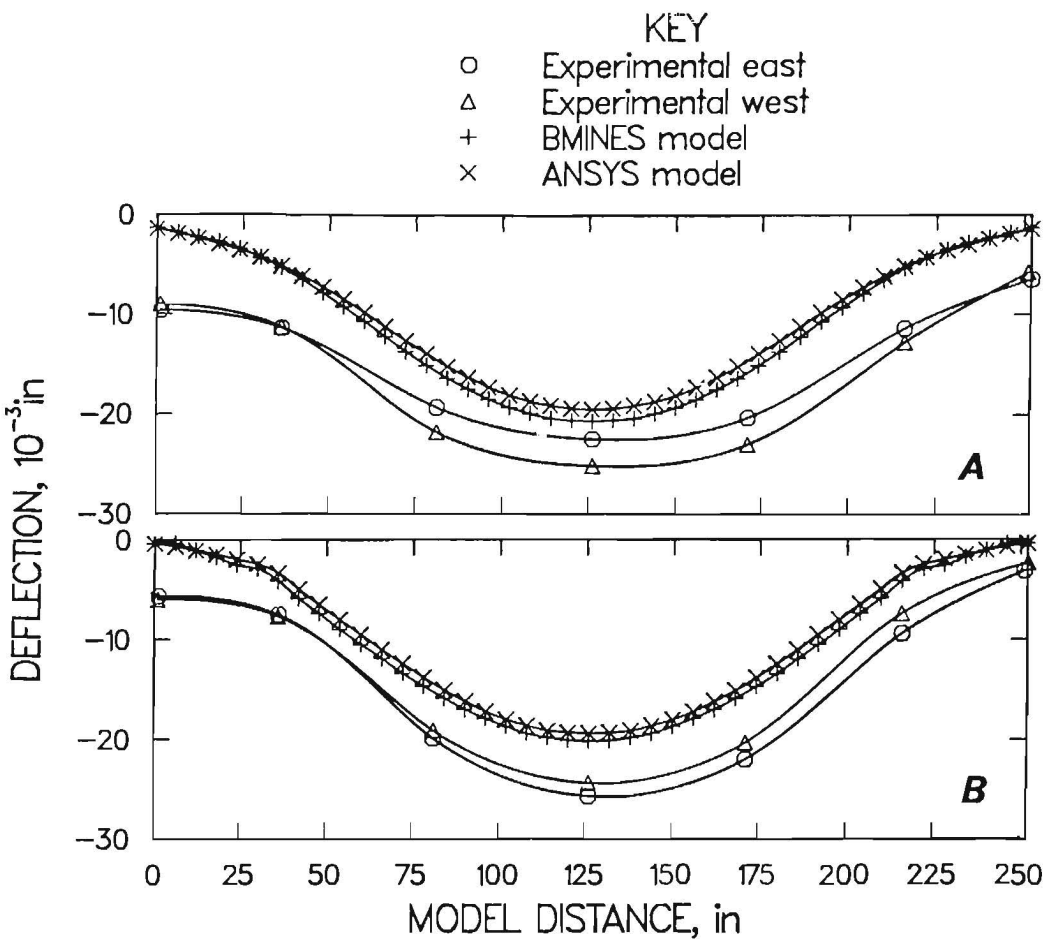

Figure 35.–Predicted and observed vertical deflection profiles under dead and 40-pct live loads using 5-ft-long resin-grouted bolts spaced 4 ft apart. *A*, Lower edge of slab 1; *B*, lower edge of slab 6.

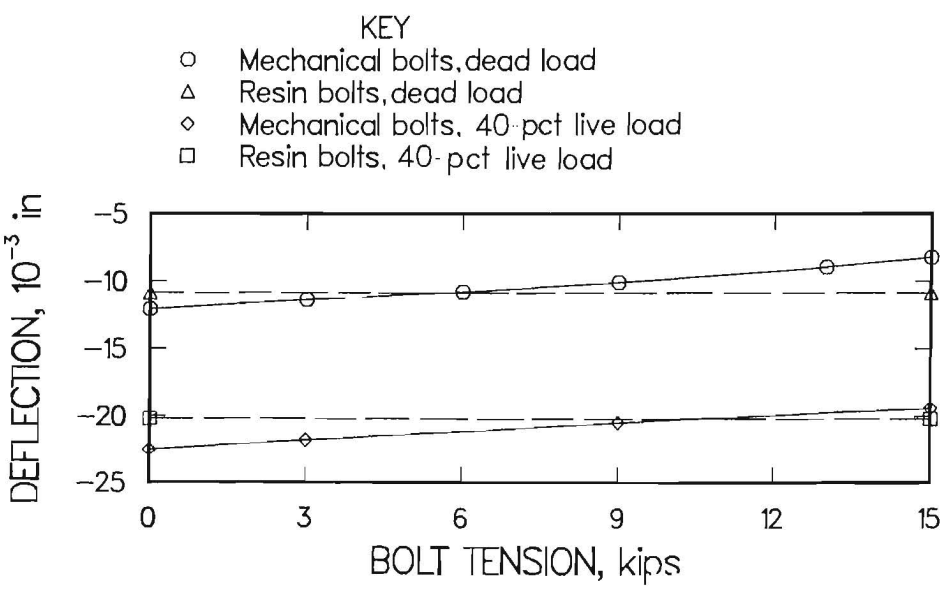

Figure 36.–Comparisons of resin-grouted bolts with mechanically anchored bolts showing predicted midspan deflections under different bolt tensions (x = 126 in and y = 72 in).

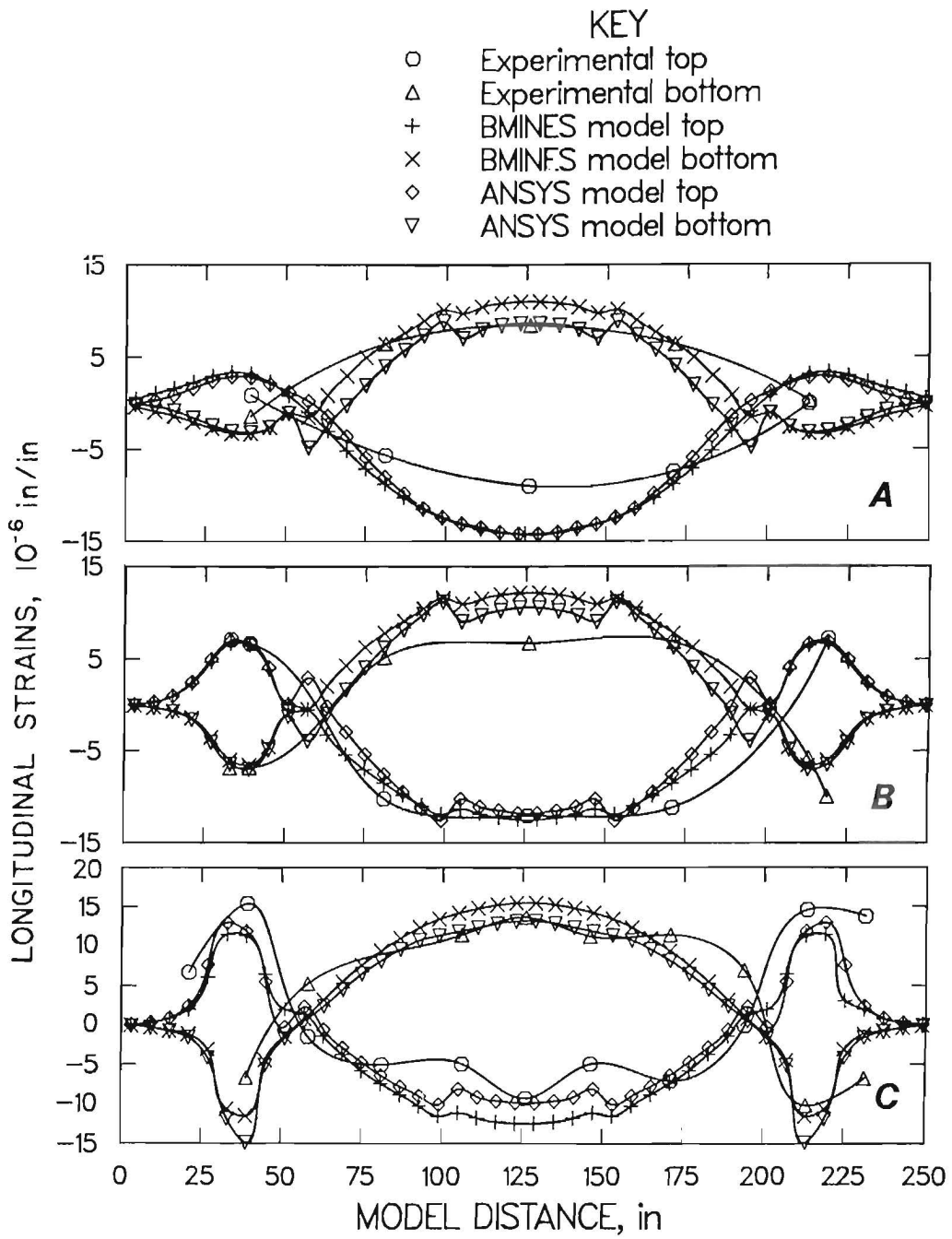

Figure 37.–Predicted and observed profiles of longitudinal strains under dead load using 5-ft-long resin-grouted bolts spaced 4 ft apart. Measurements were taken 1-1/2 in from the top and bottom edges of slab as indicated in key. *A*, Slab 2; *B*, slab 5; *C*, slab 6.

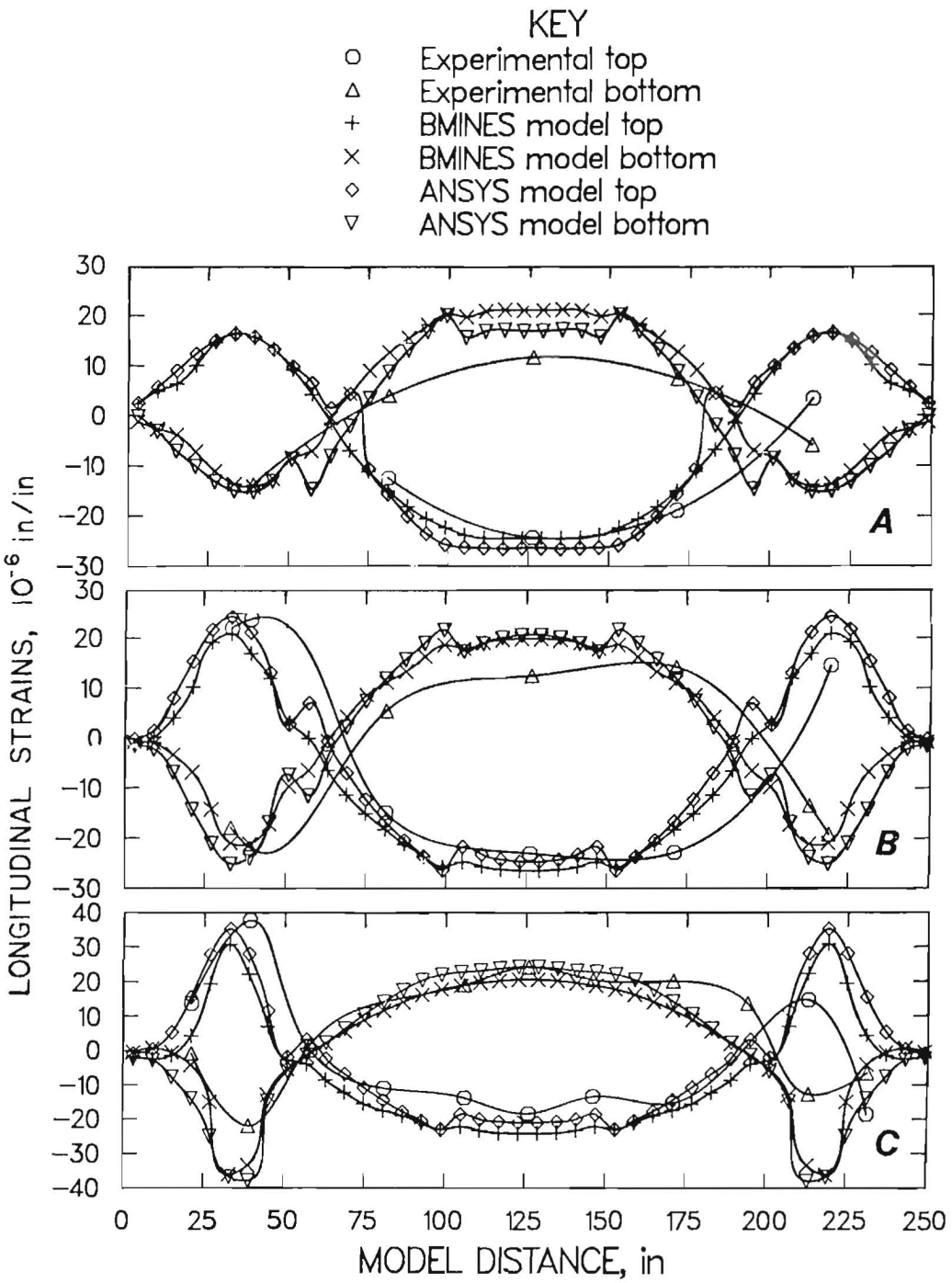

Figure 38.–Predicted and observed profiles of longitudinal strains under dead and 40-pct live loads using 5-ft-long resin-grouted bolts spaced 4 ft apart. Measurements were taken 1-1/2 in from top and bottom edges of slab as indicated in key. *A*, Slab 2; *B*, slab 5; *C*, slab 6.

The influence of bolts on longitudinal strains followed the same pattern shown by the deflections. For low bolt tensions at 3 kips, increasing the bolt length or reducing the bolt spacing did not cause any significant decreases in longitudinal strains. Figure 43 shows profiles of tensile and compressive strains in slab 6 as functions of bolt length. For higher bolt tensions, significant reductions in strain occurred only with small spacings and longer bolts. Figure 44 compares the unbolted condition with a condition incorporating bolts of different lengths under a tension of 13 kips. The decrease in compressive strain in the neighborhood of the midspan of slab 6 ranged from 10 to 15 pct, depending on the length and spacing of the bolt. For spacings of greater than 4 ft, strains did not vary appreciably even for 5-ft-long bolts. From these observations, it appears that the response of the bolted model will seldom approach the equivalent rigidity of a solid, unlayered model unless bolt spacing is extremely small and installed bolt tension very great.

Resin-Grouted Bolts

For spacings greater than 5 ft, midspan deflections were independent of the length of the bolt. Even for spacings less than 5 ft, the length of the bolt did not significantly reduce midspan deflection. This is evident from figure 45, where deflection profiles of the lower edge of slab 6 are drawn as functions of bolt lengths. The reduction of midspan deflection, compared with the unbolted condition, amounted to 6, 7, and 12 pct for bolt spacings of 12, 4, and 2 ft, respectively. A comparison of the data (fig. 42) reveals that, for the same spacing and a bolt length of 5 ft, a mechanically anchored bolt requires a bolt tension of approximately 9 kips to produce the same degree of reduction in midspan deflection as a resin-grouted bolt (fig. 45).

Longitudinal strains are also virtually independent of the length of the bolt (fig. 46); however, spacing of the bolts does affect strain. In slab 6, midspan compressive strain reductions of 21, 14, 7, and 4 pct were achieved for bolt spacings of 2, 4, 6, and 12 ft, respectively. As expected, the reduction of strains in the neighborhood of the bolts was because of the stiffer behavior of the bolt.

CONCLUSIONS

The goals of this investigation were (1) to establish the validity of finite-element methods in predicting the response of a model mine opening with and without the use of bolts as roof reinforcement and (2) to compare the relative performance (in terms of deflection and longitudinal strains) of mechanically anchored and resin-grouted bolts. The results of this research led to the following conclusions:

1. The full-scale physical model of a mine opening has proven very helpful in verifying the analytical model(s). The responses of mechanically anchored and resin-grouted bolt systems have been verified by the analytical modeling.

2. The analytical model(s) were used to study bolt systems with respect to the type, length, spacing, size, and installed tension of the bolts. These studies indicated that

a. Under low bolt tensions (3 to 7 kips), the response of a roof is independent of the length and spacing of mechanically anchored bolts.

b. Bolt lengths of 5 ft or more with bolt tensions of 9 kips or higher and bolt spacings of 4 ft or less are required for mechanically anchored bolts to cause any significant reduction in midspan roof deflections and longitudinal strains.

c. An infinite number of bolts having extremely small spacings would be required to duplicate the response of a monolithic mine roof.

d. For both types of bolts, a significant reduction in compressive strains in the immediate roof takes place in the midspan, while the tensile strains remain virtually unchanged.

e. The longitudinal strains over the pillars may even exceed those at the midspan, thereby destroying the integrity of the pillars.

f. For commonly used parameters, such as 5-ft-long bolts spaced 4 ft apart and tensioned to 9 kips, the decrease in midspan deflection may be expected to be around 10 to 15 pct and the longitudinal strain reduction around 20 to 25 pct, compared with deflections and strains of unbolted mine roof.

g. For a mechanically anchored bolt with a bolt spacing of 4 ft and a length of 5 ft, a bolt tension of 6 to 10 kips, depending on magnitude of load, is required to achieve the same response as the response given by a resin-grouted bolt.

It is recommended that pertinent field data be available for correlation with analytical predictions in order to design a safe and economical reinforcement for mine roofs.

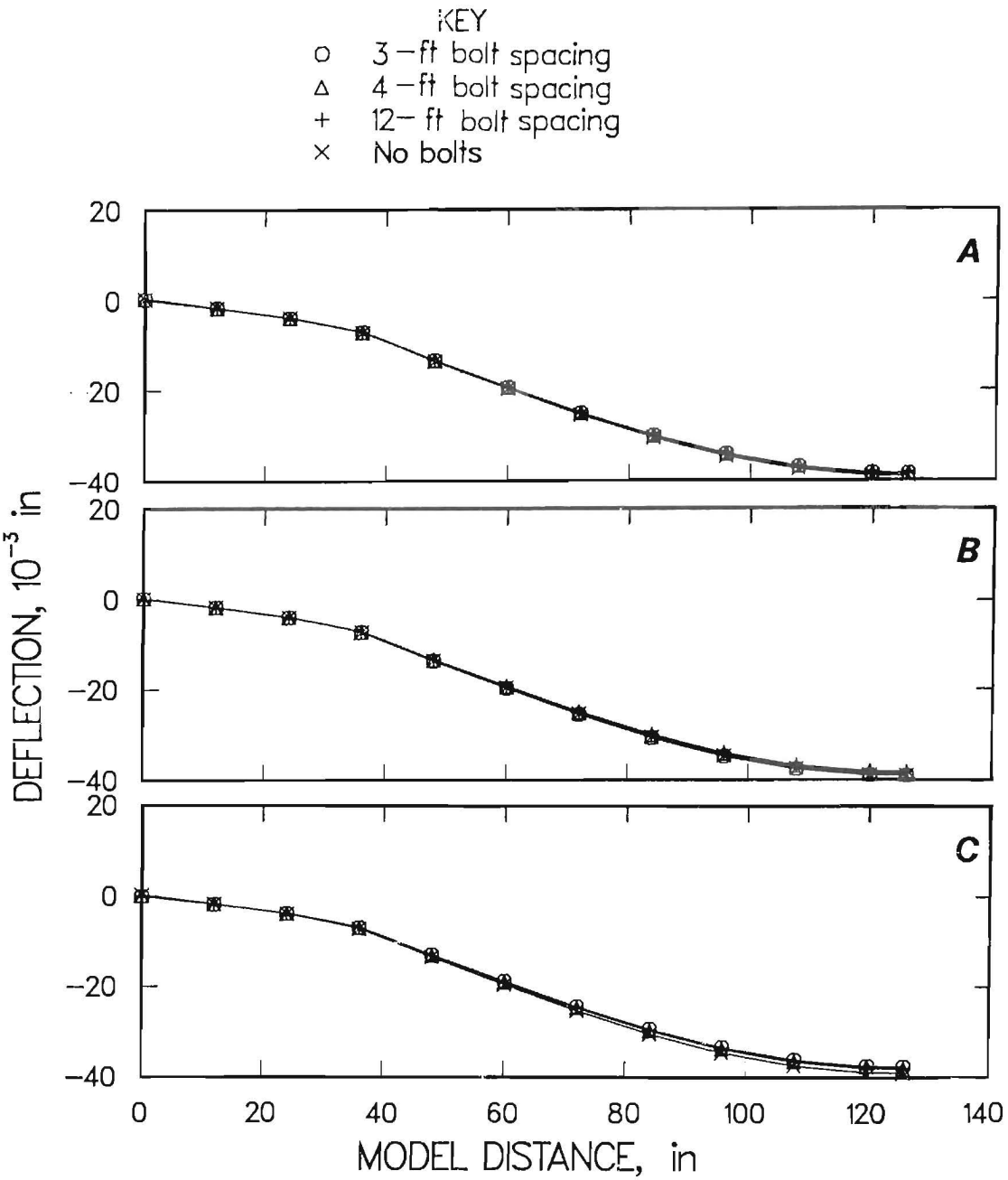

Figure 39.–Predicted vertical deflection profiles of lower edge of slab 6 under dead and live loads using mechanically anchored bolts at different spacings and lengths under a bolt tension of 3 kips. Lengths: (*A*) 3 ft, (*B*) 4 ft, (*C*) 5 ft.

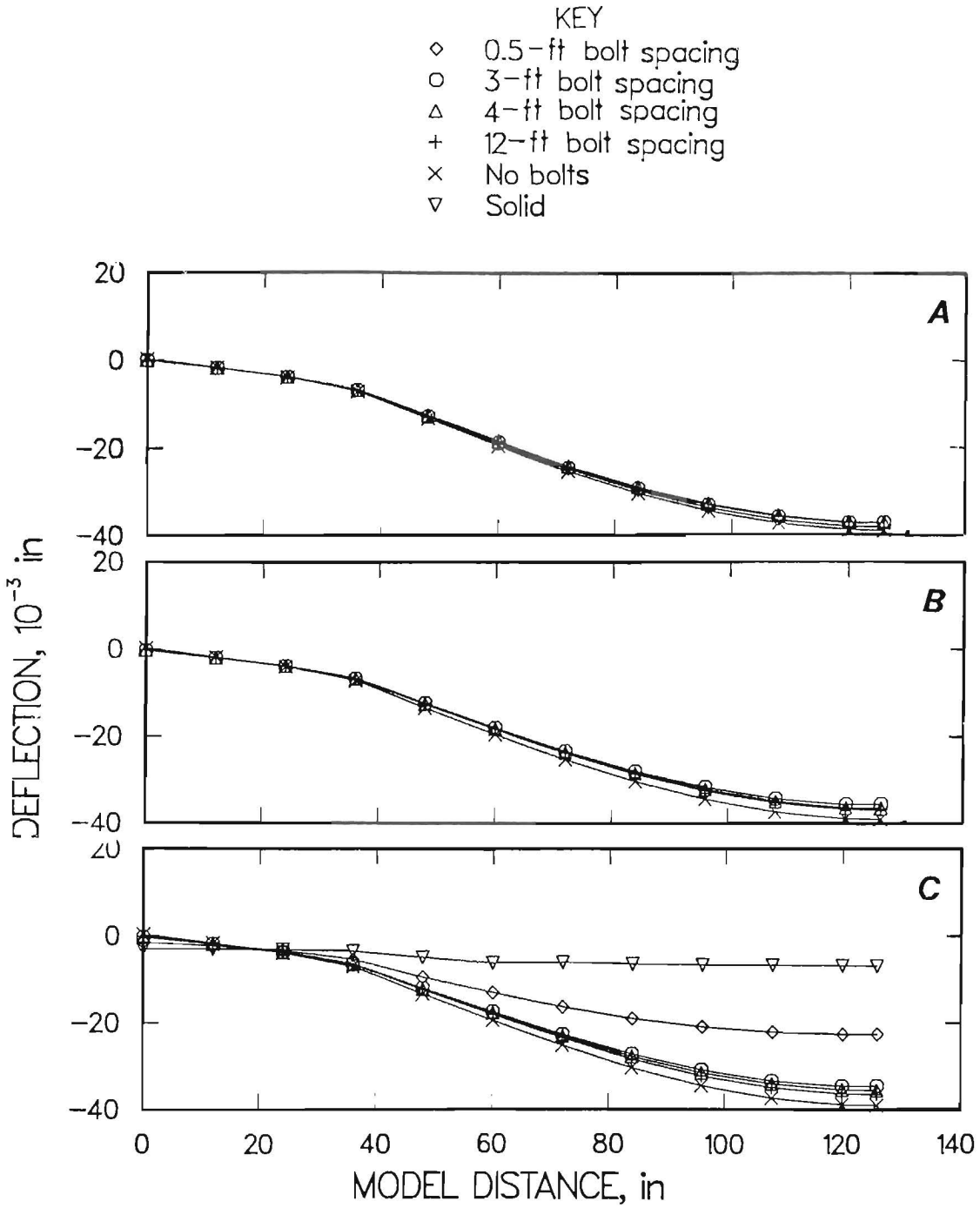

Figure 40.–Predicted vertical deflection profiles of lower edge of slab 6 under dead and live loads using mechanically anchored bolts at different spacings and lengths under a bolt tension at 15 kips. Lengths: (*A*) 3 ft, (*B*) 4 ft, (*C*) 5 ft.

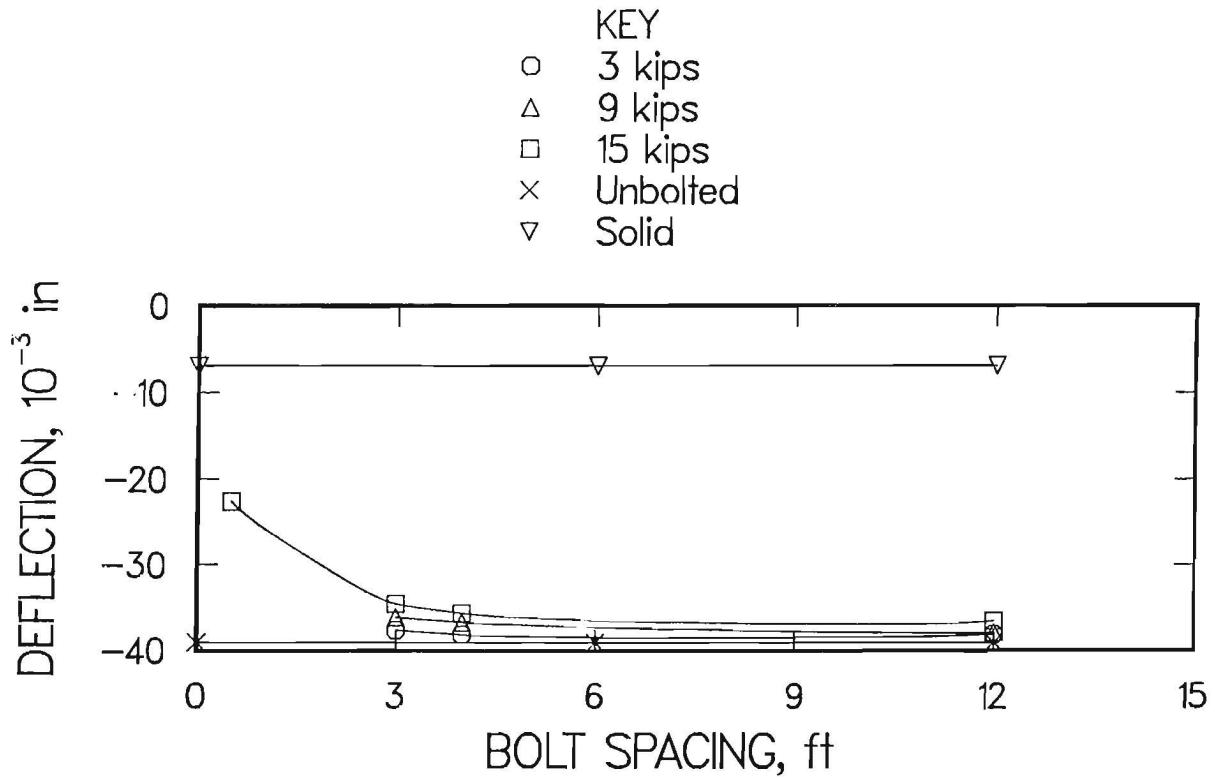

Figure 41.–Comparisons of predicted midspan deflections among solid, unbolted, and mechanically bolted models at different bolt tensions and bolt spacings.

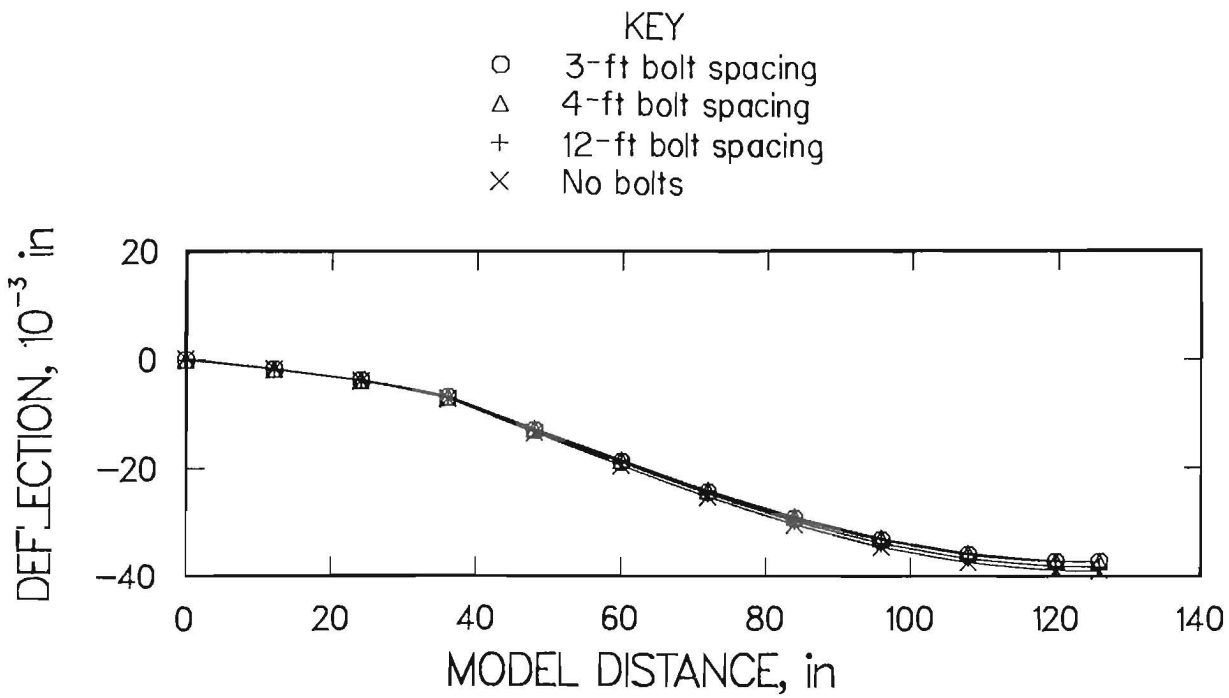

Figure 42.–Predicted vertical deflection profiles of lower edge of slab 6 under dead and 100-pct live loads using 5-ft-long mechanically anchored bolts at different spacings at a bolt tension of 9 kips.

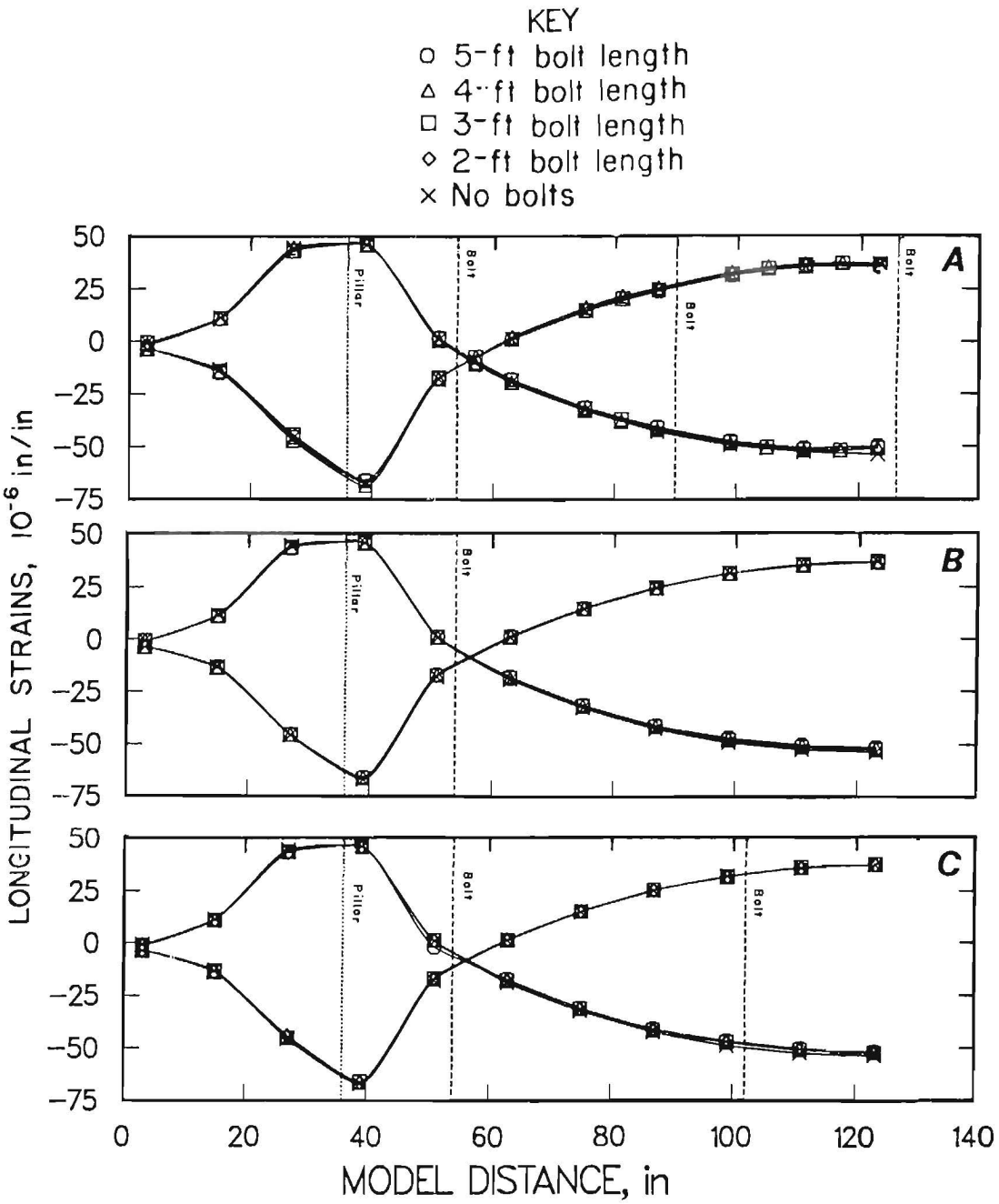

Figure 43.–Predicted longitudinal strain profiles on slab 6 under dead and 100-pct live loads using mechanically anchored bolts at different lengths and spacings under a bolt tension of 3 kips. Measurements were taken 1-1/2 in from the top and bottom edges of slab. Bolt spacings were (*A*) 3 ft, (*B*) 12 ft, (*C*) 4 ft.

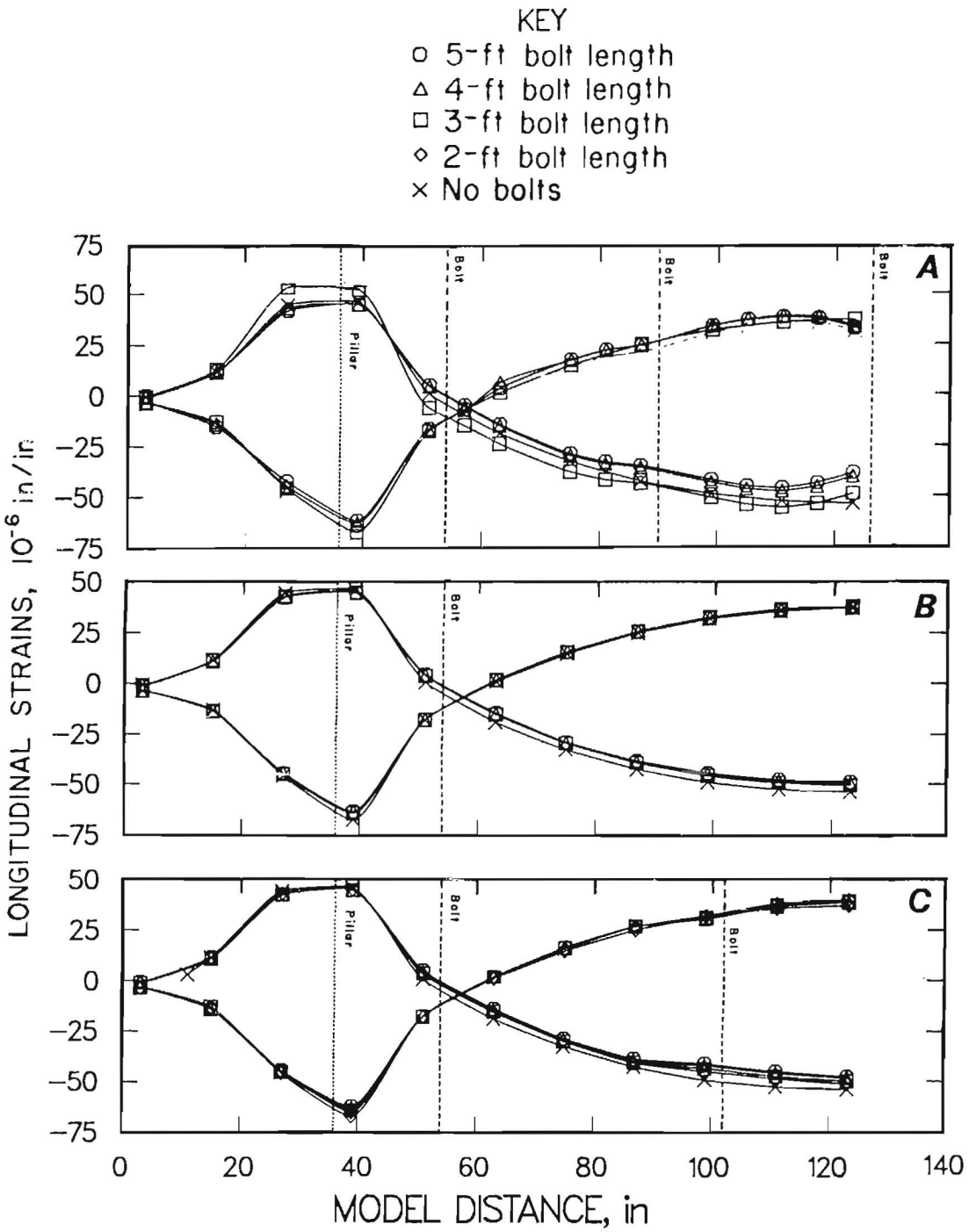

Figure 44.–Predicted longitudinal strains on slab 6 under dead and 100-pct live loads using mechanically anchored bolts at different lengths and spacings under a bolt tension of 13 kips. Measurements were taken 1-1/2 in from the top and bottom edges of slab. Bolt spacings were (*A*) 3 ft, (*B*) 12 ft, (*C*) 4 ft.

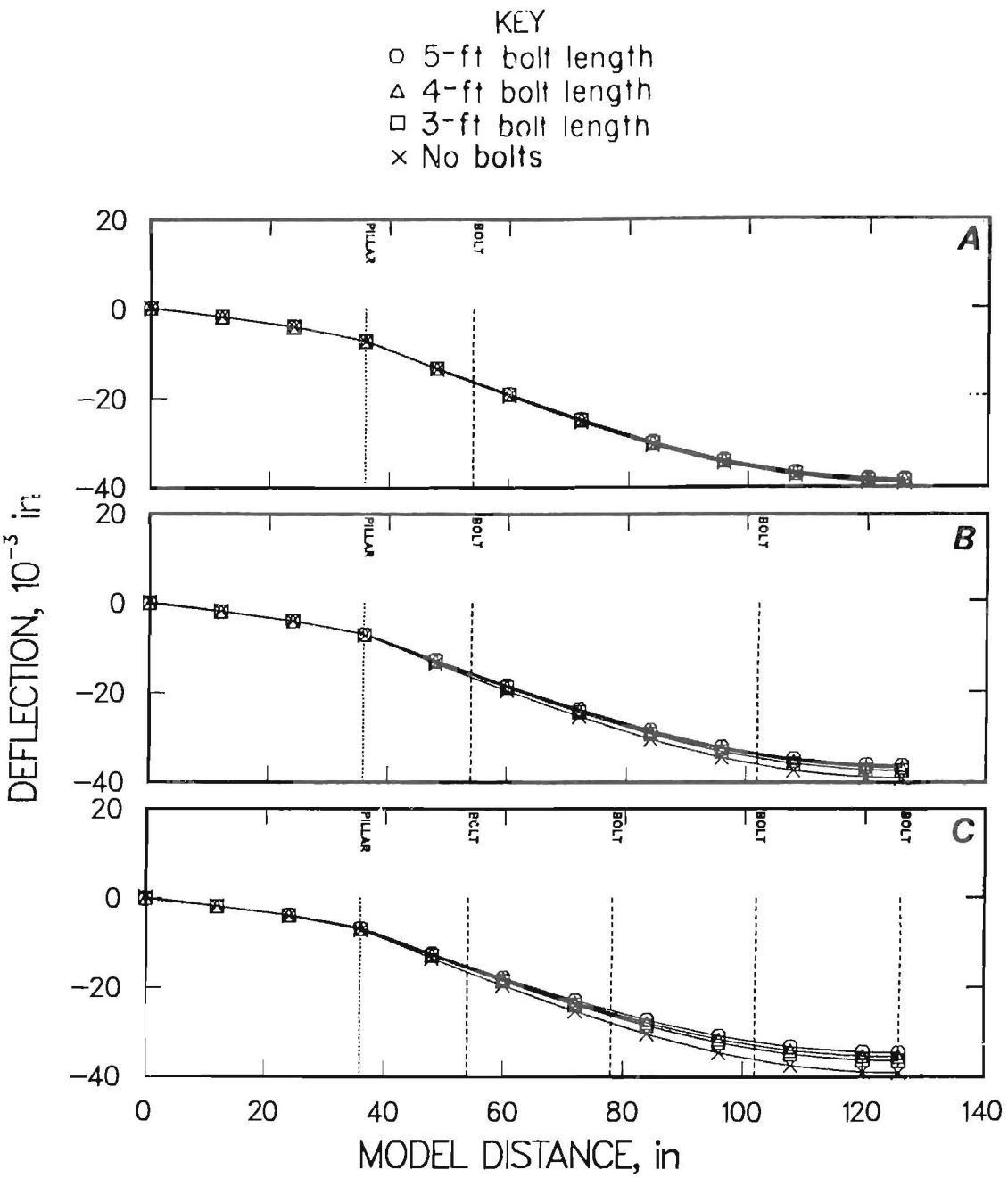

Figure 45.–Predicted vertical deflection profiles of lower edge of slab 6 under dead and 100-pct live loads using resin-grouted bolts at different lengths and spacings: (*A*) 12 ft, (*B*) 4 ft, (*C*) 2 ft.

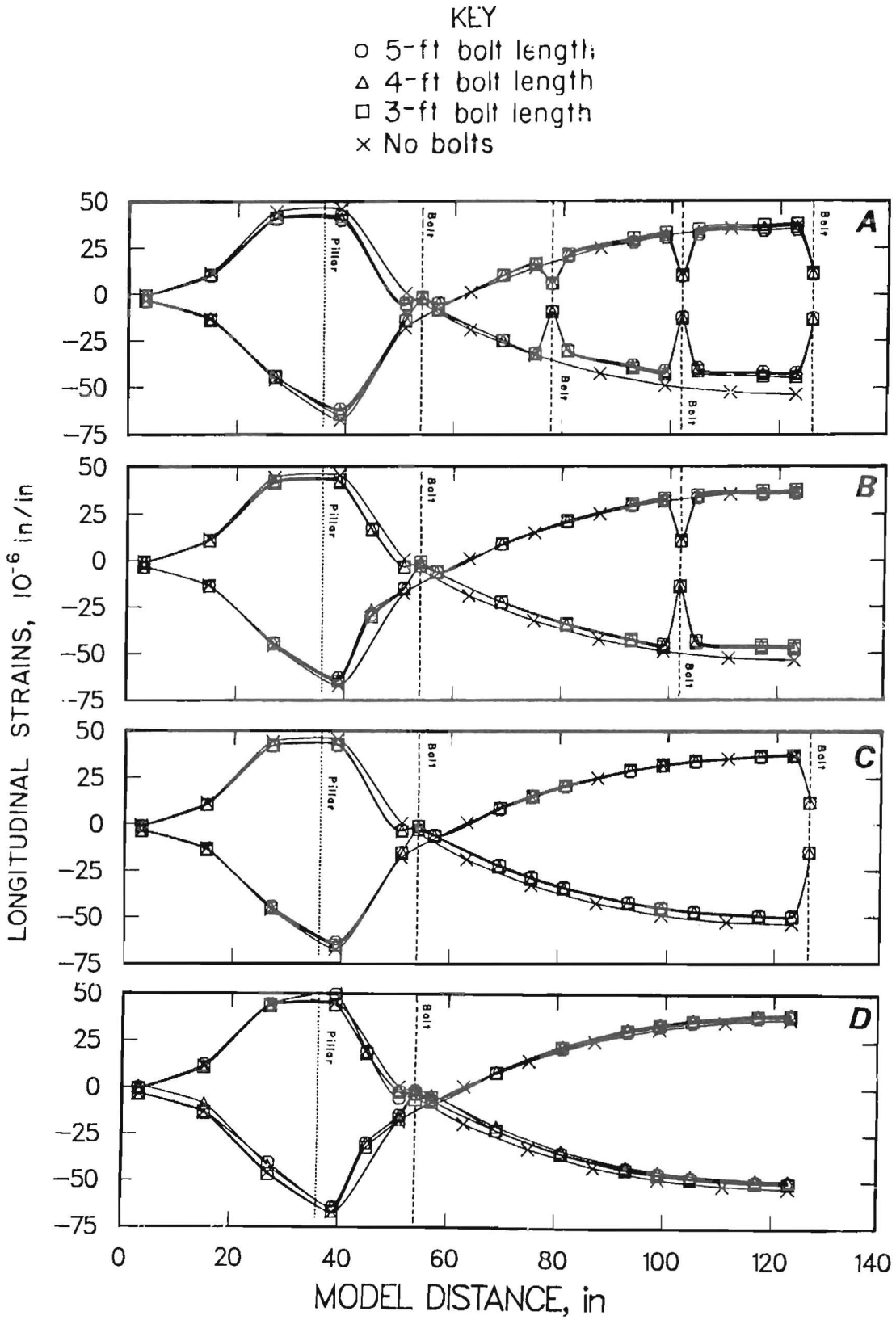

Figure 46.–Predicted longitudinal strain profiles on slab 6 under dead and 100-pct live loads using resin-grouted bolts at different lengths and spacings. Measurements were taken 1-1/2 in from the top and bottom edges of slab. Bolt spacings were (*A*) 2 ft, (*B*) 4 ft, (*C*) 6 ft, (*D*) 12 ft.

APPENDIX A.–PLACEMENT OF LOADS

This appendix establishes the magnitude and direction of the resisting forces on the boundaries of the solid structure (figure 14 in the main text) and isolated from the global model (fig. 13). The stress components from the global analysis are recorded on the elements enclosed by the boundary of the model, as shown in figure A-1. These stresses are converted to nodal forces by multiplying the stress intensities by the tributary areas of the nodes, assuming a unit thickness of the structure. When these forces are applied on the boundary, both the magnitude and the direction must necessarily satisfy the statics of the structure under consideration.

Figure A-1 shows the intensities of the stress components acting on the boundaries characterized by passing four sections in figure 14. The calculation of the balance of forces in the x and y directions of a portion of the structure, enclosed by sections 1-1, 2-2, 3-3, and 4-4, is shown in figure A-1. The calculated equilibrium in both the x and y directions agrees to within 1 pct. The insignificant differences derive from the assumption that shear stresses on each element are uniformly distributed; as is well known, shear stresses vary parabolically rather than uniformly. However, the laws of statics and compatibility must be observed in determining the directions of all stress

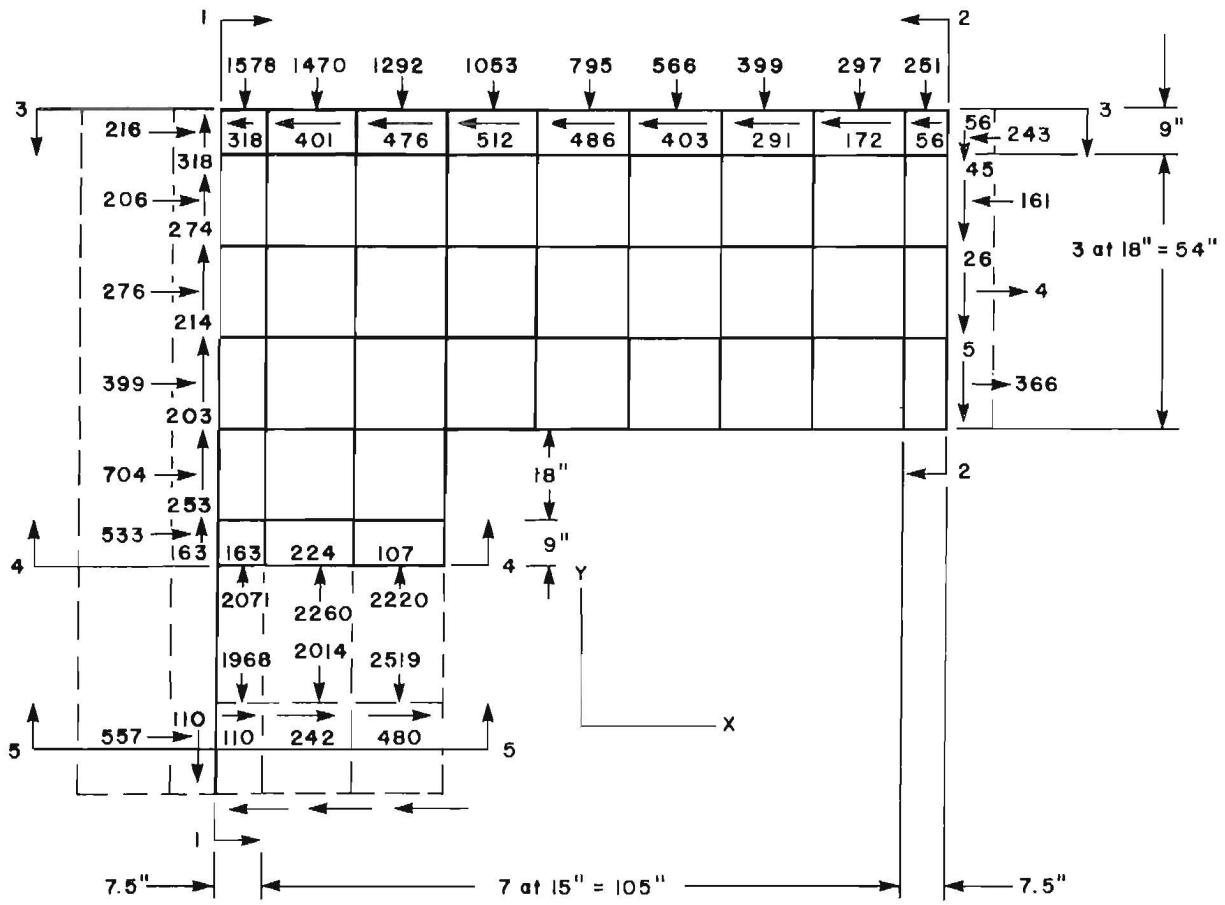

Figure A-1.–Statics checks on the mine opening caused by global loading. All values in pounds per square inch. Source, figure 14.

components. According to these laws, the assumed directions of figure A-1 are correct. Had the assumed shear stress directions been different, no equilibrium would have existed. One could arrive at the same conclusion by considering the state of stress at a point enclosed by any of the corner elements, as indicated in figure A-2.

These global stress components, when corrected for a depth of 100 ft, were not entirely applicable to the physical model. Shear forces on the pads, which transmit normal stresses and tractions, cannot exceed the normal force multiplied by coefficient of friction; that is, $F_s \leq \mu F_n$. Because most of the computer model shear forces exceeded 0.4 F_n (μ = 0.4) (coefficient of friction of steel on concrete as assumed here), the redistribution of the applied stress has to be calculated so that any possible deviation in the stress distributions in the critical regions given by global analysis of the structure is minimal. This has been discussed in detail in the main text. As a result of these conditions, the stress components were applied to the boundaries by load pads in the appropriate magnitude and direction (fig. 19).

Referring to figure A-1 and assuming uniform distribution of stresses over each element, the summation of forces in the vertical direction is as follows:

$$F_y = -[251\,(7.5) + (297 + 399 + 566 + 795 + 1{,}053 + 1{,}292 + 1{,}470)\,15 + 1{,}578\,(7.5) + 56\,(9) + (45 + 26 + 5/2)\,18] + [2{,}071\,(7.5) + (2{,}260 + 2{,}220)\,(15) + (163)\,(9) + (253 + 214 + 203 + 274)\,(18) + (318)\,(9)] = 429 \text{ lb.}$$

Balancing of forces in the x direction will require consideration of bending and direct stresses on the boundary of section 2-2:

$$\sigma_B = \left(\frac{366 + 243}{2}\right) = 304.5 \text{ psi,}$$

$$\sigma_A = \left(\frac{366 - 243}{2}\right) = 61.5 \text{ psi,}$$

where σ_B = bending stresses

and σ_A = axial stresses.

The resulting force due to axial stresses on the boundary (section 2-2) is (61.5) (63 × 1) = 3,875 lb.

The summation of forces in the horizontal direction is

$$F_x = [216\,(9) + (206 + 276 + 399 + 704)\,(18) + 533\,(9) + 163\,(7.5) + (224 + 107/2)\,(15)] + (3{,}875) - [56\,(7.5) + (172 + 291 + 403 + 486 + 512 + 476 + 401)\,(15) + 318\,(7.5)] = 610 \text{ lb.}$$

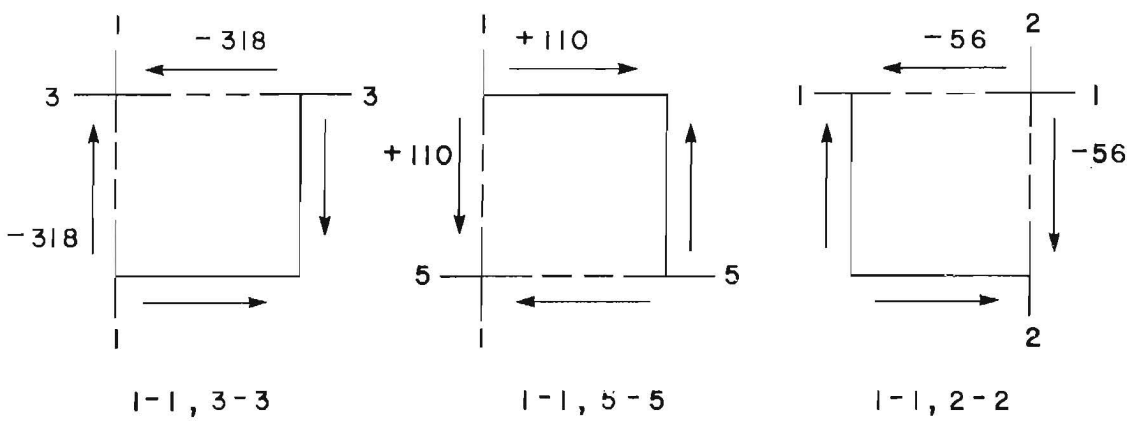

Figure A-2.–Magnitudes and directions of resisting shear stress for equilibrium of corner elements.

APPENDIX B.–STIFFNESS COEFFICIENTS

This appendix presents the results of experiments to determine the normal and shear stiffnesses of joints of the model mine roof entry. The stiffness values of the joint were necessary when using a finite-element approach with BMINES.

The basic relationships under consideration were between normal stresses and their corresponding displacements (normal stiffnesses, K_n), and between shear stresses and their resulting displacements (shear stiffnesses, K_s). The qualitative behavior of idealized stress-strain curves for determinations of K_n and K_s are shown in figures B-1 and B-2, respectively. The SRC test procedure is based on an article by Goodman and Dubois[1] and assumes smooth joints (no dilatancy).

[1]Goodman, R. E., and J. Dubois. Duplication of Dilatancy in Analysis of Jointed Rocks. J. Soil Mech. and Found. Div., ASCE, v. 98, No. SM4, Apr. 1972, pp. 399-422.

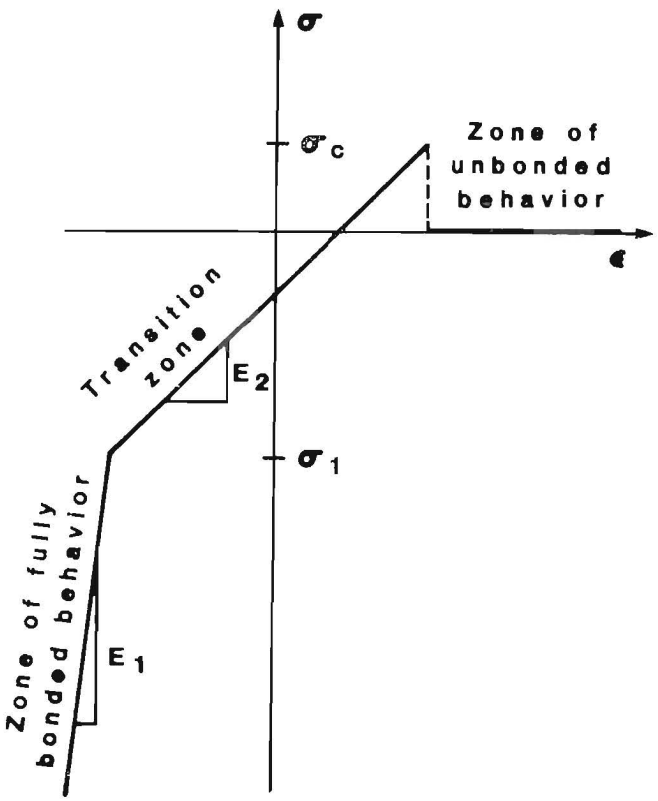

Figure B-1.–Qualitative load displacement relationship for normal stiffness of joint using BMINES.

Figure B-3 depicts one of the test curves that determined the normal stiffness coefficients needed for using the BMINES code. E_1 is the modulus for fully bonded behavior, while E_2 is the modulus in the transition zone and σ_1 is the compressive stress that acts across the boundary between two slab surfaces.

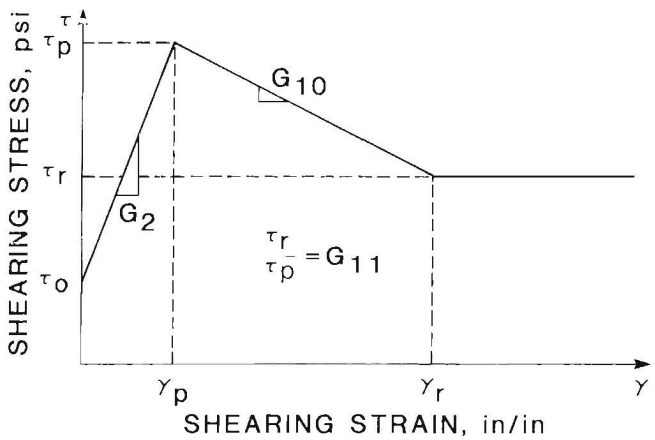

Figure B-2.–Qualitative load displacement relationship for shear stiffness of joint using BMINES.

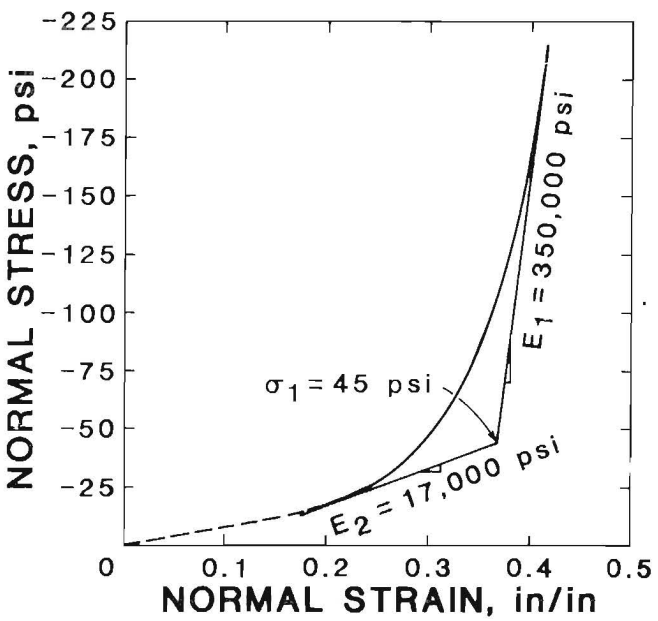

Figure B-3.–Sample plot for normal stiffness coefficient of joint as required by BMINES.

The shear modulus behavior of one of the laboratory tests is shown in figure B-4. G (G_2 in the code) is the shear modulus in the elastic range. As the asperities were worn down, the shear strength decreased to τ_r, which corresponded to cumulative shear strain, γ_r (establishing G_{10} of the code). From these data, a coefficient (G_{11}) was determined as the ratio of residual shear stress to peak shear stress, τ_r/τ_p, at low normal pressures. However, as the normal stress was increased, the shear stress necessary to produce slip increased according to the relationship:

$$\tau = C_o - \sigma_n \tan(\phi u + i),$$

where $i = C_o = 0$

The quantitative data obtained from numerous tests are given in tables B-1 through B-4. The mean values of the data used in the model are shown in tables B-3 and B-4 for normal moduli parameters, angles of friction, and shear stiffness coefficients. Typical plots of these quantities for some of the tests are shown in figures B-3 through B-5.

LABORATORY TESTS

The purpose of these tests was to determine joint stiffnesses, normal stiffnesses, and shear stiffnesses as they related to the roof bolt model; the tests were conducted along lines suggested by Goodman and DuBois.[2]

[2]Work cited in footnote 1.

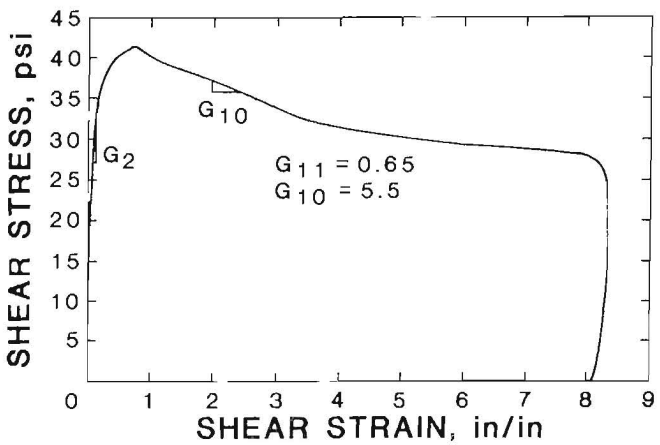

Figure B-4.–Shear stiffness curve of joint.

Table B-1.–Laboratory test results for normal stiffness coefficients, pounds per square inch

Sample	E_1	E_2	σ_1
SHEAR HELD CONSTANT AT 0 psi			
1J4	542,000	12,500	25
2J1	(1)	(1)	(1)
3J4	150,000	12,500	40
4J4	450,000	11,100	25
5J1	270,000	18,000	30
6J1	129,000	57,000	70
1J1	233,000	9,000	25
2J3	650,000	20,000	45
3J3	283,000	14,500	40
4J3	400,000	20,000	20
5J2	550,000	40,000	75
6J2	800,00	58,000	35
Mean	405,000	24,800	39.1
Std dev	215,000	18,200	18.3
SHEAR HELD CONSTANT AT 5 psi			
1J4	750,000	77,000	75
2J1	469,000	12,500	25
3J4	130,000	15,000	60
4J4	533,000	12,500	35
5J1	275,000	38,000	65
6J1	156,000	57,000	90
1J1	350,000	16,700	40
2J3	750,000	17,500	45
3J3	170,000	33,000	90
4J3	500,000	17,000	25
5J2	400,000	29,500	75
6J2	(1)	(1)	(1)
Mean	407,500	35,500	56.7
Std dev	219,000	28,400	23.1

[1]Bad data.

TABLE B-2.–Laboratory test results for normal joint stiffness coefficients (in pounds per square inch) where shear is held constant at 10 psi

Sample	E_1	E_2	σ_1
1J4	850,000	43,000	65
2J1	350,000	25,000	55
3J4	130,000	20,000	75
4J4	433,000	15,800	55
5J1	330,000	73,000	100
6J1	190,000	44,000	85
1J1	300,000	37,500	80
2J3	1,200,000	57,100	75
3J3	200,000	39,000	110
4J3	375,000	20,000	45
5J2	229,000	23,000	75
6J2	500,000	127,000	90
Mean	424,000	43,700	75.8
Std dev	309,000	31,200	19.0

Table B-3.–Laboratory test results for shear stiffness coefficients

Sample	G_2, psi			G_{11}, psi	G_{10}, psi	G_6, tan ϕu
	σ_n=10 psi	σ_n=50 psi	σ_n=150 psi			
1J4	17	100	160	0.88	4.5	0.160
2J1	180	200	375	.90	4.0	.130
3J4	100	360	(1)	.82	2.0	.188
4J4	80	240	375	.54	4.5	.225
5J1	80	120	300	.77	6.0	.200
6J1	230	210	395	1.00	3.5	.194
1J1	45	150	300	.76	7.0	.230
2J3	30	360	600	.75	4.5	.173
3J3	90	130	500	.65	5.5	.154
4J3	140	480	100	.76	4.6	.233
5J2	95	240	400	.88	5.0	.225
6J2	110	300	470	.80	3.5	.200
Mean	100	241	361	.793	4.55	.193
Std dev	60.9	116	144	.120	1.29	.033

[1]Bad data.

Table B-4.–Averaged normal and shear stiffness coefficients, pounds per square inch

Coefficients	Mean	Std dev
Normal:		
E_1	413,000	246,000
E_2	33,000	25,000
σ_1	57.8	25.2
Shear:		
G_2	150	107
G_6	.190	.033
G_{10}	4.60	1.290
G_{11}	.80	.120

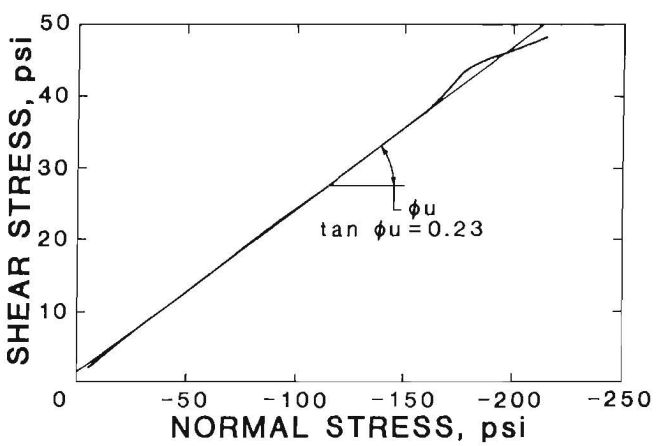

Figure B-5.–Laboratory determination of angle of friction along joints.

Each sample consisted of two circular disks each 3 in thick and 13.5 in. in diameter. These disks were separated by 6-mil polyethylene to maintain similarity between the model and test joints, thereby avoiding any bonding. The disks were poured from the concrete used in slabs of the model.

The plot for shear-versus-normal stresses was obtained by loading the sample up to 200 psi normal stress and increasing the shear load until one disk moved relative to the other. These values were recorded, the normal load was released, and the corresponding shear stress was read for set increments of normal stress. This procedure was maintained for all tests.

SAMPLE ASSEMBLY AND TESTING

1. Remove the cardboard from the perimeter and scrape the top and bottom of the sample to remove any foreign matter.
2. Measure the surface of the sample for irregularities. Measure thickness. Avoid relative movement between the two blocks.
3. Cap the top of the sample with plaster capping compound.
4. Place the sample on the aluminum block. Place the bottom ring and shim. Place the vertical direct current differential transformer (DCDT) and metal bands on the sample. Place the horizontal DCDT. Adjust the excitation voltage to 6 V and set the range of the DCDT to mid-range. Place the top ring, shim it, and place the load pad on top. Align the sample in the testing machine and tighten the backstop.
5. Where shear stress is held constant:
   a. Take an initial reading with all loads off.
   b. Place the hydraulic load pad on the top and bring the normal load up to 200 psi. Apply the shear constant and take a reading.
   c. Release the normal load in even increments while holding the shear stress constant. Take a reading at each load step until horizontal shearing takes place.
   d. Repeat for shear constants of 0, 5, and 10 psi.

6 Where normal load is held constant:

a. Reset the block and check the gauges.

b. Take an initial reading with all loads off.

c. Place the hydraulic load pad on top and bring the normal load up to the normal constant. Take a reading.

d. Slowly apply the shear load. Use the ramp loader. Take readings at even increments of horizontal deflection to obtain a well-defined stress-strain curve in the shear direction. When maximum load is reached, take readings at larger intervals until the shear stress becomes constant.

7. Shear versus normal:

a. Reset the block and check the gauges.

b. Take an initial reading with all loads off.

c. Place the hydraulic load pad and bring the normal stress to 200 psi. Increase the shear stress until sliding occurs. Take a reading. Use the ramp loader (on slow setting) to ensure constant contact in the shear direction. Unload the normal load at even intervals, wait until the shear stress levels off, and take a reading at each interval.

SAMPLES

Four samples were cast from the slab material of the roof model for each joint of the model. The forms for the samples were made from cardboard column forms cut to 3.5 in thick on a table saw. The bottom half of the form was nailed to a piece of 3/4-in plywood. A piece of 0.006-in plastic was placed between the bottom and the top. The top half of the sample was cast when the next set of slabs was placed. The samples were cured in a fog room with the cardboard forms still in place. The samples were labeled with a joint number, a "J," and a sample number; for example, 1-J-4 was taken from joint 1, the fourth sample.

DATA REDUCTION

Procedure

1. Use punched tape to create a data file.

2. Run the program "Shear/Input." This will convert and plot the data.

3. Run the program "Shear/Plot/Run" to get a hard copy on the plotter.

4. Get the values for E_1, E_2, and σ_1 by drawing tangents on the plots. The value for σ_1 is the transition point between E_1 and E_2. Draw secants to obtain a range for the values of E_1 and E_2.

5. The expanded stress-strain curve for the shear test may be obtained by plotting only the values in the elastic range. From this plot, get the values for G_1. The values of G_{10} and G_{11} may be obtained from the graph of the test with the normal stress held constant at 10 psi.

6. The slope of shear versus normal is the value for the tan ϕu.

Note: The conversion factors were calculated from the calibration runs.

Formulas

Shear load (I) = Volts (I) - Volts (0)(3000)

Displacement (I) = (Δ Volts Gage 1 * CF 1) - (Δ Volts Gage 2 * CF 2)

Normal load (I) = Volts (I) - Volts (0)(3000) - 750

Note: (I) represents any point I; the weight of the load pad is 750 lb.

DISCUSSION

The BMINES code requires various properties of the slip element. Not all of these input values are available from the shear tests. The mean values (fig. B-5) were selected from the data results (figs. B-1–B-4) and are listed here:

G_1 = 0	
G_2 = 150 psi	Elastic shear modulus of the joint material.
G_6 = 0.19	Tan ϕu, tangent of the friction angle for the joint.
G_{10} = 4.6	Slip modulus at which total degradation of the asperities has taken place.
G_{11} = 0.80	Ratio of the residual-to-peak shear strength for low normal stress.
E_1 = 413,000 psi	Joint normal stiffness for fully bonded behavior.
E_2 = 33,000 psi	Joint normal stiffness for transition zone.
σ_1 = 57.8 psi	Compressive stress required to establish full bonding.

The standard deviation shows a variation of about 50 pct in all the test results. This is a large variation and may be caused by several factors. The surfaces of the samples varied up to 1/4 in. in roughness, which was caused by variation in the sauna tube thickness and by difficulties in obtaining a flat surface in a small area. The surface variations resulted in uneven loading of the joint and rocking of the sample. Because the deflections measured are small, these factors can cause large deviations in results.

APPENDIX C.–STATICS CHECKS

This appendix establishes, in detail, statics checks on the layered analytical model. Following the procedure described in appendix A, sections 1-1 and 2-2 were passed through the model (fig. C-1). The resisting stresses were converted to forces and moments and recorded in figures C-1 and C-2 for dead load, and dead and live loads.

Force balances in the horizontal and vertical directions and moments about the z-axis are calculated below. Any deviations between applied and resisting quantities are mainly because of the assumption of a uniform shear distribution on planes 1-1 and 2-2, whereas, in actuality, a parabolic distribution on each layer should have been assumed. Despite this, the comparisons establish the statics of the layered model under dead load in a very satisfactory manner.

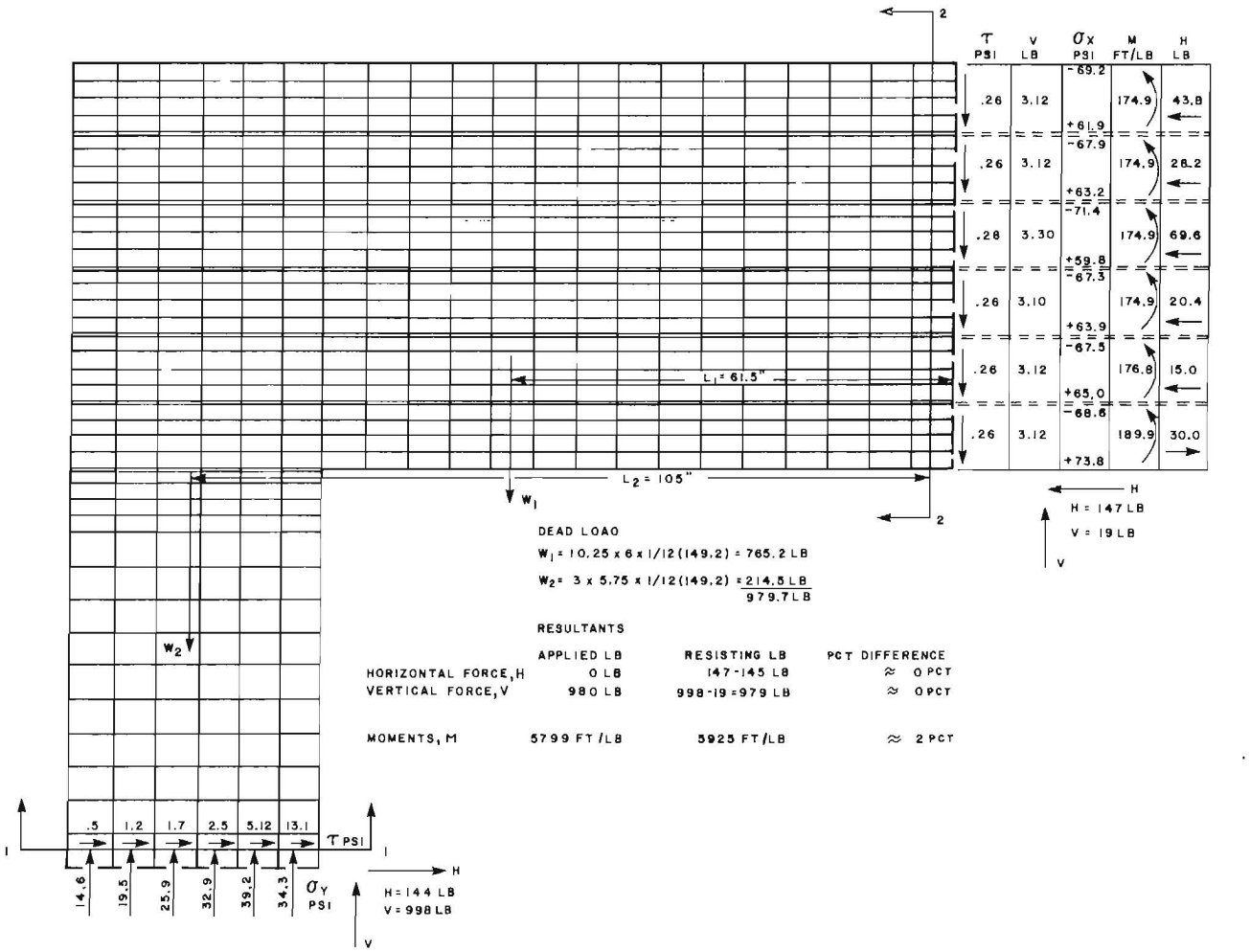

Figure C-1.–Dead-load statics checks on unbolted physical model with slip planes. Calculations are shown in text.

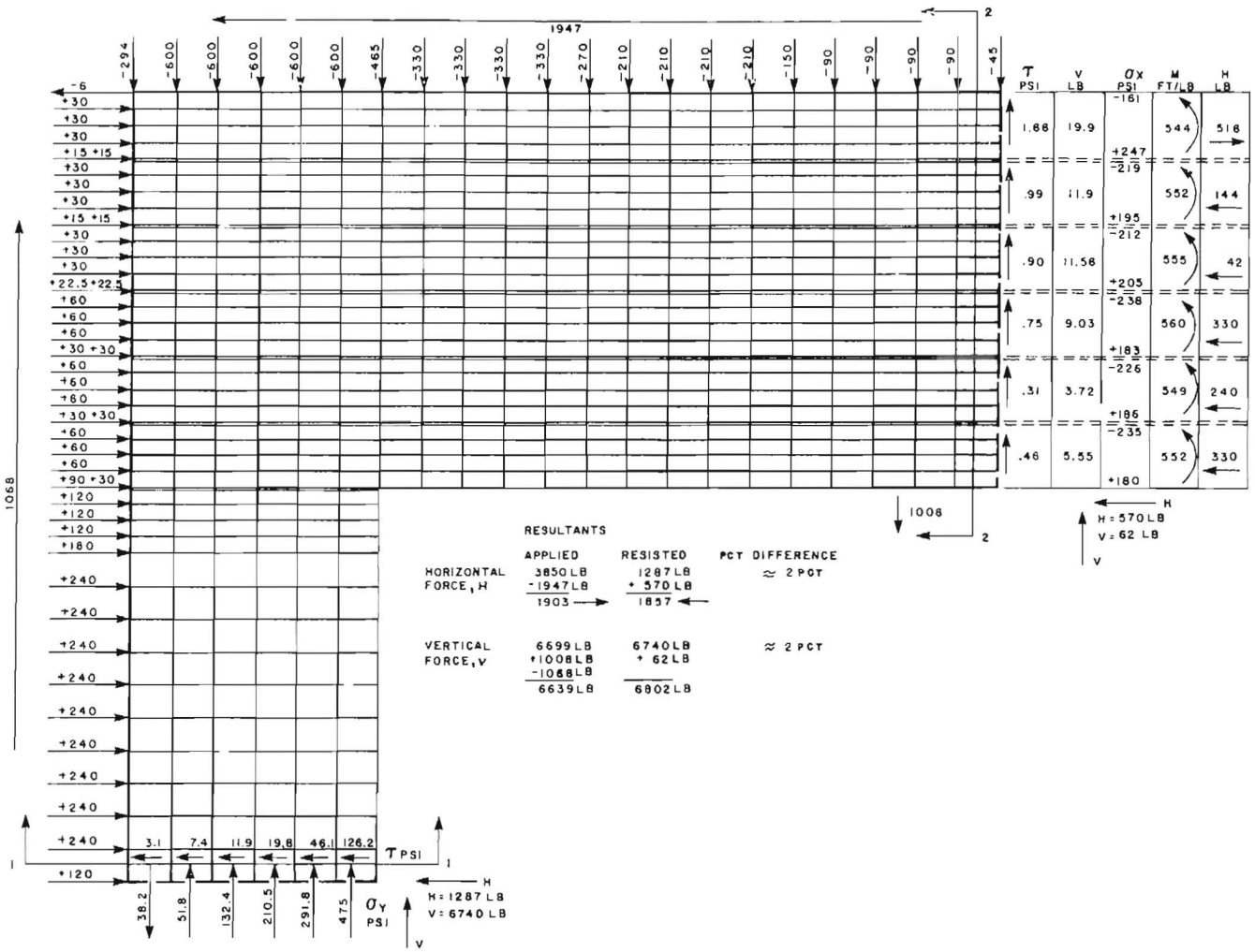

Figure C-2.–Dead- and live-load statics checks on unbolted physical model with slip planes. Source, figure 23.

HORIZONTAL FORCES: (13.1 + 5.12 + 2.5 + 1.7 + 1.2 +5) 6 + 30 - 15 - 20.4 - 69.6 - 28.2 - 43.8 = - 2 lb.

PERCENT DIFFERENCE: 0.

VERTICAL FORCES: (34.3 + 39.2 + 32.9 + 25.9 + 19.5 + 14.6) 6 - (3.12 + 3.12 - 3.30 - 3.10 - 3.12) - 979.7 = 1 lb.

PERCENT DIFFERENCE: 0.

MOMENT: 765.2 (61.5) + 214.5 (105) +12 [189.9 + 176.8+ (174.9) 4] + 145 (105) - 6[34.3 (90) + 39.2 (96) + 32.9 (102) + 25.9 (108) +19.5 (114) + 14.6 (120)] + (43.8 + 30) (30) + (28.2 - 15) (18) + (69.6 - 20.4) (6) = 126 ft/lb.

PERCENT DIFFERENCE: 2.

APPENDIX D.–SYMBOLS USED IN THIS REPORT

A	Cross-sectional area of bolt, in^2
A_g	Gross area of resin-grouted bolt, in
A_r	Cross-sectional area of resin surrounding bolt, in^2
A_s	Area of steel portion of bolt, in
C_o	Cohesion of joint, psi
D_g	Diameter of resin-grouted bolt, in
D_s	Diameter of steel portion of bolt, in
E	Modulus of elasticity in compression of material, psi
E_c	Modulus of elasticity of concrete, in
E_g	Modulus of elasticity of grouted bolt, psi
E_r	Modulus of elasticity of resin, psi
E_s	Modulus of elasticity of steel, psi
E_1	Modulus of elasticity of fully bonded behavior of joint, psi
E_2	Modulus of elasticity in transition zone after debonding of joint has started, psi
F	Force in bolt, lb
F_g	Forces resisted by gross area of bolt, lb
F_n	Force normal to joint for determination of K_n, lb
F_r	Forces resisted by resin area of bolt, lb
F_s	Force tangent to joint for determination of K_s, lb
F_{st}	Forces resisted by steel area of the bolt, lb
Fx	Resultant of forces in x direction, lb
Fy	Resultant of forces in y direction, lb
f_c'	Compressive strength of concrete, psi
G	Shear modulus in elastic range, psi
G_g	Shear modulus of grouted bolt, psi
G_1	Compressive stress required to establish full bending, psi
G_2	Shear modulus of joint in transition zone after debonding of joint has started
G_6	Tan ϕu (tangent of friction angle for joint)
G_{10}	Degradation of modulus of joint asperities
G_{11}	Ratio of the residual-to-peak shear strength for low normal stress
$G(K_s)$	Elastic shear modulus of joint, psi
I	Beginning node of an element
J	End node of an element
K_g	Bulk of modulus of resin-grouted bolt, psi
K_n	Normal joint stiffness of model material, psi
K_s	Shear joint stiffness of model material, psi
L	Axial length of bolt, in
L_g	Length of grout in bolt, in
L_o	Undefined gap of joint
L_r	Length of resin in bolt, in
L_s	Length of steel bolt, in
M	Moment
n	Direction normal to joint
s	Direction parallel to joint
U_s	Shear displacement parallel to joint
$(U_s)_J$	Shear displacement of Jth node
$(U_s)_I$	Shear displacement of Ith node
U_n	Displacement across joint
$(U_n)_J$	Normal displacement of Jth node
$(U_n)_I$	Normal displacement of Ith node
γ	Shear strain in the (x,y) plane, psi
γ_p	Shear strain corresponding to τ_p, psi

γ_r	Shear strain corresponding to τ_r, psi
Δ	Axial deformation of bolt, in
Δ_g	Axial deformation of grouted bolt, in
Δ_r	Axial deformation of resin portion of bolt, in
Δ_s	Axial deformation of steel in bolt, in
δ	Interface gap of joint, in
δy	Deflection in y direction, in
δx	Deflection in x direction, in
ϵ	Normal strain, psi
θ	Angle of inclination of the joint with the horizonal plane, deg
μ	Coefficient of friction of joint (constant)
υ	Poisson's ratio
υ_c	Poisson's ratio of concrete model
σ	Tensile normal stress, psi
σ_A	Normal axial stresses, psi
σ_B	Normal bending stresses, psi
σ_C	Tensile strength of joint, psi
σ_n	Stress normal to tangential plane, psi
σx	Normal stress in x direction, psi
σy	Normal stress in y direction, psi
σ_1	Compressive stress at which E_1 changes to E_2
τ	Shearing stress, psi
τ_p	Peak shear strength, psi
τ_o	Shear stress of unbonded behavior of joint, psi
τ_r	Residual shear strength, psi
τxy	Shear stress in the (x,y) plane, psi
ϕu	Angle of friction for joint, deg
$\tan \phi u$	Tangent of friction angle for joint

* U.S GOVERNMENT PRINTING OFFICE. 611-012/00,129